UNIVERSIDADE ESTADUAL DE CAMPINAS

INSTITUTO DE QUÍMICA

YULIANA PÉREZ SÁNCHEZ

NITRIC OXIDE-RELEASING POLYESTER COATINGS TO IMPROVE THE BIOCOMPATIBILITY OF IMPLANTABLE MEDICAL DEVICES

REVESTIMENTOS DE POLIÉSTER LIBERADORES DE ÓXIDO NÍTRICO PARA MELHORAR A BIOCOMPATIBILIDADE DE DISPOSITIVOS MÉDICOS IMPLANTÁVEIS

CAMPINAS
2019

YULIANA PÉREZ SÁNCHEZ

NITRIC OXIDE-RELEASING POLYESTER COATINGS TO IMPROVE THE BIOCOMPATIBILITY OF IMPLANTABLE MEDICAL DEVICES

REVESTIMENTOS DE POLIÉSTER LIBERADORES DE ÓXIDO NÍTRICO PARA MELHORAR A BIOCOMPATIBILIDADE DE DISPOSITIVOS MÉDICOS IMPLANTÁVEIS

Dissertação de Mestrado apresentada ao Instituto de Química da Universidade Estadual de Campinas como parte dos requisitos exigidos para a obtenção do título de Mestra em Química na área de Físico-Química

Master's thesis presented to the Institute of Chemistry of the University of Campinas as part of the requirements to obtain the title Master's in Chemistry in the area of Physical Chemistry

Supervisor: Prof. Dr. Marcelo Ganzarolli de Oliveira

O arquivo digital corresponde à versão final da Dissertação defendida pela aluna Yuliana Pérez Sánchez e orientada pelo Prof. Dr. Marcelo Ganzarolli de Oliveira.

CAMPINAS
2019

Agência(s) de fomento e nº(s) de processo(s): CAPES

Ficha catalográfica
Universidade Estadual de Campinas
Biblioteca do Instituto de Química
Camila Barleta Fullin - CRB 8462

P415n

Pérez Sánchez, Yuliana, 1993-
Nitric oxide-releasing polyester coatings to improve the biocompatibility of implantable medical devices / Yuliana Pérez Sánchez. – Campinas, SP : [s.n.], 2019.

Orientador: Marcelo Ganzarolli de Oliveira.
Dissertação (mestrado) – Universidade Estadual de Campinas, Instituto de Química.

1. Óxido nítrico. 2. Poli(ácido L-láctico). 3. Spin coating, Método de. I. Oliveira, Marcelo Ganzarolli de, 1959-. II. Universidade Estadual de Campinas. Instituto de Química. III. Título.

Informações para Biblioteca Digital

Título em outro idioma: Revestimentos de poliéster liberadores de óxido nítrico para melhorar a biocompatibilidade de dispositivos médicos implantáveis
Palavras-chave em inglês:
Nitric oxide Poly(L-lactic acid)
Spin coating method
Área de concentração: Físico-Química
Titulação: Mestra em Química na área de Físico-Química
Banca examinadora:
Marcelo Ganzarolli de Oliveira [Orientador]
Pablo Sebastian Fernandez
Amedea Barozzi Seabra
Data de defesa: 21-02-2019
Programa de Pós-Graduação: Química

BANCA EXAMINADORA

Prof. Dr. Marcelo Ganzarolli de Oliveira (Orientador)

Profa. Dra. Amedea Barozzi Seabra (UFABC/São Paulo)

Prof. Dr. Pablo Sebastian Fernandez (IQ-UNICAMP)

A Ata da defesa assinada pelos membros da Comissão Examinadora, consta no SIGA/Sistema de Fluxo de Dissertação/Tese e na Secretaria do Programa da Unidade.

Este exemplar corresponde à redação final da Dissertação de Mestrado defendida pela aluna **YULIANA PÉREZ SÁNCHEZ**, aprovada pela Comissão Julgadora em 21 de fevereiro de 2019.

To my mother, Ana Lucia and my grandparents, María Ofelia and José Jesus

ACKNOWLEDGMENTS

To Prof. Marcelo Ganzarolli de Oliveira, for the knowledge, guidance, advice and patience given.

To my mother, Ana Lucia, my sisters, Mayuly and Katherine, my brothers, Jorge and Victor, for their unconditional support, comprehension and constant encourage in this stage of my life.

To my deceased grandparents, for the absolute support on my early steps in the academic education.

To the infrastructure offered by the Institute of Chemistry of UNICAMP.

This study was financed in part by the “Coordenação de Aperfeiçoamento de Pessoal de Nível Superior - Brasil (CAPES) -Finance Code 001.

I would like to thank the São Paulo Research Foundation (FAPESP) (grant number 2016/02414-5) for financial support.

To the lab technician, Ms. Monique Ottmann, for the excellent support during the development of the project. In addition, I would like to thank the group of lab technicians and office staff of the Institute of Chemistry for the important support and training to obtain the measurements.

To the Pos-docs, Guilherme Picheth and Laura Caetano for the microscopy images, the helpful suggestions and text revision.

I would like to thank my sister Mayuly for the design of the illustrations.

To the members of Prof. Marcelo´s research group, Nitric Oxide & Biomaterials Group. Especially to Flávia Cabrini, Alexandre Dias and Sheila Alves, for the constant help and discussions during my research. Also, I would like to thank the colleagues with whom I shared the B-145 laboratory.

Finally to my partner, Andrés for his encourage in the most difficult moments. And, of course, to those who, despite of the distance, give words of support

“Será que la necedad parió conmigo,
la necedad de lo que hoy resulta necio,
la necedad de asumir al enemigo,
la necedad de vivir sin tener precio.”

Silvio Rodríguez

RESUMO

O óxido nítrico (NO) está envolvido em muitos processos biológicos e sua liberação na interface biomaterial/tecido tem mostrado diminuir a inflamação, estimular a proliferação celular e inibir a adesão plaquetária. Portanto, o revestimento de dispositivos médicos implantáveis com polímeros liberadores de NO pode melhorar significativamente a biocompatibilidade e a integração tecidual. Neste projeto é descrito o desenvolvimento de revestimentos poliméricos degradáveis com capacidade de fornecer NO durante períodos prolongados (> 1 mês). O biomaterial foi constituído por uma matriz de poli(ácido L-láctico)(PLLA, M_w 3,582 g mol^{-1}) impregnada com o doador de NO *S*-nitroso-*N*-acetil-D-penicilamina (SNAP). O método de *spin coating* foi usado para obter revestimento de mono e bicamadas partindo de soluções de PLLA-SNAP dissolvidas em tetrahidrofurano e depositadas na superfície de substratos de polipropileno. Com o fim de melhorar a hidrofilicidade do material, o PLLA foi blindado com poli(óxido de etileno)(PEO, M_v 400,000 g mol^{-1}) através de moldagem por evaporação de solvente. Caracterizações térmicas das blendas PLLA/PEO foram realizadas para investigar a miscibilidade dos polímeros. A cinética em tempo real da liberação de NO dos materiais foi analisada durante uma hora sob condições fisiológicas (pH 7.4, 37 ºC) por quimiluminescência. Os revestimentos apresentaram uma taxa de liberação na faixa de 6 - 20 pmol cm^{-2} min^{-1}, menor que a produção endógena de NO. A degradação hidrolítica dos revestimentos carregados com SNAP foi caracterizada sob condições fisiológicas e aceleradas (pH 9, 60 ºC). Revestimentos de mono e bicamada mostraram uma liberação inicial de NO rápida acima de 7 h. Depois de 30 dias de degradação hidrolítica sob condições aceleradas a liberação total de NO de monocamadas com 10 % e 20 % (m/m) de SNAP foi de 28.7 ± 0.2 nmol cm^{-2} e 67.0 ± 0.2 nmol cm^{-2}, respetivamente. No caso de bicamadas, a liberação de NO foi prolongada por mais 13 dias. Por fim, o uso de uma segunda camada de PLLA puro reduziu significativamente a liberação de NO, a qual se encontra na faixa de 2.5 - 3.2 nmol cm^{-2} que se prolongou por 72 dias. Em resumo, os revestimentos de PLLA-SNAP são capazes de manter uma liberação de NO por períodos prolongados sob condições fisiológicas.

ABSTRACT

Nitric oxide (NO) is involved in several biological processes and its release at biomaterial/tissue interface has been shown to decrease inflammation, stimulate cells proliferation and inhibit platelet adhesion. Therefore, the coating of implantable medical devices with NO-releasing polymers may significantly improve biocompatibility and tissue integration. Herein, we describe the development of biodegradable polyester coatings which are capable of delivering NO for prolonged periods (> 1 month). The biomaterial was comprised of a poly(L-lactic acid) (PLLA, M_w 3,582 g mol^{-1}) matrix impregnated with the NO donor *S*-nitroso-*N*-acetyl-D-penicillamine (SNAP). The spin coating technique was used to obtain mono and bilayer coatings of PLLA-SNAP solutions dissolved in tetrahydrofuran and deposited on top of polypropylene substrates. Poly(ethylene oxide)(PEO, M_v 400,000 g mol^{-1}) was blended with the PLLA matrix by solvent casting to improve the material´s hydrophilicity by solvent casting. PLLA/PEO blend thermal characterizations was performed in order to investigate the polymers miscibility. The real-time kinetics of NO released by the materials were analyzed during one hour under physiological conditions (pH 7.4, 37 ºC) by chemiluminescence. NO release rates were in the 6 to 20 pmol cm^{-2} min^{-1} range, which is lower than the rate of endogenous NO production. The hydrolytic degradation of the SNAP-doped coatings was characterized under physiological and accelerated (pH 9, 60 ºC) conditions; Monolayer and bilayer coatings showed an initial fast NO release profile up to 7 h at pH 7.4, 37 ºC. In 30-day experiments under accelerated conditions, the total NO release from SNAP 10 wt% and 20 wt% monolayers were, respectively, 28.7 ± 0.2 nmol cm^{-2} and 67.0 ± 0.2 nmol cm^{-2} . In the case of bilayer coatings, NO release duration was prolonged by 13 days. Finally, the use of a PLLA topcoat reduced significantly the cumulative NO release, which lasted over 72 days and was found to be in the 2.5 to 3.2 nmol cm^{-2} range. In summary, PLLA-SNAP coatings are capable of sustaining NO release over long periods under physiological conditions.

RESUMEN

El óxido nítrico (NO) está relacionado a muchos procesos biológicos y su liberación en la interface biomaterial/tejido ha demostrado disminuir la inflamación, la estimulación de proliferación celular y la inhibición de adhesión plaquetaria. Por lo tanto, el revestimiento de dispositivos médicos con polímeros liberadores de NO podría mejorar significativamente la biocompatibilidad y la integración tisular. En el presente proyecto se describe la elaboración de revestimientos poliméricos biodegradables con capacidad de liberar NO durante tiempos prolongados (> 1 mes). El biomaterial fue constituido por una matriz polimérica de poli(ácido L-lático))(PLLA, M_w 3,582 g mol^{-1}) impregnado con un donador de NO *S*-nitroso-*N*-acetil-D-penicilamina (SNAP). Revestimientos de mono y bicapa fueron fabricados mediante el método *spin coating*, usando soluciones poliméricas de PLLA-SNAP disueltas en tetrahidrofurano, las cuales fueron depositadas sobre la superficie de polipropileno usado como substrato. Con el objeto de mejorar la hidrofilicidad del material, mezclas poliméricas fueron obtenidas por *solvent casting* a partir de PLLA e con poli(óxido de etileno)(PEO, M_v 400,000 g mol^{-1}) comercial. La mezcla polimérica PLLA/PEO fue caracterizadas térmicamente para investigar la miscibilidad. La cinética en tiempo real de la liberación de NO de los revestimientos fue analizada durante una hora en condiciones fisiológicas (pH 7.4, 37 ºC) por quimioluminiscencia. Los revestimientos exhibieron una tasa de liberación en un rango de 6 - 20 pmol cm^{-2} min^{-1}, menor que la producción de NO endógena. La degradación hidrolítica de los revestimientos cargados con SNAP fue realizada en condiciones fisiológicas y aceleradas (pH 9, 60 ºC). Muestras de mono y bicapas exhibieron una liberación rápida inicial de NO después de 7 h. Después de 30 días de degradación hidrolítica en condiciones aceleradas la liberación total de NO de una monocapa con 10 % e 20 % (m/m) de SNAP fueron 28.7 ± 0.2 nmol cm^{-2} e 67.0 ± 0.2 nmol cm^{-2}, respectivamente. En el caso de la bicapa, la liberación de NO fue prolongada 13 días más. Finalmente, la aplicación de una segunda capa de PLLA puro redujo significativamente la liberación de NO entre 2.5 - 3.2 nmol cm^{-2} después de 72 días de degradación. En síntesis, los revestimientos de PLLA-SNAP demostrar poseer la capacidad de mantener una liberación de NO a lo largo de periodos extendidos en condiciones fisiológicas.

ABBREVIATIONS AND ACRONYMS LIST

Arg	L-arginine
ATR-FTIR	Attenuated total reflectance–Fourier transform infrared spectroscopy
DP_n	Number-average degree of polymerization
DSC	Differential scanning calorimetry
EDS	Energy Dispersive Spectroscopy
EDTA	Ethylenediaminetetraacetic acid
Eq(s).	Equation(s)
GPC	Gel permeation chromatography]
GSNO	S-nitroso-glutathione
HOMO	Highest occupied molecular orbital
I_r	Initial rate
IUPAC	International Union of Pure and Applied Chemistry
LA	Lactic acid
$NADP^+$	Oxidized nicotinamide adenine dinucleotide phosphate
NADPH	Reduced nicotinamide adenine dinucleotide phosphate
NAP	*N*-acetyl-penicillamine
NHA	*N*-hydroxy-L-arginine
NO	Nitric oxide
NO^-	Nitroxide ion
NO^+	Nitrosonium ion
N_2O_3	Anhydride of nitrous acid
NOA^{TM}	Nitric oxide analyzer
NONOatos	N-diazeniumdiolates
NOS	Nitric oxide synthases

cNOS	Constitutive nitric oxide synthases
eNOS	Endothelial nitric oxide synthases
iNOS	Inducible nitric oxide synthases
nNOS	Neuronal nitric oxide synthases
OM	Orbital molecular
PBS	Phosphate-buffered saline solution]
PC	Polycondensation
PDLA	Poly(D-lactic acid)
PDLLA	Poly(DL-lactic acid)
PEG	poly(ethylene glycol)
PEO	Poly(ethylene oxide)
PLA	Poly(lactic acid)
PLLA	Poly(L-lactic acid)
PLLA/PEO	Poly(L-lactic acid) and poly(ethylene oxide) blend
PP	Polypropylene
ROP	Ring-opening polymerization]
RS●	Thiyl radical
RSH	Thiol
RSNO	S-nitrosothiol
RS–SR	Disulphide dimer
SEM	Scanning electron microscopy
SNAP	S-nitroso-*N*- acetyl-D-penicillamine
THF	Tetrahydrofuran
XRD	X-Ray Diffraction

CONTENT

1. INTRODUCTION

The *in vivo* performance of biomaterials is mainly determined by their biocompatibility with the biological system they are designed for. Increasing biocompatibility especially of implantable devices is one of the major challenges involved in the development of biomaterials since some of these devices have thrombogenic surfaces that lead to serious clinical complications. Incorporating compounds in the biomaterial matrix with specific features intended to improve the tissue/biomaterial compatibility is a widely used approach to tackle this problem. Nitric oxide (NO) is an endogenously synthesized molecule, with key roles in many important cellular processes.[1-3] Due to such functions, the use of exogenous NO donor molecules for improving biocompatibility have been largely explored in the last few decades.[4-6] In recent years, most of the research concerning NO-releasing biomaterials comprising *in vivo* and *in vitro* studies highlight the therapeutic potential of NO-releasing biomaterials.

1.1. Nitric Oxide

1.1.1. NO Chemistry and physical chemistry properties

Nitric oxide (according to IUPAC) is a colorless gas at standard state.[7,8] This little molecule reacts with oxygen to form brown nitrogen dioxide and do not react with water.[7-9] It has a small dipole moment resulting in a low solubility in water (1.95 mM atm-1 at 25°C).[10] NO has a melting point of –163 °C, boiling point of –151.7 °C, and liquid density of 1.269 (at boiling point).[7] Since the discovery of NO in the 1980s as an important physiological regulator,[11] its biochemistry has been widely studied and established, and led to its selection as “the molecule of the year” in 1992 by the journal *Science.*

NO is a free radical with an odd valence electron in an anti-bonding π* molecular orbital (HOMO), as can be seen in the molecular orbital diagram of Fig.1,[12] which suggests a high reactivity as a carbon-center radicals.[A] This is not the case for NO, it is a stable free radical. For instance, it does not dimerize in the gas phase or solution under normal conditions at room temperature through the eliminating the unpaired electron; this single electron does not have preference to be centered on the nitrogen nor oxygen atom, it is delocalized between both atoms.[9,A] Its valence bond representation is also shown in Fig.1. There are two possible resonance structures, both with a double bond with a bond order of 2.5, the bond length of 1.154

Å, which is found between a bond length of a double (1.18 Å) and a triple (1.06 Å) bond.[14]

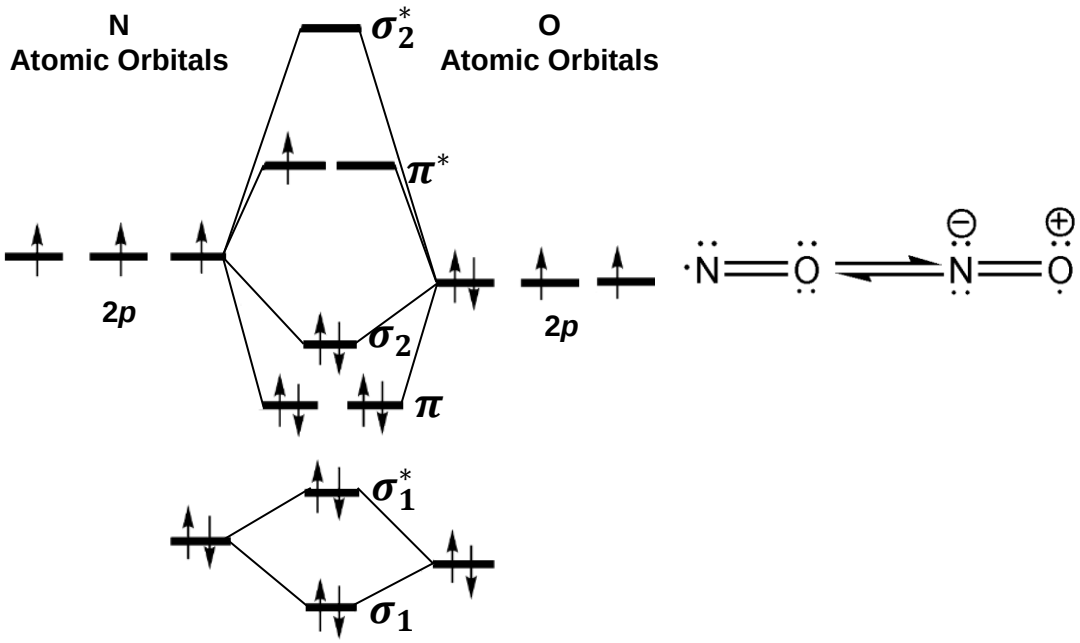

Fig. 1. Left molecular orbital diagram of NO showing the unpaired electron in an anti-bonding π* molecular orbital. Right NO valence bond representation showing the two resonance structures.

Even though NO is a stable radical, it reacts with other paramagnetic species (superoxide ion O_2^- and O_2) or metal centers.[8,9] This high reactivity is explained its radical nature, an involves its reduction to the nitroxide ion (NO^-), oxidation to the nitrosonium ion (NO^+), reaction with oxygen (yielding NO_2) and reaction with halogens.[7,14] The different redox forms undergo bond length changes; in the oxidation to NO+, the bond length is reduced to 1.06 Å (bond order 3),while in its reduction to NO^-, the bond length increases to 1.26 Å, because of the gain of one electron in the π* molecular orbital.[15,16] The infrared stretching frequencies (*ν*NO) are from 2377 cm^{-1} for NO^+, 1875 cm^{-1} for NO and 1470 cm^{-1} for NO^-.[17]

The reaction of NO with oxygen in water is well studied but the mechanism is still uncertain. The reactions involve the formation of NO_2 (Eq.1), reacts with NO to give N_2O_3 (nitrous acid anhydride) (Eq.2). Afterwards N_2O_3 hydrolyses to yield NO_2^- (Eq.3). If the NO_2 concentration is not enough for dimerization to form N_2O_4, no significant quantities of NO_3^- can be produced (Eq.4).[18,19] The concentration of nitrite and nitrate are used as markers for *in vitro* and *in vivo* NO.[18]

$$2NO + O_2 \rightarrow 2NO_2 \qquad (1)$$

$$2NO_2 + 2NO \rightleftharpoons 2N_2O_3 \quad (2)$$

$$2N_2O_3 + 2H_2O \rightleftharpoons 4NO_2^- + 4H^+ \quad (3)$$

$$N_2O_4 + H_2O \rightleftharpoons NO_2^- + NO_3^- + 2H^+ \quad (4)$$

For overall NO oxidation reaction (Eq.5), the rate law for the oxidation of NO is second order relative to NO and first order relative to O_2 (Eq.6). The rate constant, k_{aq} is reported as 9 x 10^6 M^{-2} s^{-1}, at 23 ºC.[9,20]

$$2NO + O_2 + 2H_2O \xrightarrow{k_1} 4NO_2^- + 4H^+ \quad (5)$$

$$-\frac{d[NO]}{dt} = 4k_{aq}[NO]^2[O_2] \quad (6)$$

The NO behavior in water is much simpler than in the biological environment. The biological activity of NO is complex; it reacts in the cellular environment to give a variety of products with different biological effects.[9] Its high solubility in membranes or hydrophobic environment accelerates the rate of NO oxidation by a factor of about 300 and its reacts with radical species eliminating dangerous radical species from biological systems.[8,21] In conclusion, features such as the small size, the lipophilicity and the high diffusion rate are important factors in the biological role of NO.

1.1.2. Nitric oxide biological syntheses

Endogenous NO is produced by most cell types by the aerobic oxidation of one the terminal guanidino nitrogen atoms of L-arginine (Arg) to L-citrulline, catalyzed by nitric oxide synthases (NOSs) (Fig.2).[22] In the first step, Arg is hydroxylated to *N*-hydroxy-L-arginine (NHA), where 1 mol of NADPH (nicotinamide adenine dinucleotide phosphate, reduced form) and O_2 are consumed. Afterwards, NHA is oxidized to L-citrulline with the consumption of 0.5 mol of NADPH and 1 mol of O_2, yielding NO and 1.5 mol of $NADP^+$ (oxidized nicotinamide adenine dinucleotide phosphate).Once NO is produced, it diffuses until reaching the target cells.[23]

In mammals, three distinct isoforms of NOS have been identified: neuronal nNOS, inducible iNOS and endothelial eNOS types.[22] Each one is associated with a

particular physiological process. The constitutive isoforms (nNOS and eNOS) are Ca^{2+} dependent and required calmodulin, a calcium sensor. On the other hand, the inducible isoform (iNOS) is Ca^{2+} independent (Ca^{2+} and calmodulin are already bond) and produces larger NO amounts (> μM).[8] Constitutive nNOS or NOS I is involved in the neurotransmission process; iNOS or NOS II act as a cytotoxic agent in normal immune defense against microorganisms and tumor cells; finally, constitutive eNOS or NOS III regulate smooth muscle relaxation and blood pressure.[23]

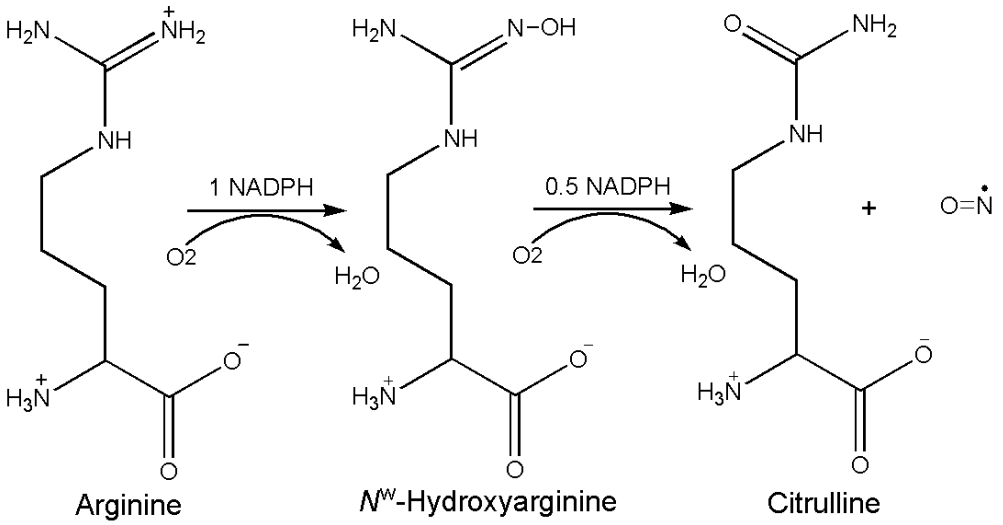

Fig. 2. Endogenous synthesis of nitric oxide from the oxidation of arginine into citrulline in the presence of the cofactor NADPH.[23]

1.1.3. Physiological NO actions

NO takes part in several cellular processes, to mention some, the vasodilation, the inhibition of platelet adhesion, thrombosis prevention,[24] the promotion of endothelial proliferation, re-epithelialization and collagen production in the wound healing process;[25] the reduction of bacterial adhesion[26] as well as stimulate blood flow increase (vasodilation),[27] which is related to many biological responses such as female sexual dysfunction.[28]

The most interesting NO participation in the cellular process for the aim in this project is the physiological action of NO in the vascular vessel. In situ, endothelial cells continuously produce low amounts of NO as the principal physiological source of NO in the vascular system by the eNOS constitutive isoform as was aforementioned (≤ 2 nM).[8,29,30] The NO produced controls the blood flow, which is the most important function, supplying indirectly oxygen to organs and governing the blood cell interaction with the vascular wall.[31] The production of this constitutive NO is known as basal production which is modulated when the endothelial cells suffer

shear stress, which stimulates the expression of NO synthase.[32,33] Fig.3 shows the biological actions of NO occurring at physiological levels; the cytoprotection against ischemia (lack of blood) and the regulation of blood flow to tissues:[8] NO enhances the development of blood vessel (angiogenesis) as a response of ischemia in tissues. In the cell, NO also attenuates mitochondrial respiration, programmed cell death (apoptosis), as well as the antioxidant function as mentioned before. Additionally, NO promotes vasodilation and inhibits both platelet and leukocyte aggregation. In summary, all these effects maintain blood homeostasis.[8]

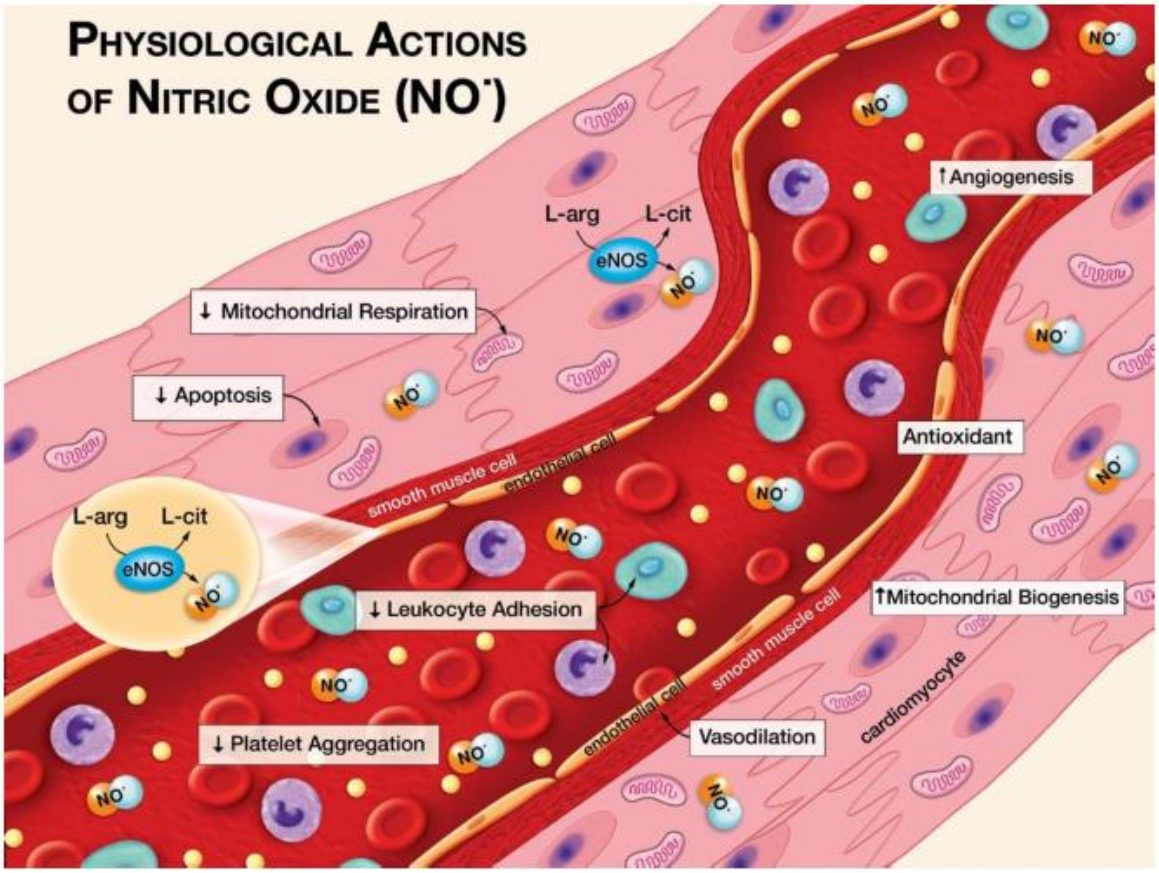

Fig. 3. Biological action of NO in the vascular vessel depicting the vasodilatation and antioxidant effect; the role in the mitochondrial respiration, cellular apoptosis and mitochondrial biogenesis. Reproduced with permission.[8] Copyright 2010, Elselvier

Novel potential therapeutic application of NO has been explored, such as anti-cancer since NO may act as a cytotoxic species against tumor cells leading to apoptosis.[34,35] Additionally, an antiviral action of NO is proposed and studied as well, due to it can pass through the cells, acting as a defense mechanism before the development of a specific immune response.[23]

1.2. *S*-nitrosothiols (RSNOs) as NO donors

1.2.1. NO release from RSNO

A compound can be classified as NO donor when its chemical structure has a functional moiety which can generate NO. Each class of NO donors has structural differences leading to large range of chemical relativities conferring advantages and disadvantages related to the NO release triggering and delivery system.[36] Basically, there are three NO release mechanisms; the first one is the spontaneous NO release, by means of thermal or photochemical self-decomposition of compounds such as N-diazeniumdiolates (NONOates) and S-nitrosothiols (RSNOs); the second mechanism comprises chemical reactions with other species and the last one is the enzymatic oxidation.[23]

1.2.2. RSNO chemistry, biochemical function and some applications

It has been demonstrated in several studies that RSNOs represent a source of endogenous NO, and have better biocompatibility compared to NONOates as exogenous NO donors. [37] Nevertheless, RSNOs are not yet approved for clinical practice.[37] Fig.4 shows the generic thio-ester structure of tionitrite highlighting the sulfur-nitrogen bond, which is a stable covalent bond, slightly polar which may be easily synthesized through the S-nitrosation of the parent thiol (RSH).[38] The most common nitrosation method involves reacting thiols with the nitrosonium ion (NO^+) in a highly acidic environment.[39,40] NO^+ is generated by the conversion of NO_2^- added as a sodium nitrite. RSNOs have two configurational isomers which have been computational studied, analyzing HSNO and CH_3SNO configuration and calculating the bond lengths of the lowest energy conformation for *trans* and *cis* configuration.[23]

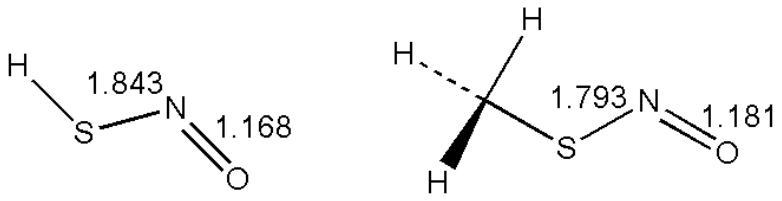

Fig. 4. RSNO configurational isomers and computational calculated bond lengths. Left *trans* HSNO configuration. Right *cis* CH_3SNO configuration.[23]

The chemical nature of the R group, heat as well as light influence the thio-ester formation and stability. A bulky protecting group confers stability making difficult the nucleophile attack. For instance the thionitrite derivatives of N-

acetylpenicillamine (NAP) and t-butyl-thionitrite are compounds that have steric hindrance.[41,42] Pure solid SNAP has shown to be a stable solid which decomposes above 150 °C releasing NO.[18,41] Additionally, RSNOs solutions are sensitive to catalytic decomposition by copper ions that may be present in the solution.[40,43,44] Also RSNOs solutions undergo acid catalyzed hydrolysis (Eq.7) or heterolytic fission in the alkaline pH case as shown in Eq.8. Therefore, such factors must be taken into account to guarantee RSNO stability in the polymeric matrix.

$$\mathrm{RSNO} + \mathrm{H^+} \rightleftharpoons \mathrm{RSH} + \mathrm{NO^+} \quad (7)$$

$$\mathrm{RSNO} + \mathrm{OH^-} \rightarrow \mathrm{NO_2^-} + \mathrm{RS^-} + \mathrm{H^+} \quad (8)$$

The RSNOs typical ultraviolet absorption peaks are found approximately at 200 nm, 335 nm, 500 nm and 550 nm with molar absortivities equal to 10,000, 1,000, 5 and 5 M^{-1} cm^{-1}, respectively.[42,45] RSNOs infrared analysis are given NO stretching values around 1490 to 1700 cm^{-1} and bending frequencies around 610-660 cm^{-1}.[42,46] For ^{16}N-NMR RSNOs spectra analysis, there are shifts in comparison with $NaNO_2$ spectrum (587 ppm) in the 750-790 ppm range.[47] In respect to the RSNO quantification, there are fluorescence methods (using dyes) and the Saville reaction (nitrosyl replacement by mercury of the thiol group).[7] Nevertheless, these methods are not sensitive enough to measure the RSNOs physiological levels (nM range, or pM range). Undeniably, the chemiluminescence method using Sievers NOA™ 280i instrument is one of the most sensitive to quantify low NO concentrations cleaving the linkage between sulfur and NO.[7]

Although RSNOs do not spontaneously release NO, this process can be triggered by different approaches such as the catalytic decomposition using transition metals (Cu^+ ions), the direct reactions with ascorbate salts, heat and light. In the latter cases, NO release is a result of the homolytic cleavage of the S–NO bond, which leads to the formation of thiyl radicals (Eq.9). These radicals can recombine leading to the formation of the RS-SR dimer (Eq.11), or may react with a second S-NO group, leading to the formation of a sulfur bridge with simultaneous release of a second NO molecule (Eq.10).[36,39,40,43]

$$\mathrm{RSNO} \xrightarrow[\Delta]{h\nu} \mathrm{RS\bullet} + \mathrm{NO\bullet} \quad (9)$$

$$\mathrm{RSNO} + \mathrm{RS\bullet} \rightarrow \mathrm{RS-SR} + \mathrm{NO\bullet} \quad (10)$$

$$RS\bullet + RS\bullet \rightarrow RS - SR \quad (11)$$

In biological systems, RSNOs have been identified in nanomolar concentrations in cells and body fluids.[7,27] In the case of vascular vessel, the surface flux rate by healthy endothelial cells from the inner walls of the blood stream, has been reported as 5 - 40 nmol cm^{-2} min^{-1}.[48-50] For instance, low molecular weight RS-NOs was identified in the plasma of human subjects treated with nitroglycerin;[51] S-nitroso-glutathione (GSNO) has been identified as well in concentrations sufficient to influence basal brachial tone.[52] RSNOs have shown biological actions such as antimicrobial actions and inherently possess the aforementioned NO biological action.[27]

The antimicrobial action of NO was associated with the covalent modification of bacterial membrane sulfhydryl groups by the thiyl group inductive effect which is independent of the spontaneous NO release.[53,54] Also, this antimicrobial action comprehends a chemical alteration of DNA, due to the reaction of NO with superoxides to form nitrogen and oxygen intermediates, which induce the DNA alterations such as nitrosylation of nuclei acids, avoiding the DNA replication of bacteria.[55,56] Additionally, this antimicrobial action was shown to be independent of RSNOs size, shape, charge, hydrophobicity and membrane permeability.[27]

The incorporation of RSNO groups into polymeric matrices, includes the use of SNAP (Fig.5a), which is a hydrophobic NO donor extensively used in scientific research.[40,57-64] Its hydrophobic character favors its location in the hydrophobic polymer phase.[59] For SNAP syntheses, the acid nitrosation of N-acetylpenicillamine proposed in 1978 by Field *et al* has been widely used and barely modified.[41] Fig.5b. shows the absorption maxima in 341 nm and a second weak absorption in 595 nm.[65] The stability of tertiary RSNO in the face of primary RSNO has been highlighted in studies of SNAP-doped polymers, with respect to the loss of NO;[60] tertiary RSNO stability is conferred by the steric hindrance of the sulfur atom imposed by the methyl group. This is important considering that NO-donors in polymeric systems must remain stable throughout the entire preparation process, resist storage and release NO only during or after the application time. However, this kind of NO donors decomposes following the same pathways mentioned before, yielding NO and the dimer of NAP. The chelator property of NAP is widely studied and used in treatment of heavy metal intoxication, such as mercury poisoning and excessive cupper accumulation know as a Wilson´s disease.[61-66] Hence, the SNAP decomposition will not represent any toxicity risk for materials loaded with SNAP employed for medical proposed.

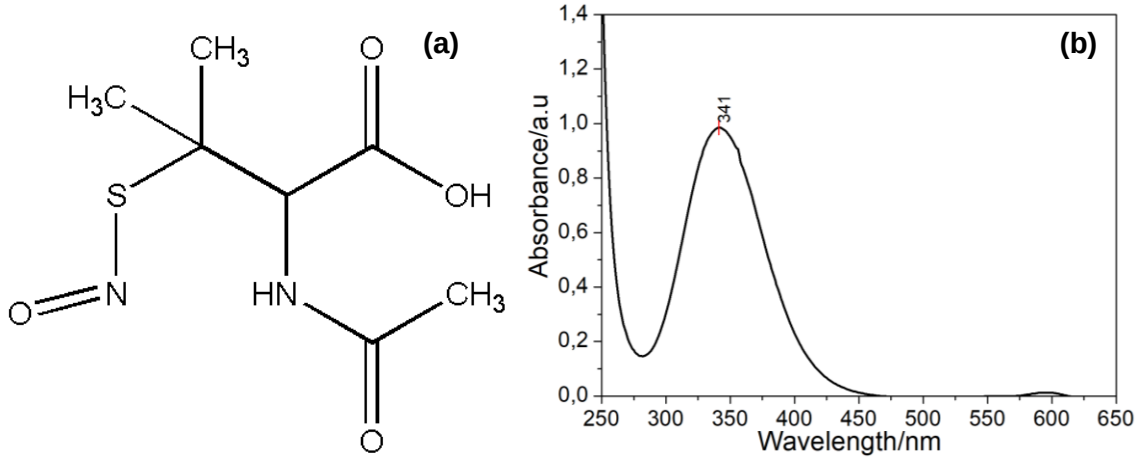

Fig. 5(a) SNAP chemical structure showing the tertiary *S*-nitrosothiol and **(b)** UV- Vis spectra of 1.6 mM SNAP in methanol.[65]

The loaded SNAP in hydrophobic polymeric matrix has shown to be a good strategy to improve the lifetime of NO donors, to administrate NO exogenously and simulate the biological NO flux. Meyerhof's research group have studied the SNAP solubility in hydrophobic polymers and found that SNAP barely dissolves (solubility: ca. 3.4 - 4.0 wt%), the SNAP excess crystallizes in orthorhombic form, contributing to shelf stability and slow dissolution of the crystals due to the hydrogen bonding between SNAP molecules, resulting in a long term release under physiological conditions.[67] Besides, they suggested that the NO release rate from SNAP-doped hydrophobic materials is controlled by the total water contacting the surface area of the polymer film and depends on the SNAP concentration within the film, where NO release rate does not increase as the thickness of the film increases; if this area remains the same, the NO release rate decreases as the SNAP concentration decreases. Also, the SNAP concentration and the thickness of the film determine the long-term NO release.[68] Additionally, other studies performed by that research group observed that SNAP can be leached out from the film at lower rate than the NO release from the polymer, which can be counteracted by the deposition of a polymer topcoat.[68]

Fig.6 shows the representation of the NO release mechanism proposed by Yaqi Wo., *et al.* [67], which describes an interesting theory for SNAP decomposition in biomaterials that shows low water uptake (hydrophobic), which is summarized by three factors: 1) the SNAP concentration in the polymer matrix; as SNAP crystals slowly dissolve into the solid polymer SNAP molecules are released; 2) the polymer surface area exposed to the aqueous solution where free SNAP molecules dissolve in the aqueous media and decomposes releasing NO; and 3) the film thickness of the specific material. These factors lead to long-term NO release, being directly proportional to the SNAP loading. In conclusion, SNAP solubilizes in the polymer

matrix, later, in water-rich regions near the polymer/solution interface, SNAP decomposes and releases NO. Additionally, the SNAP crystal dissolution leads to a decrease in the dissolution of more crystalline SNAP because the bulk polymeric phase becomes saturated.

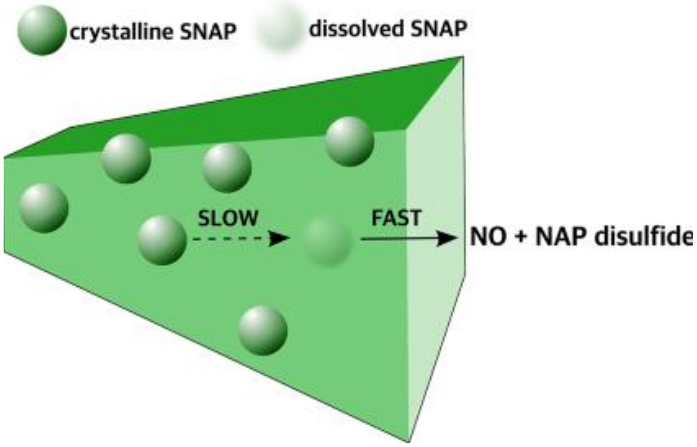

Fig. 6. Schematic representation of NO release mechanism from a hydrophobic polymer showing the three determining factors; the SNAP concentration, the water contacting surface area and the film thickness. Reproduced with permission.[68] Copyright 2015, American Chemical society.

1.3. NO releasing materials

Biomedical advances have encouraged the development of biodegradable platform materials. For instance, regenerative medicine, tissue engineering and controlled drug delivery are biomedical technologies that require biomaterial-based platforms.[69] According to Willians D.F, a biomaterial can be defined as a material intended to interface with biological systems to evaluate, treat, augment or replace any tissue, organ or function of the body.[70]

The biodegradability is an important concern for the biomaterial applications. Some important properties of a biodegradable biomaterial are sited: biologic inertness, non-toxic degradation products; ability to be metabolized and cleared from the body; the biomaterial/biological system contact should not evoke inflammation or toxic response; the mechanical properties of the material should be appropriate for the intended application. Besides, during the biomaterial degradation, those mechanical properties should be compatible with the biological process for which it was designed. Finally, the degradation time should be enough to accomplish the function.[71]

Polymeric materials have a variety of mechanical and degradation properties that confer special features for the biomaterial applications. Due to their versatility, in some cases they replace other biomaterial, such as metals, alloys and ceramics. The material chemistry, the molecular weight, the solubility, the hydrophobicity and degradation affect their biocompatibility. Among the biomedical applications it is included the controlled drug delivery: the bioactive agents are loaded inside the polymeric matrix from which they are released by the erosion or diffusion (or both) processes.[71]

For the NO delivery, several biomaterial-based platforms have been used, involving strategies to link NO-donors with delivery systems, acting as a source of circulating NO for sustained release (Fig.7); These delivery systems comprehend micelles, liposomes, polysaccharides, zeolites, inorganic silica nanoparticles, inorganic multifunctional nanoparticles (such as gold particles), self-assembled polymeric monolayers and sol-gel coating.[36,37]

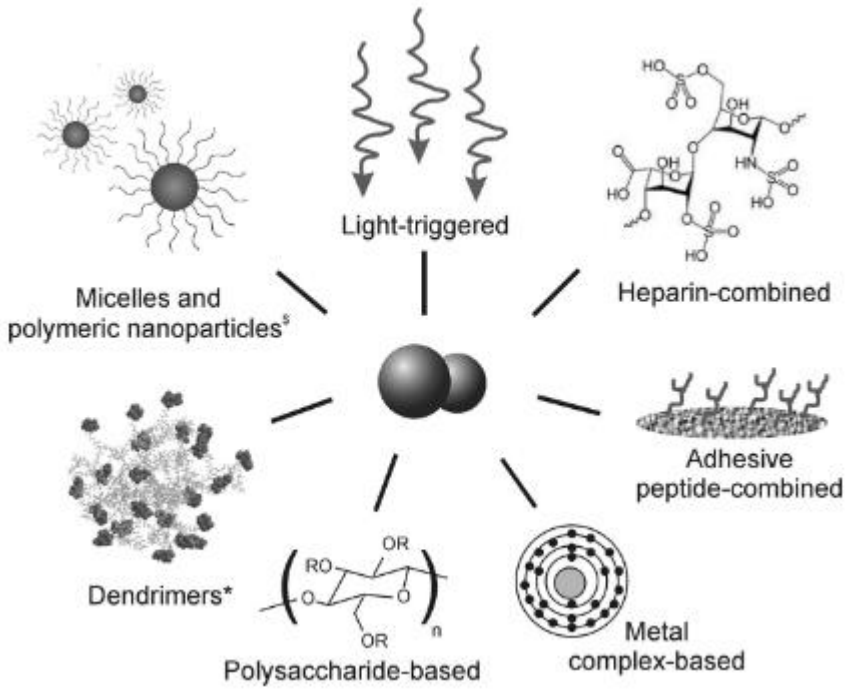

Fig. 7. Biomaterial-based platforms strategies for sustained NO delivery. Reproduced with permission.[37] Copyright 2012, Wiley-VCH. $Reproduced with permission.[72] Copyright 2009, American Chemical society. *Reproduced with permission.[73] Copyright 2010, Elservier.

The coating platform strategy can be used for localized delivery by means of adsorption. NO donors can be blended with polymers and afterwards adhered physically to the surface of a substrate using dip-coating, spin-coating or spray coating techniques.[74,75] In particular, spin coating represents an excellent strategy to obtain high-quality multilayer thin coatings on different substrates, when using polymeric solutions with volatile solvents. This technique can be divided into four steps: 1) solution deposition, in which the liquid is dropped on the substrate held by a disk which is rotating at a low rotating speed, so that the liquid can flow over until the edge of the disk; 2) spin-up, in which the disk rotating speed is accelerated to a set speed, ω, and the liquid flows radially, due to centrifugal force, covering the whole substrate area; 3) spin-off, in which the excess liquid flies off the edges, and a thin uniform liquid film is formed under the constant rotating speed; and 4) film drying, in which the liquid solidifies due to the solvent evaporation.[76] This technique was used in this project to coat model surfaces of polypropylene.

Meyerhoff and coworkers have been explored a varieties of strategies to load materials with NO donors and have been characterized the NO release profiles for the obtained NO release biomaterials doped with SNAP, as well as biological assays to evaluated the potential as biomaterial. Among the polymeric materials, polyurethane (Carbosil® 20 80A) films doped with SNAP were analyzed and demonstrated to be effective to control the bacterial adhesion and microbial infection on the material surface, due to the synergistic effect of physical topographic surface modification and the NO action, that decreased the available surface area, while the decomposition of SNAP within polymer film initiated the NO release at flux levels higher than 50 nmol $min^{-1}cm^{-2}$ up to 10 days. [77,78]

On the other hand, the stability of SNAP within the polymer is other important matter in NO releasing materials. For instance coatings of E2As polymer load with SNAP exhibited an excellent storage stability, after 2 months storage at 37 °C 82% of the initial SNAP was retained.[59] The same platforms strategy was tackled for sustained NO delivery by catalytic decomposition of SNAP in blood, via copper mechanism, using NO generating material polymeric coating, composed of copper nanoparticle-containing polyurethane combined with systemic SNAP administration (0.1182 mmol/kg/min), after 4 h of blood exposure, the extracorporeal circulation circuits in a rabbit thrombogenicity model yielded significantly reduced of thrombus formation and platelet aggregation.[79] The same catalytic decomposition (copper ions mechanism) was used in studies of tunable NO release from Carbosil coatings with top-coated polymer composites with copper nanoparticles, which increased the NO release flux from 132 nmol min^{-1} cm^{-2} to 448 and 1170 nmol min^{-1} cm^{-} with 1 and 5 wt % copper nanoparticles; increased the antimicrobial activity and decreased the platelet adhesion.[80]

Studies related to poly(lactic acid) (PLA) matrix doped with SNAP were realized by the Meyerhoff´s group. They encapsulated the SNAP within poly(lactic-co-glycolic acid) 50:50 (PLGA) microspheres to sustain NO release (*ca* 0.56 µmol SNAP/mg microspheres.), which was governed by the erosion of PLGA microspheres. They observed that using the ester capped PLGA (M_w = 38,000–54,000) the NO released was prolonged for over 4 weeks. Additionally, they analyzed the different catalytic decomposition to obtain sustained NO release such as copper ions and/or ascorbate salts and light.[57]

Other reported strategy such as silica has been studied as system for NO releasing materials at controlled rates, especially as particles, which are covalently attached with NAP and by reaction with *t*-butylnitrite, tertiary RSNO-modified materials are obtained.[60,80,82] The incorporation of SNAP-fumed silica in polymeric materials shown maintained NO release and possessed biological potential such as antimicrobial activity, inhibition of bacteria adhesion. For instance, the system of SNAP-fumed silica particles (21–138 nmol/mg) were blended with polyurethane to create films and generated NO fluxes of approximately of 750 nmol cm^{-2} min^{-1} catalyzed by copper ions. Contrary to the silicone rubber films, which only liberated NO by photolytic decomposition.[82]

1.3.1. Poly(lactic acid)

Polymeric matrices may exert an important effect on the kinetics of NO release. Several studies report the use of hydrophobic aliphatic polyesters such as poly(glycolic acid), poly(vinyl chloride), poly(caprolactone) and poly(lactic acid) (PLA) among others as matrices for the incorporation of NO donors.[83-86] PLA, in special, is considered a versatile biodegradable polymer, which is degraded by simple hydrolysis generating non-toxic byproducts, which are eliminated through normal cellular activity. The chemical properties and characteristics of PLLA will be cited in the subsequent sections, especially, the factors that contribute with the PLLA degradation.

1.3.1.1. PLLA chemical properties

PLA is a thermoplastic polymer constituted by aliphatic ester linkages in their backbone.[71] PLA or polylactide has a structural variety (Fig.8) due to its monomer, the lactic acid (LA), which has a chiral carbon, resulting in configurational isomers consisting of enantiomeric D- and L-lactic acid units in different sequences

and ratios. Enantiomeric polymers are commonly called PLLA and poly(D-lactic acid) (PDLA). While a racemic polymer consisting of a random sequence of both enantiomeric units is called poly(DL-lactic acid) (PDLLA).[71,87]

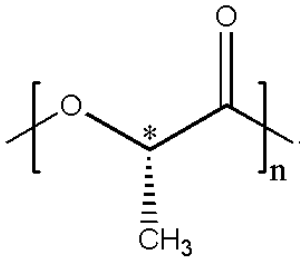

Fig. 8. Structural formula of PLLA. The asterisk shows the chiral carbon.

Basically, PLA can be synthetized by two routes according to Fig.9:[87] direct polycondensation (PC) of LA by the elimination of water (byproduct), in the presence of single (metal-compound) or binary (metal compounds activated with proton acids) catalysts.[88,89] The challenge to obtain high molecular weight PLA is to drive the dehydration equilibrium in the direction of esterification by using an organic solvent.[69] For instance, there is a PLA synthetic method, in which water/xylene azeotropic mixture is collected using a Dean Stark trap. The other route is the ring opening polymerization (ROP) of cyclic diester of LA, known as lactide, obtained through dimerization of LA catalyzed by metal-based or organic compounds.[87] The polymerization can be performed through cationic, anionic, coordination or free radical polymerization.[69,90]

However, these common routes have disadvantages. In the PC, the azeotropic distillation of solvent used, the complete removal of solvent and the difficulty in driving the dehydration equilibrium to the direction of esterification are some of the challenges to deal with.[69] On the other hand, the ROP route requires high cost of production due to the demanding purification process of the lactide.[69,88,89,91] For that reason, alternative synthetic routes have been suggested such as melt polycondensation followed by solid-state polycondensation, offering high molecular weight PLA with high yield in comparison to the ROP route.[69]

PLLA is a semicrystalline, slow-degrading polymer, with good tensile strength and a high modulus of approximately 4.8 GPa. The crystallinity degree depends on the molecular weight and the polymer processing parameters. Its thermal properties have been widely studied; the glass transition temperature, T_g has been reported in the range of 50 to 65 °C; the melting temperature, T_m has been reported as well, ranging from 160 to 180 °C.[87,92] The melting enthalpy of 100% crystalline

PLLA varies from 82 to 203 J/g and the degradation temperature was estimated at around 307 to 310 °C.[87,93-95] Additionally, the heat capacity of the solid state, Cp_{solid} below T_g is related to the vibrational motion of the PLLA macromolecule. Conversely, the heat capacity of the liquid state C_{liquid} is associated to the vibrational and conformational motions.[94]

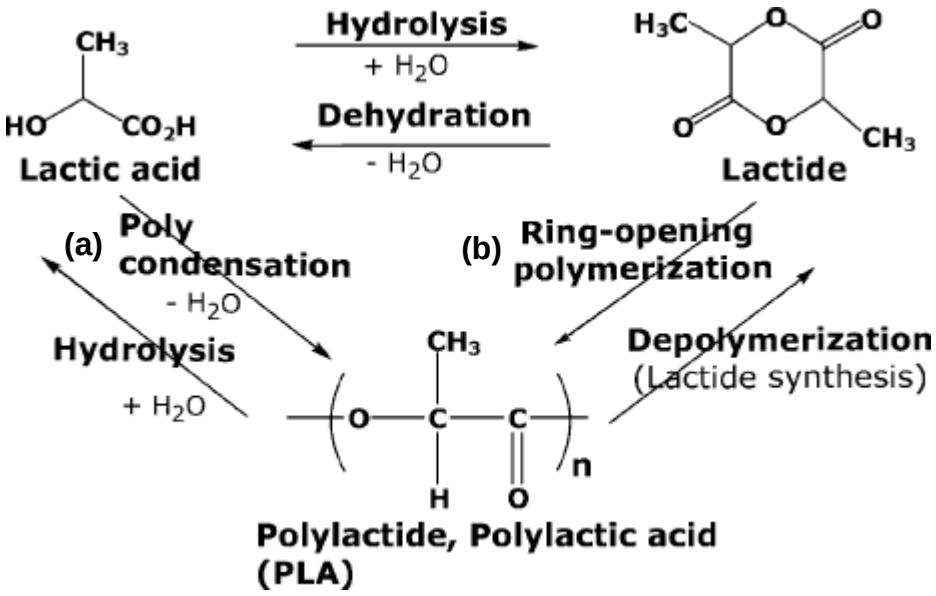

Fig. 9. PLA synthesis routes **(a)** direct polycondensation of LA by the elimination of water as a byproduct and the inverse reaction, the PLA hydrolysis with the consumption of water; **(b)** ring opening polymerization ROP of lactide and the inverse reaction, the depolymerization of PLLA. Additionally, the route to produce the lactide by the LA hydrolysis. Reproduced with permission.[96] Copyright 2006, Wiley-VCH.

The preparation conditions, the molecular weight and the thermal history influence the crystalline preference of PLLA and its thermal transitions. In addition, PLLA can undergo crystal reorganization through polymorphic transitions during heating. For instance, without a controlled process the obtained PLLA is generally amorphous due to the slow crystallization rate. [87,94,97,98]

The most stable crystallographic form of PLLA is the orthorhombic α-crystal, with parameters a = 10.683 Å, b = 6.170 Å, and c(chain axis) = 28.860 Å.[99] This crystal form is obtained upon crystallization at temperatures higher than about 120 °C.[93-95] Isotactic macromolecular chains adopt this crystallographic form by taking a 10_3 helical conformation (*i.e*. 10 units in 3 turns).[100,101] The orthorhombic unit cell have two chains and the a/b ratio indicates that the helices pack in a hexagonal manner even though the symmetry of the cell is orthorhombic.[100] On the other hand,

the metastable α'-crystals (or δ-crystal) is produced by bulk crystallization at temperatures lower than 120 °C. This phase is considered as a disordered α-form crystal and can be transformed into the α-form.[102,103] Other crystallographic form that PLLA can adopt is the ß-form crystals comprised by 3_1 configuration (*i.e*. 3 units per turn) with a trigonal unit cell.[104] This crystallographic form is known as "frustrated ß-Phase" because of the central helix cannot establish the same interactions with its neighbors as the other surrounding six helix do in this structure, and must adapt to an unlikely environment.[87] Finally, the last crystallographic form for the PLLA is γ-form, it can be obtained by epitaxial crystallization.[87]

1.3.1.2. PLLA hydrolytic degradation

Polylactides undergo hydrolytic degradation, taking place at bulk or surface erosion by the random scission of the ester backbone, which is a chemical group easily hydrolysable. In the bulk erosion the water diffusion is faster than polymer degradation, the material degradation is homogeneous. Instead, in surface erosion, the degradation is faster than water diffusion, and the material is eroded from the external surface and the erosion moves towards the interior of polymeric matrix.[71,87] This hydrolytic chain cleavage has shown to occur preferentially in the amorphous regions, resulting in an increase in polymer crystallinity.[105] The polymeric degradation product is the LA, which is also the human metabolic byproduct and is converted into water and carbon dioxide, representing no toxicity issue.[106] The hydrolytic degradation and therefore the degradation rate of PLA depends on a plenty of variables, including molecular weight, chemical composition, crystallinity degree, stereochemistry, morphology (*e.g*. porosity of the matrix), as well as the environmental conditions.[71,87] Table.1 summarizes the effect of some main parameters on the PLA hydrolytic degradation

The control of the mentioned variables and the prior knowledge of the hydrolytic degradation mechanism, including the biodegradation conditions are fundamental for the medical applications of PLLA.[87] Thus, the stages of the PLA hydrolytic degradation can be summarized in: 1) diffusion of water into the material; 2) hydrolysis of chains in the amorphous region due to the lower resistance to water attack; 3) decrease of molecular weight as a result of hydrolytic cleavage of ester bonds and formation of water-soluble compounds; finally 4) hydrolysis of the lamellae of the crystalline phase, which can undergo autocatalytic degradation due to the acidic degradation products and the increasing concentration of carboxylic acid at chain ends.[87,107]

Table 1. Effect of temperature, pH, M_w and crystallinity on the hydrolytic degradation of PLA

Property	Effect on the hydrolytic degradation of PLLA
Temperature	Mathematical deduction of kinetic degradation´s temperature dependence, assuming an Arrhenius-like dependence : $$K_R = K_R(T_{ref})e^{-E_R\left(\frac{1}{T}-\frac{1}{T_{ref}}\right)}$$ where T is the temperature, K_R is the rate constant of hydrolysis from experimental data, T_{ref} is the reference temperature, E_R is the Arrhenius constant, which is about 10,000 K. At T values lower than T_g (T_{ref}) the K_R becomes much slower.[87]
pH	pH influence on the reaction mechanism and on the kinetics of degradation. The hydrolytic degradation can be acid-catalyzed, base-catalyzed, and uncatalyzed.[108,109] pH dependence is also related to the different reactivity of the ester bonds: terminal esters degrade faster than backbone esters according to the preferential chain-end scission mechanism.[87] However, the cleavage of backbone esters results in a faster Mw drop.[110] De Jong S., *et al*. [111] report the degradation kinetics constants collected at 37 °C at different pH values for LA oligomer with an average polymerization degree of 7. They increased the pH from 1 to 10 and observed that initially the rate constant decreases reaching a minimum at pH of about 4, and then increases at higher pH values.
M_w	M_w influence was reported by Sara KS., *et al*.[116] They observed that lower M_w values accelerates the hydrolytic degradation, due to the higher molecular mobility, higher density of hydroxyl groups and hydrophilic terminal carboxyl groups, as well as higher probability of formation of water-soluble oligomers and monomers. Thus, the water diffusion and water content increase, catalyzing the PLLA degradation.
Crystallinity	The crystallinity influence lays in the preference of hydrolytic cleavage of chains in the amorphous regions rather than the crystalline regions of PLA as a result of the restriction imposed by the rigid crystalline regions on the water molecules to access the polymeric chains. Likewise, as the amorphous regions hydrolyzes, the ratio of crystalline regions increases.[113]

1.3.1.3. Commercial application

Currently, the biopolymers can be classified into 3 groups: first, second and third generation related to bioabsorbable (degradable), biodegradable (eco-friendly) and biobased (renewable resource) polymers, respectively. The historical application of PLA material allows its classification in each group.[87] Though the PLLA brittle character, modifications made to PLA since its early application enabled the unlimited options to use PLA materials.[114] As first generation, PLLA was used for fabrication of sutures, prostheses and scaffolds. As second generation, PLLA was developed to replace some plastics for short-life applications. Finally, as third generation polymers, PLLA was for long-term applications such as automobile parts.[87]

As biobased polymer, the PLA and its copolymers are manufacture by pharmaceutical and food companies such as Durect and Purac (now Total Corbion) corporations to supply bioplastics, commercializing products such as Durect LACTEL® Absorbable Polymers and Luminy® PLA. Specifically, because of the PLLA mechanical, thermal and degradable properties, it has been considered an ideal biomaterial for applications, such as orthopedic fixation devices. Medical devices companies such as Depuy Synthes and Arthrex manufacture a variety of PLLA-based orthopedic products including materials for medical interventions of hip, knee and shoulder.

1.3.2. Poly(ethylene oxide)

The PLA hydrolytic degradation can be controlled or tailored by some strategies and approaches such as increasing the hydrophilicity of PLA.[115-117] For instance, generating hydrophilic surfaces by copolymerization or crosslinking; modifying the morphology (e.g. generation of pores); and enabling the hydrolytic attack by blending with a hydrophilic polymer. [118-120] The development of polymeric blends containing PLLA and poly(ethylene oxide)(PEO) (PLLA/PEO) has been widely reported, to study the influence of hydrophilicity of PEO to modify the degradation of PLLA as well as the drug release.[115-117] PEO is a hydrophilic polymer that possesses interesting chemical properties. Some chemical characteristics of PEO, studies of polymeric blends with PLLA will be cited latter herein.

1.3.2.1. PEO chemical properties

The common name of the polymer of ethylene oxide is poly(ethylene oxide) or poly(ethylene glycol)(PEG) and according to IUPAC the name is poly(ethylene oxide).[121] PEO is a crystalline, thermoplastic, hydrophilic and uncharged polyether, characterized for being a water-soluble polymer, with the linear formula H-[-OCH_2CH_2O-]-H. The chemical structure shows the end hydroxyl for low M_w PEO (Fig.10).[126,123] PEO is commercially available in a wide range of molecular weights from ethylene glycol, diethylene glycol to several million or more (Mn 120-136,000).[121-123] According to the M_w the adopted nomenclature is polyethylene glycols for lower M_w, which are relatively viscous fluids to wax-like solids, while higher M_w polymers are named as PEO and are thermoplastics. Both polymeric classes display different properties conferred by the M_w difference since the concentration of end-groups in the low M_w PEGs is higher than PEOs.[126] The thermal properties depend on M_w. For instance, in low M_w PEO (600 g/mol) the T_m is about 20 to 25 °C and for high M_w PEO (50,000 – 160,000 g/mol) the T_m is about 67 °C. Moreover, the T_g has been reported as well, ranging from -50 to -70°C.[121,126,124]

The PEO synthesis was initially explored by Lourenco and Wurtz,[125,126] at almost in the same time. The early synthesis used ethylene oxide, which is a three-membered ring containing an oxygen atom, highly reactive due to large strain energy (Fig.10).[125] The polymerization of ethylene oxide may be classified into anionic using an alkali, cationic using a Lewis acid, and coordinate anionic polymerization.[126] The first high M_w PEO synthesis was reported in 1958 using alkaline earth carbonates.[127] Currently, anionic polymerization using ethylene glycols yield low polydispersity polymers.[121,126]

PEO can crystallize from the melt. Initially, crystal nucleation occurs and afterwards the growth of the nuclei takes place. In the crystalline state, the crystallographic form adopted by PEO is a 7_2 helical conformation (*i.e.*7 units in 2 turns).The crystallographic unit cell contains four molecular chains and is monoclinic with parameters a = 8.16 Å, b = 12.99 Å c (chain axis) = 19.30 Å, and β=126°5'.[126,123]

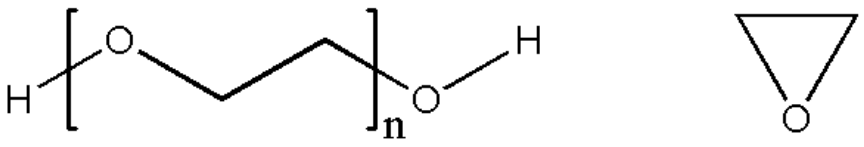

Fig. 10. Structural formula of PEO (left) and structural formula of ethylene oxide (right).

PEO undergoes oxidative attack resulting in the degradation of the polymer, which is accelerated by heavy metal ions, oxidizing agents, strong acids, and ultraviolet light.[122] Besides, this polyether can be enzymatically biodegraded, by PEO-dehydrogenase, PEO-aldehyde-dehydrogenase and PEO-carboxylate-dehydrogenase yielding terminal carbonyl groups followed by the release of C2 units as glyoxylic acid.[121] Also, the polymer degrades by autoxidation forming hydroperoxide species, which decompose and cause polymer chain cleavage.[122]

One of the most interesting properties of PEO is its solubility in water in spite of being soluble in organic solvents such as chloroform. However, PEO is insoluble in aliphatic hydrocarbons and at low room temperature is soluble in aromatic hydrocarbons. In water, PEO has an inverse solubility-temperature relationship, in which, increasing the temperature of aqueous solution (near to the boiling point of water), leads to the polymer precipitation. PEO also exhibits an upper consolute temperature or an upper critical solution temperature, which depends on polymer concentration and molecular weight.[122,127] For instance, for polymeric concentrations lower than 0.2% the observed precipitation is known as a cloud point.[122]

According to Kjellander and Florin,[128] the solubility of PEO in water is conferred by the suitable structural fit between them. They suggested that PEO can be fitted into the tetrahedral water lattice with minimal perturbation of the water structure, where the lattice points are occupied, either by water or by ether oxygen.. Additionally, the inverse solubility-temperature relationship aforementioned can be interpreted as disordering of ‘hydration shells’, which are conformed by highly oriented water molecules that surround the polymer molecule. This hydration shell water is characterized by unfavorable entropy that is overcome by the low enthalpy due to the water and PEO interaction. With increasing temperatures, the hydration shell is disrupted due to thermal motion and entropy contribution overcomes the enthalpy contribution, allowing a better polymer-polymer interaction causing the system phase-separation. [122,123,130]

The hydrophilic character of PEO confers a biological advantage in its application as a biomaterial. It seems that the suitable properties of PEO such as the minimal interfacial free energy with water and good structural fit; high mobility and large excluded volume are related to the decreased protein adhesion, making it protein-resistant. The protein adhesion represents a problem that may lead to further thrombus formation in the material surface. The effectiveness in the protein-resistance of PEO suggests that it could improve the blood-compatibility of

biomaterials. Thus, immobilizing hydrophilic polymers in surfaces, such as PEO could enhance some biomaterial properties.[123] Some strategies are used to accomplish the PEO mobilization surface. For example, the non-covalently attachment in the surface, using of a common solvent that allows the surface of biomaterial to swell and the water soluble polymer molecules entrance into the loosed polymeric network, followed by, the fast collapse of the swollen interface provoked by water, entrapping the hydrophilic polymer within the biopolymer network.[129]

Among the different applications of PEO in materials, the blending with PLLA has been explored to improve some mechanical and thermal properties. These properties are influenced by the polymeric interactions, which are nothing but the miscibility of the system that explains the phase behavior and the morphology of the blend. The understanding of the polymeric interactions can be archived by thermodynamic studies, such as Differential Scanning Calorimetry (DSC).[130] Currently, the miscibility of PLLA/PEO blends with different M_w and concentrations obtained by solvent casting technique or melt-blending are widely studied according to their thermal properties by DSC,.[131] Younes *et al.*[132] studied the miscibility of PLLA/PEO blends comprising high M_w PLLA with high and low M_w PEO. Analyzing the T_m depression, they concluded that the T_m of PEO is more susceptible to the PLLA presence and when one of the components is present at more than 20 wt%, it is able to crystallize.

Other miscibility studies by DSC showed that blends containing up to 50 wt% of high M_w PLLA with high M_w PEO displayed both single T_g and T_m decreased on blending, suggesting miscibility in the amorphous phase.[133] Besides, the hydrolytic degradation rate of blends was also increased compare to pure PLLA. On the other hand, for high M_w PLLA and low M_w PEO blended films, the T_m of PLLA linearly decreased with the increase in the PEO content. In addition with 20 wt% PEO, the alkali hydrolysis rate was accelerated due to the porous structure of the blend. [134] Same trend was observed in other study.[135] Studies of enzymatic hydrolysis were reported as well. The degradation of the blends containing high M_w PLLA and low M_w PEO was accelerated and it was shown that blends with up to 30 wt% and 20 wt% PEG are miscible for amorphous and semicrystalline PLAs. [136,137]

Finally, applications of PLLA/PEO blend comprehend a variety of options as biomaterials, especially for drug delivery purpose. Such studies includes development of nanoparticles,[138] hydrogel structures,[139] nanofibers[140] and 3D-printed scaffolds,[141] highlighting the helpful influence of PEO in both processing and degradation of PLLA in biomaterials.

The purpose of this project was the development of polymeric coatings of PLLA doped with SNAP by spin coating, capable of releasing NO in a sustainable fashion with the aim to enhancing the biocompatibility of medical devices, which could contribute to the studies related to NO release by materials. In addition, as the kinetics of NO release in the exogenous administration by hydrophobic polymeric coatings using PLLA may be governed by the low rate of PLLA degradation, due to its hydrophobicity of PLLA, coatings of PLLA/PEO may to increase the permeation of water into the polymer bulk and accelerate NO release from SNAP, thereby offering a new way of controlling the release of NO from the material.

2. AIMS

2.1. General aim

The main aim of this project was the characterization of NO-releasing coatings prepared by spin coating, comprised of poly(L-lactic acid) (PLLA) containing S-nitroso-*N*-acetyl-D-penicillamine (SNAP) as a NO-donor, capable of delivering NO locally during prolonged periods.

2.2. Specific aims

- To characterize the kinetics of hydrolytic degradation of materials and its impact on the modulation of NO release profiles.
- To characterize the effect of multi coatings on the kinetic profile of NO released from the materials.
- To characterize the effect of blending PLLA with poly(ethylene oxide) (PEO) on the NO-releasing and hydrolytic properties of the materials.

3. EXPERIMENTAL SECTION

3.1. Materials

L-lactic acid 84.5-85.5 %, stannous(II) chloride dehydrate 98 %, m-xylene 99 %, p-toluenesulfonic acid monohydrate 98 %, N-acetyl-D-penicillamine (NAP) 99 %, hydrochloric acid (HCl) 37 %, sodium nitrite ($NaNO_2$) 99 %, vanadium (III) chloride (VCl_3) 97 %, potassium chloride 99 %, PEO M_v 400,000 g mol^{-1} (Sigma-Aldrich Chem. Co, USA), sodium iodide (NaI) 95 %, sodium nitrate ($NaNO_3$) 99 % (Fischer Scientifgic, USA), tetrahydrofuran (THF), chloroform ($CHCl_3$), acetone, EDTA disodium salt dehydrate 99 %, methanol 99.8 %, sodium chloride 99 %, sodium phosphate dibasic anhydrous 99 %, potassium phosphate monobasic anhydrous 99 % (Labsynth, Brazil) and sulfuric acid 98 % (Tedia Company, Inc., USA) were used as received. Ultrapure water (resistivity 18.2 MΩ cm at 25 °C) obtained from a Milli-Q® Direct-Q® 3 UV purification system (MerckMillipore, USA) was used in all procedures. Commercial polypropylene (PP) sheets were used without further treatment.

3.2. Methods

3.2.1. Poly(L-lactic acid) (PLLA) synthesis

PLLA was synthesized by a research group member, based on the procedure described in previous work.[65] Briefly, lactic acid solution (85 wt%) was heated in a reaction flask under reflux and magnetic stirring in the presence of stannous (II) chloride dihydrate as a catalyst, p-toluenesulfonic acid monohydrate as co-catalyst and m-xylene as a solvent. A Dean-Stark trap was used to collect the water/m-xylene azeotropic mixture distilled from the reaction. The reaction was allowed to proceed for 24 h. PLLA was further purified by recrystallization/dissolution in methanol/chloroform. Afterwards, dried in vacuum oven (Büchi, Glass Oven B-585) at 60 ºC and 15 mbar for 24h and post-dried by lyophilization for 24 h.

3.2.2. *S*-nitroso-*N*-acetyl-D-penicillamine (SNAP) synthesis

SNAP was synthesized by a research group member, based on the procedure described in previous work.[65] Briefly, the S-nitrosation of NAP was carry out with a molar ratio 1:2 (NAP:$NaNO_2$) in an acidified methanol solution with molar ratio 1:2 (HCL:H_2SO_4) for 30 min. Subsequently, the solution was stirred in an ice bath for SNAP precipitation. Crystals were collected by vacuum filtration, washed with cold water and dried by lyophilization for 24 h.

3.2.3. Coating model surfaces by spin coating

PP sheets (*ca.* 4 cm^2) (Fig.11) used as model surface were cleaned ultrasonically twice using ethanol, isopropyl alcohol and deionized water during 5 min and dried at room temperature. The choice of PP as a model surface was based on its previous applications in clinical interventions as implantable material.[142] In order to obtain a homogeneous thin film a spin-coater (Laurell Technologies Corporation, WS-650MZ-23NPP) was used to coat the PP surface. Different concentrations of polymeric solutions were used, 5, 10, 20 and 40 g L^{-1} of PLLA. The spin coater program used comprehended basically 3 programming steps; 1) solution deposition, 2) spin up and 3) spin-off. Two variables in each step, target speed and the corresponding time were fixed. Table 2 shows the different spin coating used for each step in the coating process.

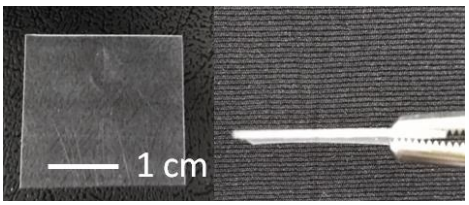

Fig. 11. Cleaned polypropylene sheets used as a model surface for spin coating.

In the first step, solution deposition, at which the polymeric solutions is poured on the substrate, two speeds were tested, 100 and 300 rpm. The 300 rpm rotating speed allowed a uniform deposition of the polymeric solution; there was a good pre-spread of the solution without drop formation. The 100 rpm seemed to be too slow and led to the formation of a drop, resulting in a heterogeneous coating.

In the second step, spin-up, 4 speeds were tested: 500, 1,000, 1,500 and 2,000 rpm. The lowest speed led to heterogeneous coatings with spots and solids in the 4 concentrations. Similar results were obtained with 1,000 rpm except for the 40 g L^{-1} concentration. The 500 and 1,000 rpm speeds showed to insufficient to spread the polymer solution uniformly before solvent evaporates. The 1,500 rpm speed gave better results than 500 and 1000 rpm speeds in terms of uniform spreading; although opaque films were obtained. Finally, the best speed was 2,000 rpm, which led to homogeneously spread films all the concentration used.

Table 2. Spin coater conditions used to coat model PP surfaces with PLLA solution.

Step	Time/s	Rotating speed/rpm
1	3	100
		300
2	60	500
		1,000
		1,500
		2,000
3	30	500

In the third step, the speed was decreases until 500 rpm during 30 s for allowing solvent evaporation in the coating already formed. It is important to note that in addition to finding the optimal programming steps, the final result obtained in the coatings depends also on standardizing the manual addition of the polymeric solution whose 100 µL must be added at the same rate during 3 s. The above mentioned steps are represented in the speed profiles shown in Fig.12a, for the addition of 100 µL of polymeric solution in THF.

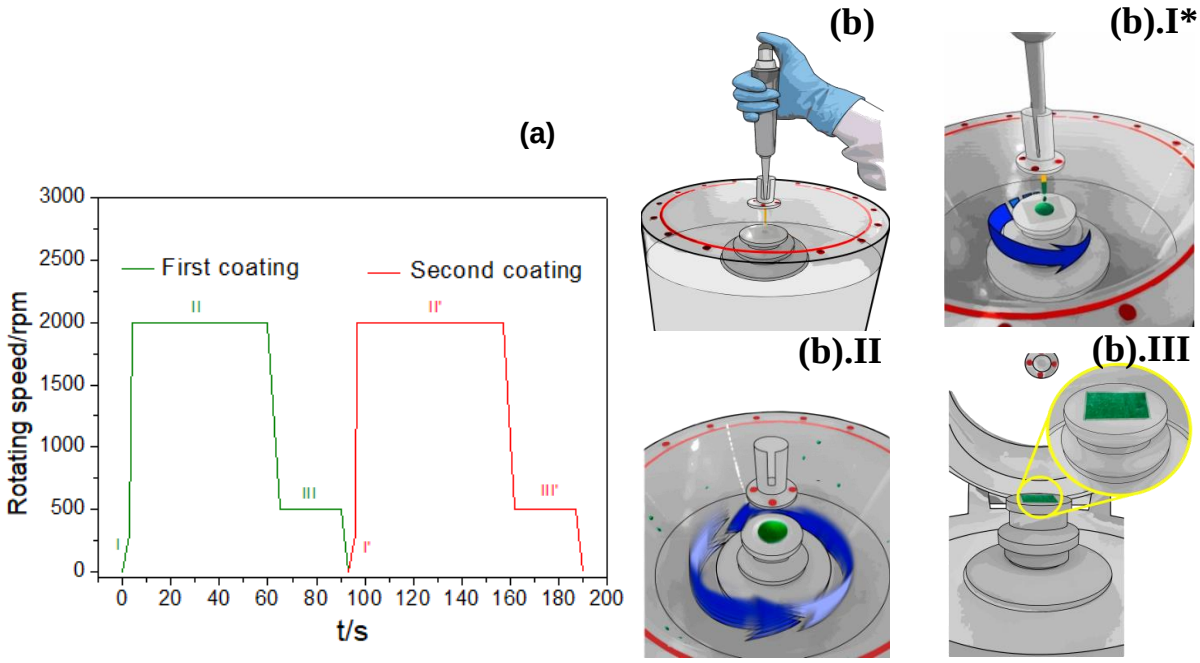

Fig. 12(a) Spin coating speed profile used for coating of PP substrates with PLLA-SNAP solutions in THF, **(b)** schematic procedure related to each step: **(I)** solution deposition, **(II)** spin up, **(III)** spin off and coated film.
*The green color is just for schematic illustration purpose.

In the case of blend-coated films of PLLA/PEO, 60 g $^{L-1}$ of polymeric solution was prepared with mass ratio 70:30 (PLLA:PEO). The blended solutions were doped with SNAP 10 wt% relative to the mass of the solid polymer, by previously dissolving SNAP in an appropriate amount of THF. Afterwards, the SNAP-doped solution was deposited on PP substrates by spin coating as described above (Fig.12b).

Fig.12b schematically shows the main steps in the coating process: solution deposition (I), spin-up (II) and spin-off (III) respectively. In some cases, a second deposition on the same surface was realized. No drying time was used between depositions. Afterwards, the coated model surfaces were dried in a vacuum oven (40 °C, 30 mbar) during 3 h, protected from light, and then stored at room temperature also protected from light.

3.2.4. PLLA/PEO blend film preparation

In order to study the polymeric interactions, the miscibility of the PLLA/PEO blend was characterized based on the thermal characterization by Differential Scanning Calorimetry (DSC). PLLA/PEO 70:30 (wt/wt) blends were previously obtained by solvent casting (Fig.13). The PLLA/PEO solution (60 g L^{-1}) in $CHCl_3$ was prepared using a vortex spinning machine (Daigger, Vortex Genie® 2). 2.5 mL of blended polymeric solution was poured on a Teflon® plate (diameter 3 cm) and solvent evaporation was conducted at room temperature for *ca.* 24 h. Afterwards, to complete solvent removal the sample was dried in a vacuum oven (40 °C, 30 mbar) for 3 h.

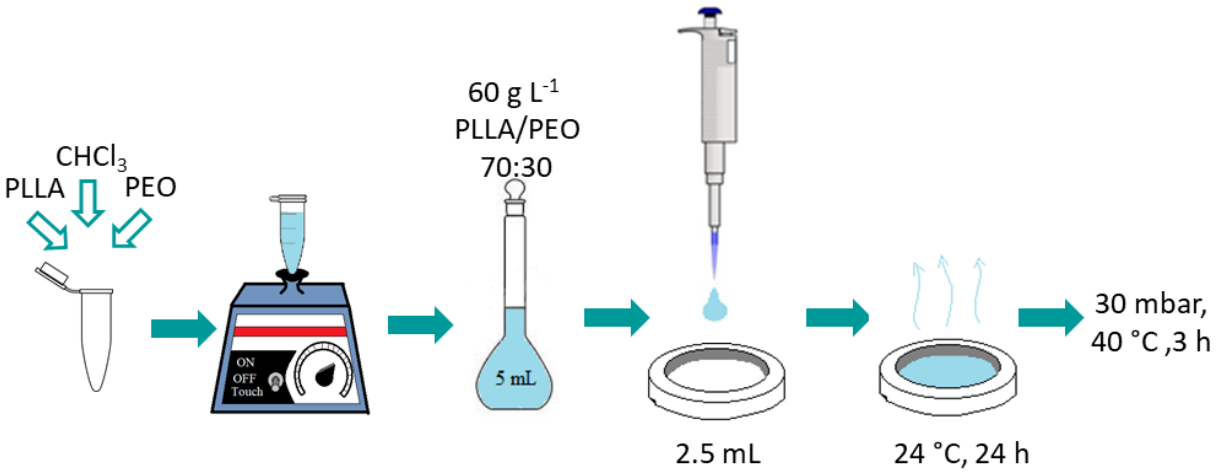

Fig. 13. Schematic ilutration of the procedure used to obtain blended PLLA/PEO films by solvent casting.

3.2.5. Physical chemical characterizations

3.2.5.1. Attenuated Total Reflectance-Fourier Transform Infrared Spectroscopy (ATR-FTIR)

Infrared spectra were obtained in Attenuated Total Reflectance (ATR) mode in a FTIR Cary 630 spectrometer (Agilent, Santa Clara CA) fitted with a diamond crystal type II ATR accessory (penetration 2 mm, active sampling diameter 200 mm) in the range of 4000 – 400 cm^{-1}. The coatings were pressed directly against the crystal for analyses.

3.2.5.2. X-Ray Diffraction (XRD)

An X-ray diffractometer (Shimadzu, XRD7000), operating at 40 kV with Cu Ka radiation (λ=0.154 nm), was used to obtain diffractograms in the 5 – 50º 2θ range. Pure solid PLLA and SNAP were analyzed as well as the PLLA-SNAP coatings.

3.2.5.3. Gel Permeation Chromatography (GPC)

PLLA molecular weight distribution was determined by GPC using a Viscotek chromatograph (Model GPCmax VE 2001), equipped with a refractometric detector (Viscotek Model VE 3580) and three columns Shodex KF-806M (300 mm x 8 mm, 10 µm) connected in series using polystyrene standards. Experiments were performed at 40 ºC. Filtered and degassed THF (HPLC grade) was used to prepare the PLLA solution in a 7.5 mg mL^{-1} concentration. 100 µL of polymeric solution (filtered with a PTFE membrane with a pore size of 0.45 µm) was injected with a 1 mL min^{-1} eluent flow rate. The calibration curve was plotted by OmniSEC (Vicotek) software from the peak molecular weight (Mp) of polystyrene standards (Viscotek) (1,080-1,900,000 g mol^{-1}).

3.2.5.4. Thermal properties

Differential Scanning Calorimetry (DSC) was carried out to determine the glass transition temperature of pure solid PLLA in the range of -10 °C to 220 °C at a 10 °C min^{-1} heating rate; as well as pure solid PEO and PLLA/PEO blend obtained in the range of -90 °C to 220 °C at a 20 °C min^{-1} heating rate. DSC curves were normalized with respect to sample mass (*ca* 5 - 10 mg). The thermograms were

obtained in a calorimeter TA Q-100 (New Castle, DE) and recorded using the software of TA Instruments Universal Analysis 2000.

3.2.5.5. Contact angle measurements

Contact angles between the air/water interfaces were measured with an optical tensiometer (Theta Attension, KSV Intruments), at 17 °C, using Milli-Q water drops. The images of the water drops on the coated substrate were recorded with a digital camera and were analyzed using the software provided by the manufacturer. Right and left angles obtained were used to calculate the average angles, expressed herein as mean ± SD.

3.2.5.6. Scanning electron microscopy / Energy Dispersive Spectroscopy

The morphology of the samples was investigated in a Quanta FEG 250 (FEI) scanning electron microscope (SEM) equipped with an energy dispersive X-ray spectrometer (EDS, Oxford). Films were mounted on aluminum stubs with a double-side carbon tape, sputter coated in a high-vacuum gold-palladium (80/20) sputter-coating unit (Balt-Tec, MCS 010) for SEM investigation, while samples used for EDS were coated with evaporated carbon.

3.2.5.7. NO release measurements

NO released was measured by chemiluminescence, using a NO analyzer (NOA^{TM}, Sievers 280i), operated with an O_2 pressure of 6.0 psig and N_2 pressure 0.4 psig above the equilibrium pressure (*ca.* 7.2 Torr). The NO detection is based on a gas-phase chemiluminescent reaction between ozone (generated by an electrostatic ozone generator and high voltage transformer, *ca.* 2 v/v% from oxygen) and the NO released, according to Eq.12. Afterwards, the excited $NO_2^{\bullet}$ specie releases energy (Eq.13), which is quantified by the NOA´s detector.

$$NO + O_3 \rightarrow NO_2^{\bullet} + O_2 \quad (12)$$

$$NO_2^{\bullet} \rightarrow NO_2 + h\nu \quad (13)$$

The NOA was calibrated according to the manual for measurements of NO and nitrate/nitrite (Fig.S-1). All NO release measurements were conducted in triplicate. Data reported herein are all expressed as mean ± SD. Comparison of means using student's *t*-test was used to analyze the statistical differences between different sets of samples. For these calculations GraphPad QuickCalcs statistical calculator was used. Values were considered statistically significant for all tests considering the $p < 0.001$ (one asterisk) and $p < 0.02$ (two asterisks).

3.2.5.7.1. NO release profile and kinetics

The real time NO release under physiological conditions was obtained by chemiluminescence. Briefly, samples (*ca*. 2 - 3 cm^2) were placed into an inert sample holder (polyethylene mesh) kept pending by a stainless steel wire and submerged into a phosphate-buffered saline solution (PBS) (100 µM EDTA, pH 7.44) contained in the sample vessel at 37 °C in dark (Fig.14a). The NO released was carried to the chemiluminescence detection chamber by N_2. Finally, the NO released per squared area was calculated assuming a flat surface on a single side of the sample.

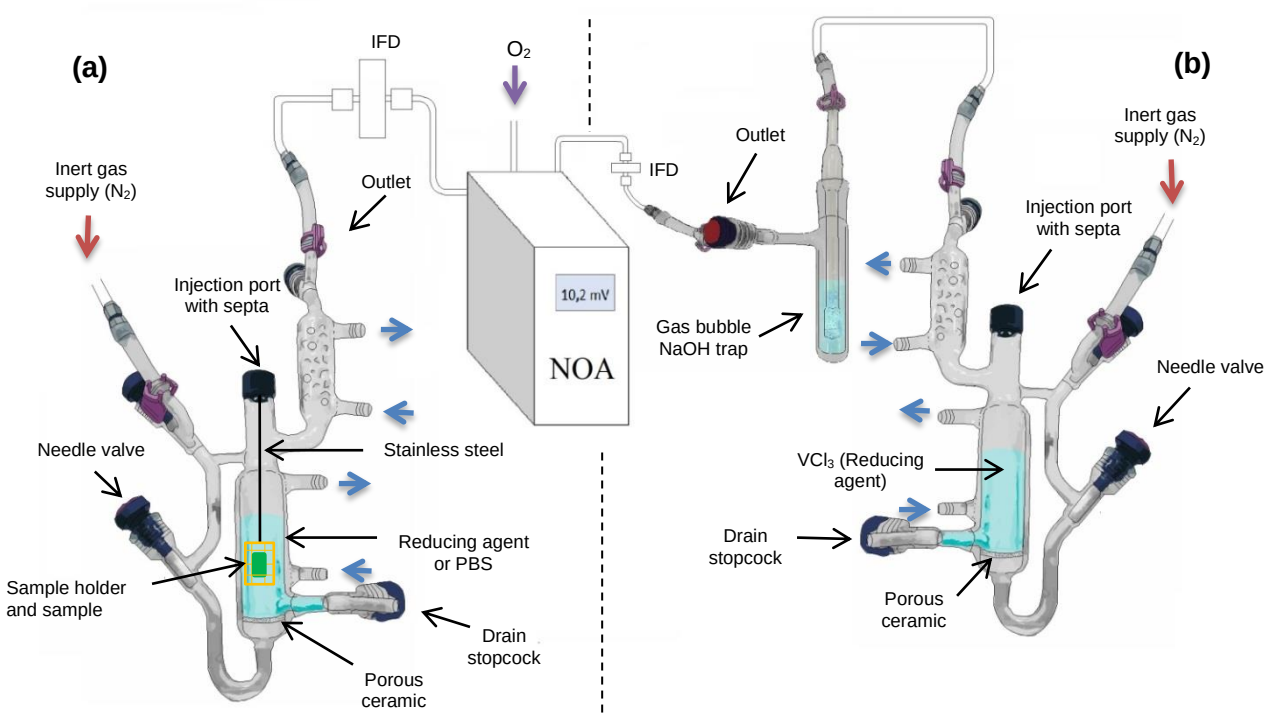

Fig. 14 Schematic illustration for NO detection using a Nitric Oxide Analyzer **(a)** setup for short-term kinetic NO release and quantification measurements. The sample was placed into an inert sample holder pending from a stainless steel wire. **(b)** setup for quantification of long -term NO release.

3.2.5.7.2. Quantification of short-term NO release

The quantification of SNAP superficial of the coatings under accelerated conditions was obtained by chemiluminescence. The SNAP quantification is reflected by a short-term NO release, obtained by SNAP reduction by an alkaline ascorbate medium (160 mM, pH 11), in which the SNAP´s SNO groups are selectively reduced to free NO and its parent thiolates.[143] These experiments were also performed in the NOA using the setup shown in Fig.14a and similar precautions described above. Impregnated SNAP was decomposed simultaneously through both ascorbate reduction pathway and the photoinitiated decomposition pathway using a LED fiber optic illuminator (LMI-6000, Fiber-Lite®) with a visible light source.

3.2.5.7.3. Quantification of long-term NO release, *in vitro* hydrolysis

The NO release under physiological conditions for prolonged periods was obtained by chemiluminescence. This indirect NO quantification was based on the reduction of nitrite and nitrate species, using the vanadium (III) chloride method, according to the NOA manufacturer's specifications. VCl_3 in hydrochloric acid was used to reduce nitrite and nitrate species to NO, in order to quantify the cumulative NO release (Eq.14). Nitrite and nitrate species were produced by the NO oxidation during the incubation period (Eq.4). The samples were immersed in PBS at 37 ºC protected from light. Aliquots of 50 µL were taken for the determination of long-term NO release. After aliquot extraction the samples were placed in fresh PBS. The analysis was performed at 85 °C, containing a saturated VCl_3 solution in HCl. The gas flow was previously washed in a washing flask containing NaOH solution to prevent HCl to reach the detector (Fig.14b). The calibration curve was performed using nitrate standard solutions. (Fig.S-2).

$$3V^{+3} + 2NO_3^- + H_2O \rightarrow 2NO + 3VO_2^+ + 4H^+ \quad (14)$$

4. RESULTS AND DISCUSSION

4.1. PLLA-SNAP coatings preparation and characterization

PLLA was obtained as a white fine powder, soluble in THF and chloroform, with weight average molecular weight (M_w) of 3,582 g mol^{-1}. Molecular weight and distribution obtained by GPC is shown in Fig.15. The chromatogram indicates the presence of two distinct populations, in which the higher M_w is in a lower concentration (represented by a shoulder in approximately 31 mL). As a result, the low molecular weight PLLA, so-called a PLLA oligomer, showed dispersity (Đ) equal to 1.292. This is characteristic of a step-growth polymerization reaction. The number average polymerization degree DP_n (Eq.15) given by the quotient between the M_n (2,771 g mol^{-1}) and the repeat unit (lactic acid) average molecular weight (M_0 = 72.06 g mol^{-1}), corresponds to an average value of 38 repeat units per polymeric chain.

$$DP_n = \frac{\bar{M}_n}{\bar{M}_0} \tag{15}$$

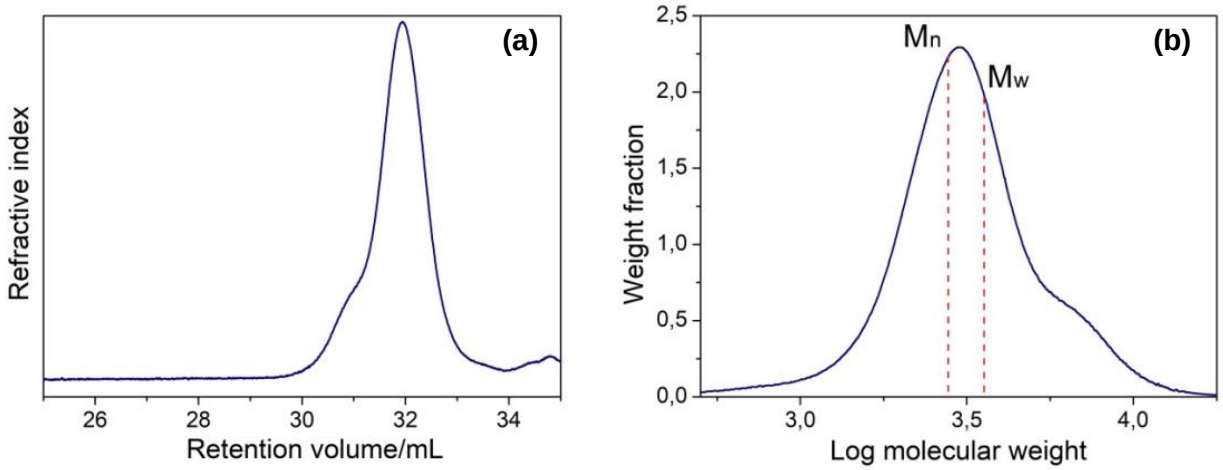

Fig. 15. GPC chromatogram of PLLA **(a)** and its corresponding molecular weight distribution **(b)**. Number average molecular weight (M_n) and weight average molecular weight (M_w) are indicated by the red dashed lines.

The pure solid PLLA thermogram is shown in Fig.16. Three thermal events can be observed; the glass transition temperature (T_g), the crystallization temperature (T_c) and the melting temperature (T_m). The T_g at 39.5 ºC can be observed in the magnification of the inset corresponding to the temperature at which the polymer undergoes phase transition from a glassy state into a rubbery.

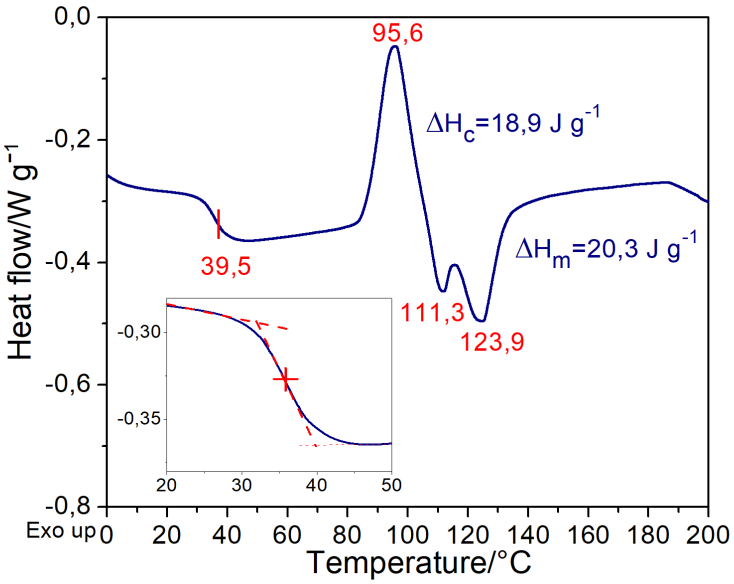

Fig. 16. Thermogram of PLLA by DSC (second heating after erasing the thermal history) showing the thermal events. From the left to the right; the glass transition temperature, the crystallization temperature and the melting temperature (bimodal event). Additionally, the crystallization and melting enthalpies values are shown. The inset figure shows a magnification of the T_g region.

The T_g value allows estimating M_n can be through the empirical Flory-Fox equation (Eq. 16).[144]

$$T_g = T_g^{\infty} - \frac{k}{M_n} \qquad (16)$$

where T_g^{∞} is the limiting value of the glass transition temperature at very high M_n and k is a constant of a given polymer, which represents the excess free volume, associated with the dependence of the T_g with the molecular weight.

This approximation implies considering that the lower the molecular weight the higher the chain ends contribution to the overall polymer free volume.[145] In this case, the M_n calculated was 2,477.5 g mol^{-1} for T_g = 39.5 ºC, T_g^{∞} = 58 ºC and k = 5.50 x 10^4, values extracted from the literature for PLLA.[146] The empirical M_n obtained was found to have about the same order of magnitude as the M_n obtained by GPC.

After T_g event, an exothermic T_c is observed at 95.6 ºC, due to PLLA cold crystallization and finally, two endothermic peaks at 111.3 and 123.9 ºC, T_m, due to the melting of the crystalline phase are observed. The occurrence of two distinct endothermic peaks (bimodal event) is caused by the recrystallization and change in PLLA crystal structure during heating:[147] The α´ crystal is obtained at T_c below 120 ºC as a disordered crystal with hexagonal packing, that upon heating, gain mobility and is transformed into and ordered α form.[148] These endothermic peaks are not observed in the thermal history (Fig.S-3), which only depicts multiple melting peaks during heating, due to the PLLA polymorphism, whereas during cooling no crystallization peaks are observed, since the crystallization kinetics from the melt is slow and cannot be detected. Furthermore, the enthalpies of crystallization (ΔH_c) and melting (ΔH_m) calculated by the quotient between the peak area and the heat rate, are very similar (19.9 J g^{-1} and 20.3 J g^{-1}, respectively), as expected.

Solid pure SNAP was characterized by ATR-IR as shown in Fig.17a. The main peaks related to the ν(N-H) and ν(N=O) stretching vibrations are shown by the black arrows. A sharp peak at 3337 cm^{-1} is assigned to the N-H bond stretching vibration of secondary amines (Fig.17b).[149] A second weaker band at 1930 cm^{-1} and the intense peak around 1493 cm^{-1} can be assigned to stretching vibrations of the N=O.[39] These results confirm SNAP synthesis.

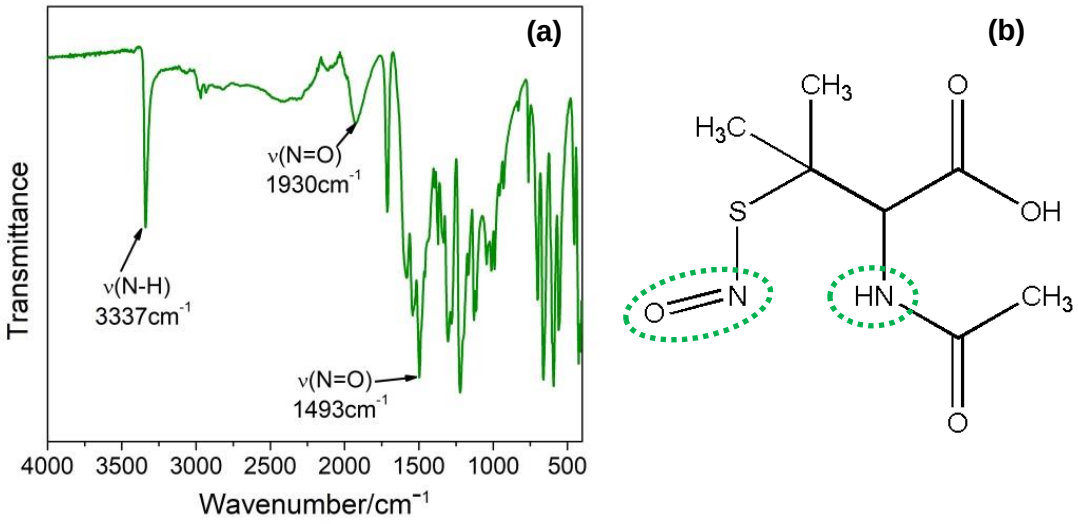

Fig. 17(a) Vibrational spectra of powdered SNAP. Main peaks, ν(N-H) and ν(N=O) stretching shown by the black arrows. **(b)** SNAP chemical structure highlighting the amine group and NO groups responsible for the peaks highlighted in (a).

Fig.18 shows a schematic illustration of the coating conformation and the different PLLA-SNAP coated films obtained. Fig.18a shows a schematic illustration of

a monolayer sample where the orange coils represent the PLLA matrix, the green solids represent the SNAP molecules dissolved in the polymeric matrix and the smooth base represents the PP substrate. Fig.18b and c depicts the schematic illustration of a bilayer samples, PLLA-doped second deposition and pure PLLA second deposition, respectively.

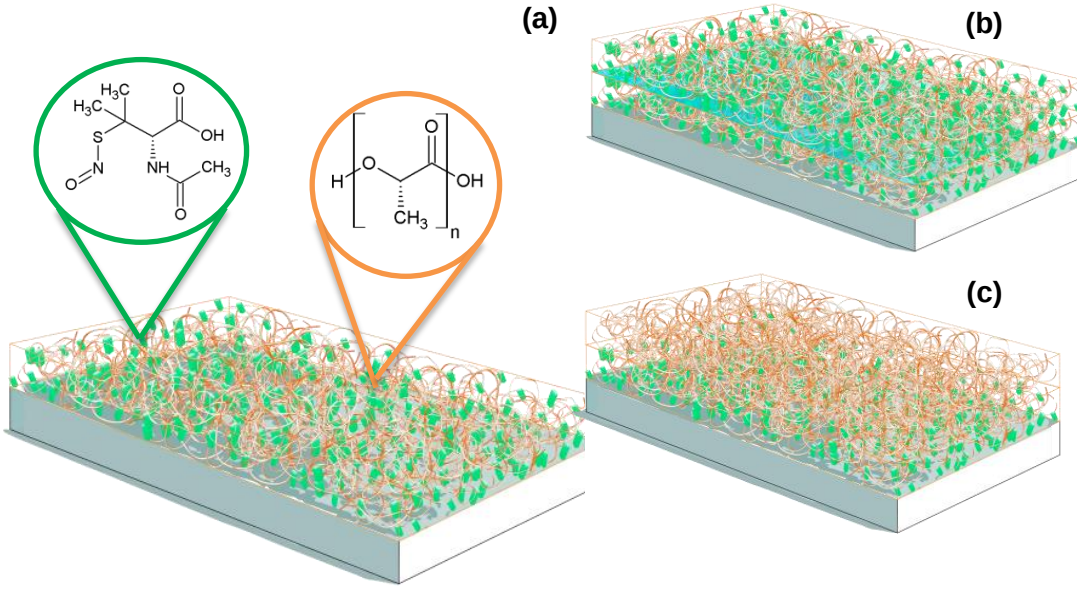

Fig. 18. Schematic illustration of PLLA-SNAP coated films **(a)** PLLA-SNAP showing the composition of the coating. Green circle represent SNAP molecules and orange coils represents PLLA chains **(b)** Scheme of PLLA-SNAP/ PLLA-SNAP. **(c)** Scheme of PLLA/ PLLA-SNAP.

Table.3 describes the different coatings obtained; along with the names of the coating, the SNAP concentration and the number of coatings onto the same PP substrate.

The ATR-IR spectra of PLLA coat and SNAP-doped PLLA coatings are shown in Fig.19. The main characteristic peaks of PLLA, ν(C=O), $\nu(CH_3)$ and ν(C-O-C) stretching confirm the complete coating of the PP substrate as shown Fig.19a, blue spectrum. Table.4 shows the corresponding band assignments. Fig.19a shows the spectrum SNAP (in green), including the weak band at 3347 cm^{-1}, assigned to the N-H bond stretching. Fig.19b shows a magnification of the spectrum in (a), showing the band at 1505 cm^{-1}, assigned to the N=O bond stretching vibration. These results confirm that SNAP is effectively embedded into the PLLA matrix.

Table 3. Samples obtained by spin coating showing the concentration of SNAP relative to the solid polymer (50 g L^{-1}) or to the solid polymeric blend 70:30 (60 g L^{-1}) and the number of layers.

Name	SNAP wt%	Coating
PLLA-SNAP 10	10	Monolayer
PLLA-SNAP 20	20	Monolayer
PLLA-SNAP/PLLA-SNAP 10	10	Bilayer
PLLA-SNAP/PLLA-SNAP 20	20	Bilayer
PLLA coat	0	Monolayer
PLLA/PLLA-SNAP 10	10	Bilayer
PLLA/PLLA-SNAP 20	20	Bilayer
PLLA/PEO-SNAP 10	10	Monolayer

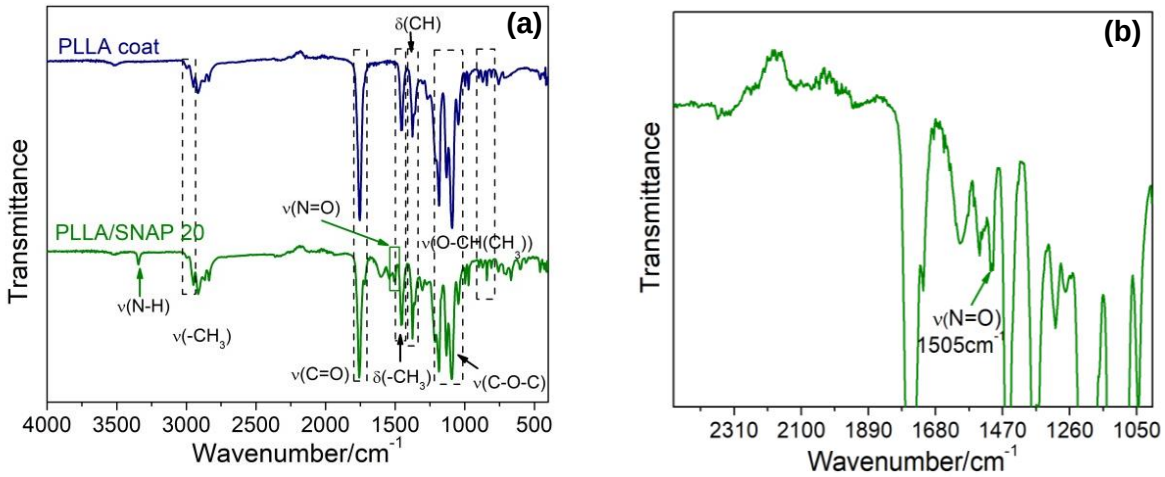

Fig. 19. Vibrational spectra of PLLA coat and PLLA-SNAP 20 **(a)** dashed rectangles show the main PLLA peaks and the green arrows indicate main SNAP peaks.**(b)** Scaling up the spectra region showing the stretching vibration of N=O in 1505 cm^{-1}.

In order to further characterize the coating crystallinity, X-ray diffractometry was performed. Fig.20a shows the X-ray diffractograms of pure solid PLLA, solid SNAP and the bare PP substrate. The PP diffractogram shows characteristic peaks at 2θ of 14.2; 17.1; 18.8; 21.3 and 22.0º, which correspond to α crystalline form of PP.[150] The XRD patterns of powdered PLLA at 2θ of 12.5; 14.8; 16.8; 19.1 and 22.4º exhibited the typical characteristic peaks of PLLA which correspond to the *β*-form, an orthorhombic unit cell or the *α*-form, a pseudo-orthorhombic unit cell. The last is the

most stable crystal phases among the different types of PLLA crystal modifications.[151,152] The diffractogram of the powdered SNAP, corresponds to the orthorhombic SNAP crystal structure already reported by Yaqi Wo., *et al.*[68] The diffractograms in Fig.20b**,** shows the diffractograms of monolayer of PLLA-SNAP 10 and PLLA onto PP, were only peaks of PP can be seen. The absence of PLLA and SNAP peaks in these samples can be attributed to the reduced thickness of the coatings, whose X-ray signals are insufficient to overcome the strong PP signals.

Table 4. Wavenumber and assignments for the main characteristic vibrational bands of PLLA.[153]

Absorption band position (wavenumber/ cm^{-1})	**Vibrational mode***
2995	ν_{as} (CH_3)
2945	ν_s CH_3)
1750	ν (C=O)
1457	δ_{ab} (CH_3)
1386	δ_s (CH)
1186,1083 and 1045	ν (C-O-C)
869	ν (O-CH(CH_3)-)

*ν: stretching, ν_{as}: antisymmetric stretching, ν_s: symmetric stretching, δ_{ab}: antisymmetric bending, δ_s: antisymmetric bending.

SEM images allowed evaluating the surface morphology of PLLA and PLLA-SNAP coated films (Fig.21). It can be seen in Fig.21a and b that all PLLA coating surface displays cavities with polydisperse diameters in the range of 1 to 2 µm. The high rate of solvent evaporation in the spin coating process is probably the origin of these cavities. The interaction time between the solvent and the polymer will define the morphology according to Neumann *et al*:[154] If the interactions are weak the rate of solvent evaporation is high resulting in a heterogeneous surface, whereas strong interaction between the polymer and solvent will decrease the rate of solvent evaporation, allowing the formation of a more homogeneous surface.

In comparison, the PLLA-SNAP 10 micrographs (Fig.21c and d) show a different morphology: no cavities can be observed on the surface and the coating is homogeneously distributed due to the colligative effect exerted by the SNAP in the polymeric matrix. SEM micrographs of the PP substrate showed a smooth surface with the absence any relevant morphological feature (Fig.S-4).

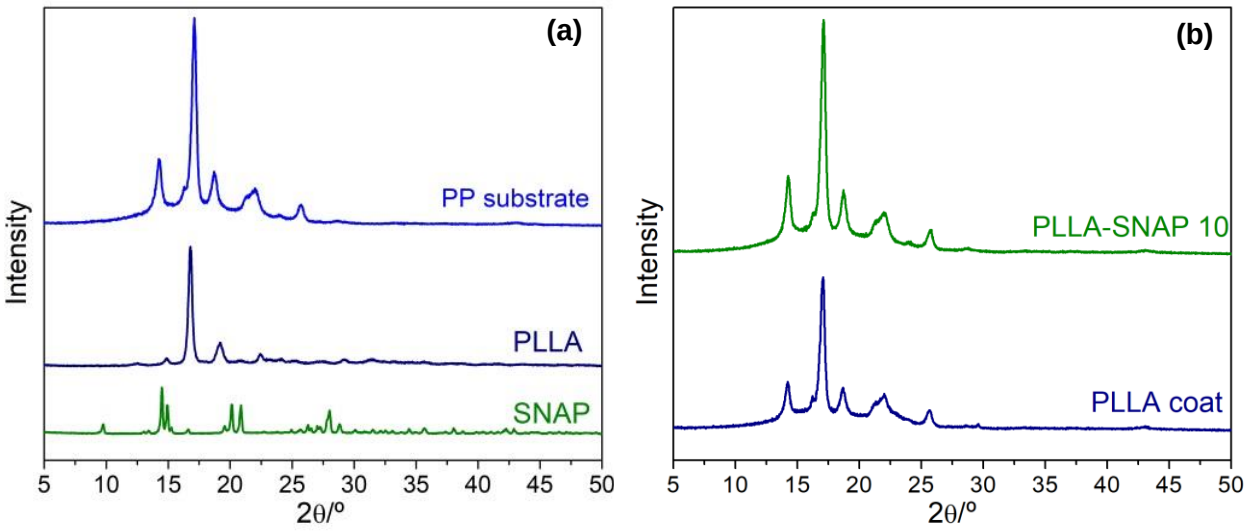

Fig. 20. X-ray diffractograms of pure samples PLLA, SNAP and PP substrate **(a)** and monolayers of PLLA and PLLA-SNAP coating **(b)**.

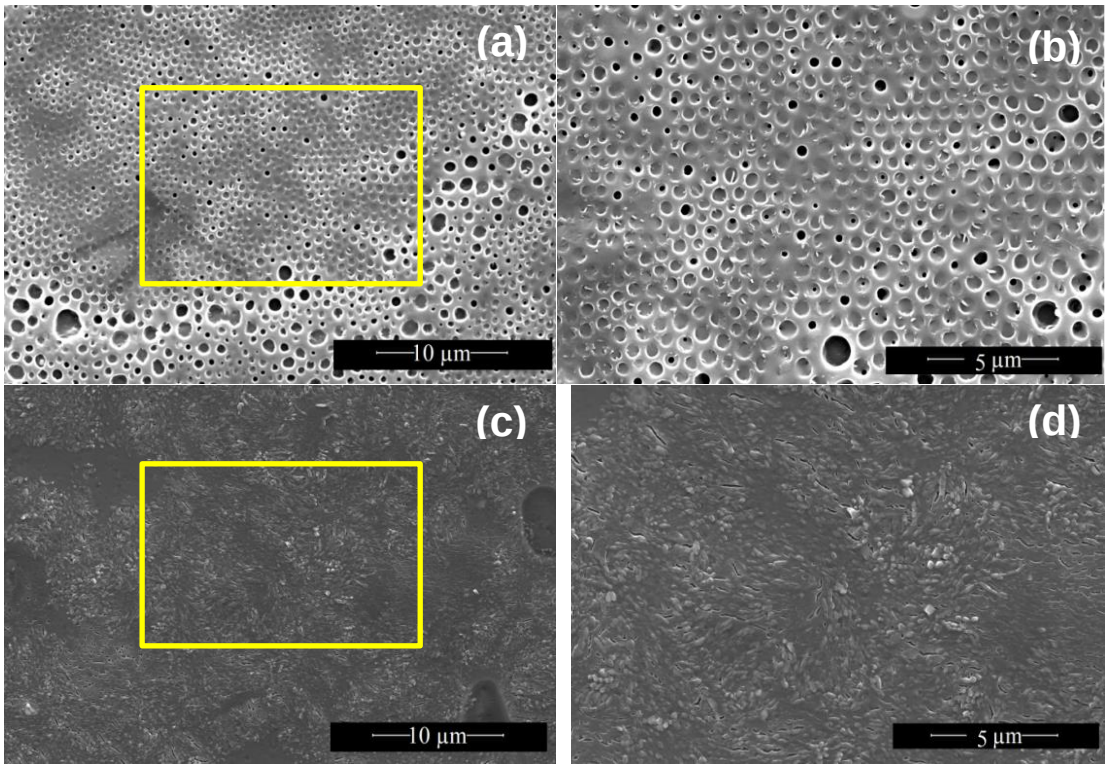

Fig. 21. SEM micrographs of monolayer coatings of PLLA coat **(a)** with magnification of the yellow square of (a) **(b).** PLLA-SNAP 10 **(c)** with magnification of the yellow square of (c) **(d)**.

In order to obtain a cross section image of PLLA coat sample, the Cryo-Ultramicrotome (Reichert ultracut, FC6) was used to slice the coated PP substrate. A representative cross section micrograph is shown in Fig.22. The thickness of single monolayer was found to be *ca.* 10 µm approximately.

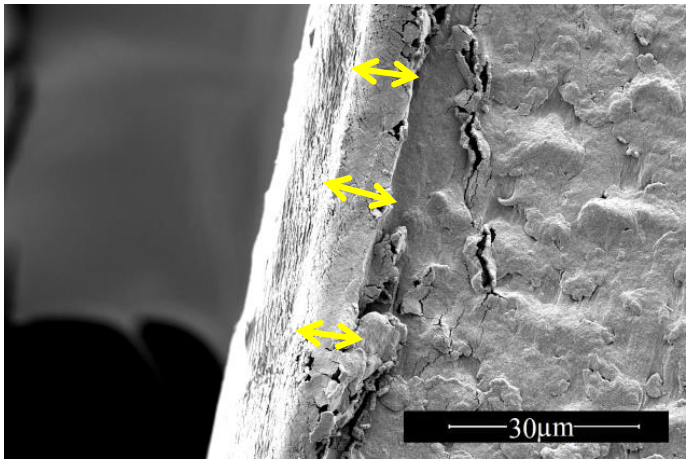

Fig. 22. SEM cross section micrograph of a monolayer of PLLA coating. Yellow arrows indicate the coating thickness.

Micrographs of bilayer of PLLA-SNAP 10 also showed absence of cavities (Fig.23) and are similar to the morphology of the monolayer shown in Fig.21c and d. The small section of the second layer that can be seen in the bottom left of Fig.23, shows that there is an interface between the two coatings. This feature shows that during the deposition of the second coating there is not time enough for the solvent present in the second coating to dissolve the PLLA of the first coating, before is evaporates.

The micrograph shown in Fig.24 displays a second deposition of pure PLLA layer above the first PLLA-SNAP layer. Pores (or cavities) appear in smaller amount and lager size. This morphology could be the result of the decreased solvent evaporation rate, due to a possible interaction with the first layer. The inner parts of the cavities resemble the morphology of PLLA-SNAP monolayer sample

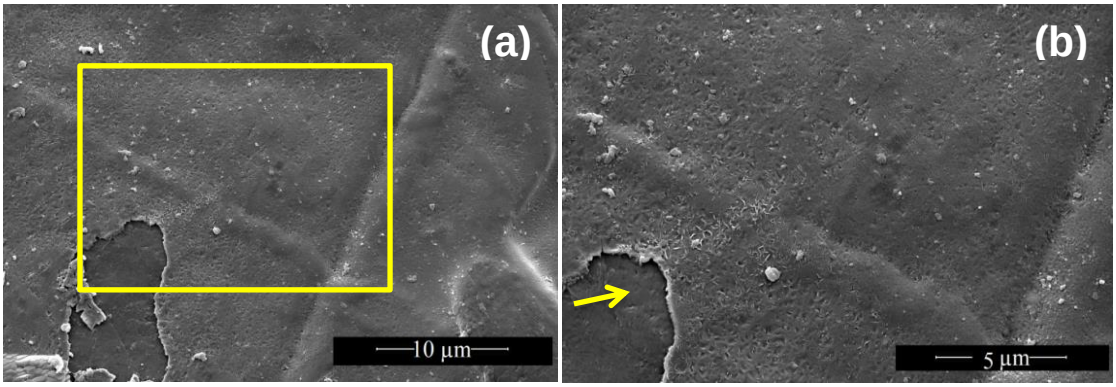

Fig. 23 SEM micrographs of a bilayer coating of PLLA-SNAP 10 **(a)** and with magnification of the yellow square **(b)**. The yellow arrow shows the first layer.

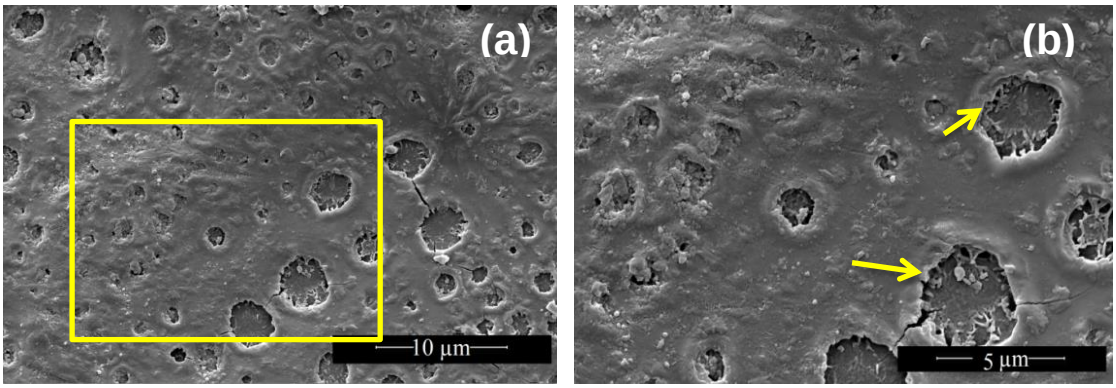

Fig. 24. SEM micrographs of bilayer coatings of PLLA/PLLA-SNAP 10 **(a)** with magnification of the yellow square **(d).** The yellow arrows show two pores in the second PLLA layer.

4.2. Blend coatings preparations and characterization

The viscous PLLA/PEO solution was poured on a Teflon® plate to obtain the blend by solvent casting as aforementioned. A white translucent film was obtained and used for the thermal characterization. Fig.25 and Fig.26 show the thermograms of pure solid PEO and of a PLLA/PEO 70:30 blend, respectively. Table.5 summarizes the thermal event values for pure PLLA, PEO and for the PLLA/PEO 70:30 blend. The PEO T_g could not be observed in the first heating (Fig.S-5a). Possibly, this is due to its high crystallinity degree, which decreases the amorphous phase volumetric fraction, impairing T_g visualization. A large sharp endothermic peak, which is related to the melting process, with T_m is seen at 74.6 °C. In the cooling run, PEO crystallization is revealed by an intense exothermic peak, which is observed at 39.2 °C (Fig.S-5b). In the second heating (Fig.25), the T_g is located at -50.1 °C, in agreement with the literature.[115,116] In the second heating, the melting enthalpy is smaller than in the first heating, due to the distinct thermal history and lack of an annealing time, which leads to incomplete crystallization.

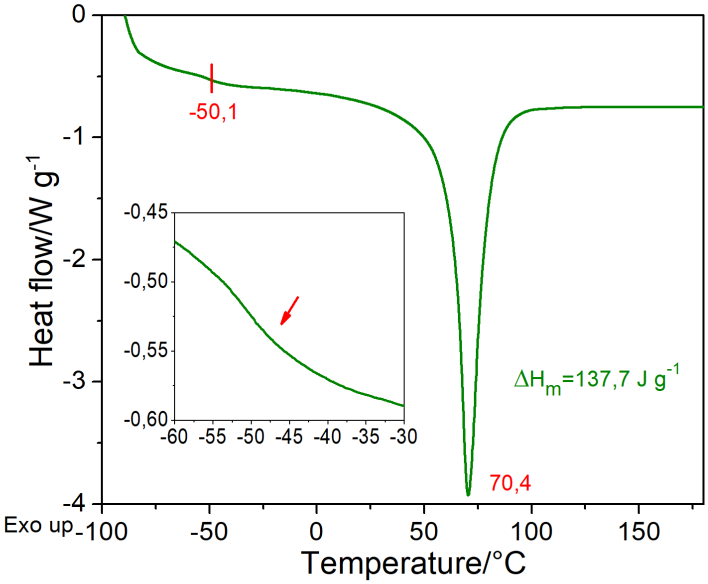

Fig. 25. Thermogram obtained by DSC (second heating after erasing the thermal history of the sample) of PEO. The inset shows the magnification of the T_g region. From the left to the right; the glass transition temperature and the melting temperature with the melting enthalpy value are indicated.

The PLLA/PEO miscibility is related to the formation of a homogeneous system at a molecular level. It is found that most blends are immiscible due to the poor entropy contribution in polymer mixtures associated with the enthalpy of mixing

being positive or near to zero.[115] Consequently, the free energy of mixing becomes positive, originating two crystalline phases. In contrast, in semi-miscible blends, intermediate dispersion or phase separation with a diffuse interface, due to the interpenetration of the different polymeric chains, may be observed. Miscibility can be evaluated by the T_g method, in which the blend is classified as miscible if it shows a single T_g and immiscible if the presence of distinct glass transitions is verified.[115] Fig.S-6 and Fig.26 show the first and second heating of PLLA/PEO blend, respectively. The T_g of the blend cannot be seen due to its overlap with PEO melting peak as well as the PLLA T_g. On the other hand, Fig.26 displays what seems to be the T_g for both polymers, -29.8 ºC for PEO and -20.5 ºC for PLLA. For this reason, the T_g cannot be used as a guide to determine the PLLA-SNAP miscibility in the present case.

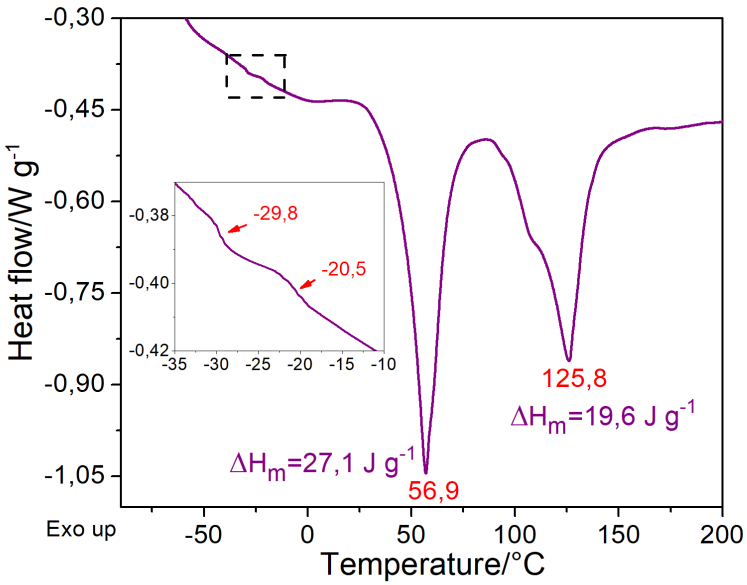

Fig. 26 Thermogram obtained by DSC (second heating after erasing the thermal history of the sample) of the PLLA/PEO 70:30 blend. The inset shows the magnification of the T_g region. From the left to the right; the glass transition temperature and the melting temperatures with the melting enthalpies values are indicated

The melting temperature depression is another method that has been used for characterizing blends containing crystalline polymers. Depending on the composition the melting peaks are expected to display a shift indicating a miscible blend, whereas a constant T_m indicates an immiscible system. Each of the crystallizable polymer of the mixture should display the T_m of the corresponding pure

polymer.[115,155] It can be seen in Fig.26 that in the PLLA/PEO 70:30 blend the endothermic peak underwent a great reduction in the crystallization (table 5). In addition, the melting peak was also shifted to a significant lower temperature (56,9 ºC). The decreased T_m found for PEO is an indication of thinner crystalline lamellae which might be the result of PLLA templating effect, as shown by Rufino *et al.*[124] Moreover, significant reduction on both PLLA and PEO melting enthalpies suggests some miscibility degree between PLLA and PEO due to crystallization restriction imposed by one phase on the other. Finally, the increased PLLA Tm indicates increased lamellae thickness and might also be the result of miscibility.

Table 5. Thermal properties of PLLA, PEO and PLLA/PEO blends.

Thermal event		PEO	PLLA	PLLA/PEO
T_g/ºC	First heating	Unnoticeable	56.9	Unnoticeable
	Second heating	-50.1	39.5	-20.5 -29.8
T_c /ºC	First heating	-	-	-
	Cooling	39.2	-	69.5**
	Second heating	-	95.6	-
ΔH_c/J g^{-1}	First heating	-	-	-
	Cooling	130.9	-	21.3**
	Second heating	-	18.9	-
T_m/ºC	First heating	74.6	121	128.6* 61.3**
	Second heating	70.4	111.3 and 123.9	125.8* 56.9**
ΔH_m/J g^{-1}	First heating	181.1	Undefined	30.2* 33.8**
	Second heating	137.7	20.3	19.6* 27.1**

Values corresponding to *PLLA and ** PEO in the blends.

It is interesting to notice the change of the bimodal melting of pure PLLA to the almost monomodal melting of the PLLA in the blend, which suggests that the presence of PEO changes the preferential PLLA crystalline phase. However, the PLLA affects much more the PEO crystallinity of the other polymer because as seen in the large T_m depression, especially in the first heating. In conclusion, the shifts of T_m and T_m depressions indicate partial miscibility between PLLA and PEO.

Similar T_m shifts have been reported for PLLA/PEO blends with high molecular weight PLLA. Usually it is verified that larger T_m drops are exhibited for the lower molecular weight polymer or the one in the lowest concentration.[115,117] Therefore, it is possible to conclude that in this work the blend film consists of two semi-miscible polymers with distinct crystalline phases dispersed in a miscible amorphous matrix. In fact, the most accurate influence of PEO was observed in the blend coating related to the PLLA degradation therefore the NO release, which are discussed latter,

SNAP-doped coatings were obtained by spin coating using PLLA/PEO solution for the blend described above. Visually, the coating obtained was similar to the monolayer and bilayer samples PLLA-SNAP. The ATR-IR spectra of SNAP-doped blend coatings are shown in Fig.27. The main characteristic peaks of PLLA appear again in the coating. The spectrum of the PLLA/PEO-SNAP 10 coating depicts the characteristic bands of PEO around at 3500 cm^{-1} for ν(OH), 2885 cm^{-1}, ν_{as}(CH) of CH_2, 1455 cm^{-1} of CH_2 scissoring, 1345 cm^{-1} of $\delta_{ab}(CH_2)$, 1078 cm^{-1} for ν(C-O),[156,157] confirming the deposition of the polymer onto the PP substrate. The peak assigned to the N=O stretching vibration is unnoticed, indicating that SNAP is not exposed at the surface or is present at the concentration not enough to be detected by reflectance IR spectroscopy. One may consider that the presence of PEO increases the amorphous PLLA phase resulting in an increased of SNAP solubility and its depletion from the surface.

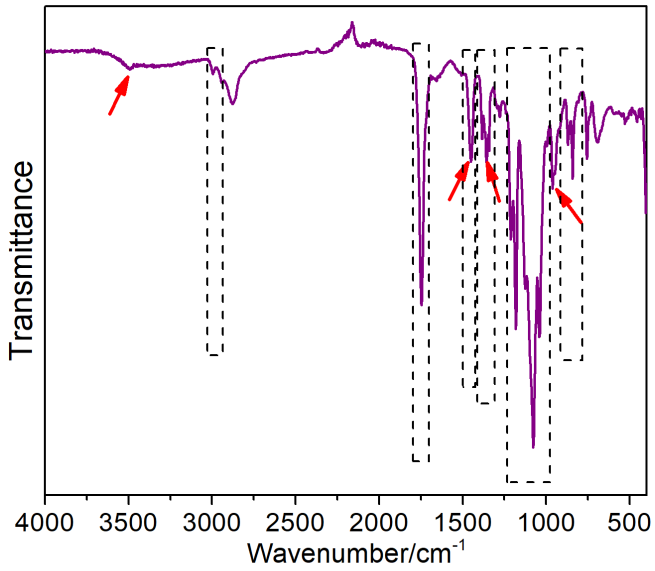

Fig. 27. Vibrational spectra of SNAP-doped PLLA/PEO-SNAP 10: red arrows show the main peaks of PEO in the blend. The dashed rectangles depict the mean peaks of PLLA shown in Fig.19a.

Fig.28 shows micrographs of PLLA/PEO-SNAP 10. The observed morphology is similar to that observed for the PLLA-SNAP coatings, with the presence of larger cavities. However, needle-like crystals are seen inside a close to the borders of cavities, which may be assigned to SNAP segregation during solvent evaporation. This segregation may be due to a decrease SNAP solubility in the PEO matrix. Further experiments are necessary to confirm this hypothesis.

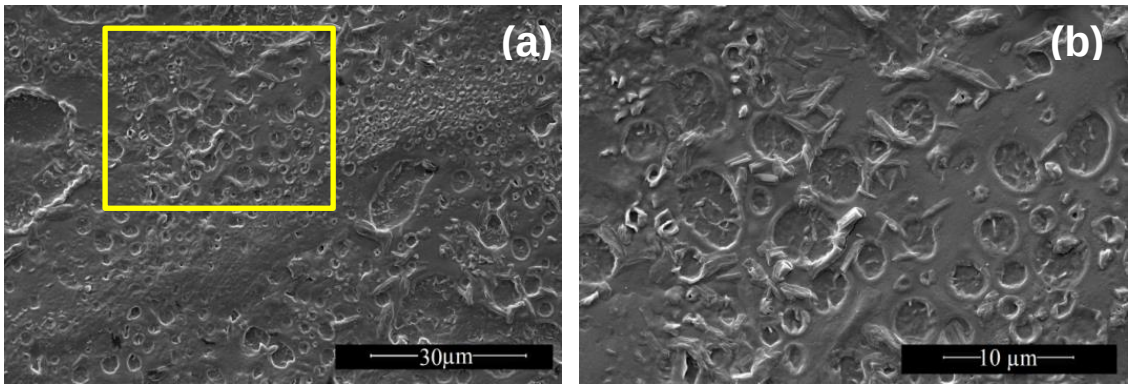

Fig. 28. SEM micrographs of a SNAP-doped monolayer of PLLA/PEO-SNAP 10 **(a)** with magnification of the yellow square of (a) **(b)**

4.3. Kinetics of NO release from PLLA-SNAP and PLLA/PEO-SNAP coatings

As aforementioned, the decomposition of RSNOs comprehends several pathways. Thermal (Δ) and photochemical ($h\nu$) decomposition take place through the homolytic cleavage of the S–NO bond, the simplest and lowest energy pathway (Eq.17 to 19), releasing NO and yielding the dimer RS–SR (disulphide). According to the initial step, there is a homolytic cleavage of the S-N bond to give NO and thiyl radicals (RS•), followed by the reaction between the RS• formed with a second RSNO molecule, leading to the formation of a sulfur bridge with simultaneous release of a second NO molecule (Eq.18). Eq.19 shows the possible bimolecular reaction between two thiyl radicals to yield a disulfide product. However, a bimolecular reaction between two reactive species present at low concentrations is unlikely. For this reason, the formation of the disulphide species is more likely to involve the reaction between a thiyl radical and an intact RSNO molecule, which is present at a higher concentration.[43,158,159]

$$\mathrm{RSNO} \xrightarrow[\Delta]{h\nu} \mathrm{RS}\bullet + \mathrm{NO}\bullet \quad (17)$$

$$\mathrm{RSNO} + \mathrm{RS}\bullet \rightarrow \mathrm{RS-SR} + \mathrm{NO}\bullet \quad (18)$$

$$\mathrm{RS}\bullet + \mathrm{RS}\bullet \rightarrow \mathrm{RS-SR} \quad (19)$$

This set of reactions, for the case of SNAP occurs in the aqueous medium. Therefore, SNAP stability within the polymeric matrix and its sustained lixiviation by diffusion or polymeric degradation are factors that contribute to the NO release in a sustainable fashion. For instance, due to the hydrophobic character of SNAP, this molecule tends to remain in the more hydrophobic polymer matrix, which is stabilized by intermolecular hydrogen bonding between crystallized molecules. [59,77] Related to that factors and based on the NO release obtained from PLLA-SNAP and PLLA/PEO-SNAP coatings, the mechanism of NO release from the SNAP leached in aqueous media (physiological conditions) will be purposed and discussed latter, for its greater understanding.

Firstly, in order to obtain the release rate of the total amount of SNAP contained in the volume of polymeric solution used to coat the PP films, the NO release rate from dissolved SNAP was analyzed under physiological conditions. A solution of SNAP 9 mM containing 100 µM EDTA was prepared considering the poor SNAP solubility in water (2 mg mL^{-1}), 333 µL (300 nmol) of this solution were added into the NOA sample vessel containing PBS with 100 µM EDTA at 37 ºC, protected from light. The real time release was measured for 1 h. This control experiment was

conducted in triplicate. The NO release profile from dissolved SNAP is depicted in the Fig.29, showing an initial burst at the first minute of measurement, followed by a plateau with a NO releasing rate of 1.0 ± 0.2 nmol min^{-1}. The cumulative NO release before 1 h of analysis was 64 ± 9 nmol, corresponding to 21 % of the total molar amount of SNAP added.

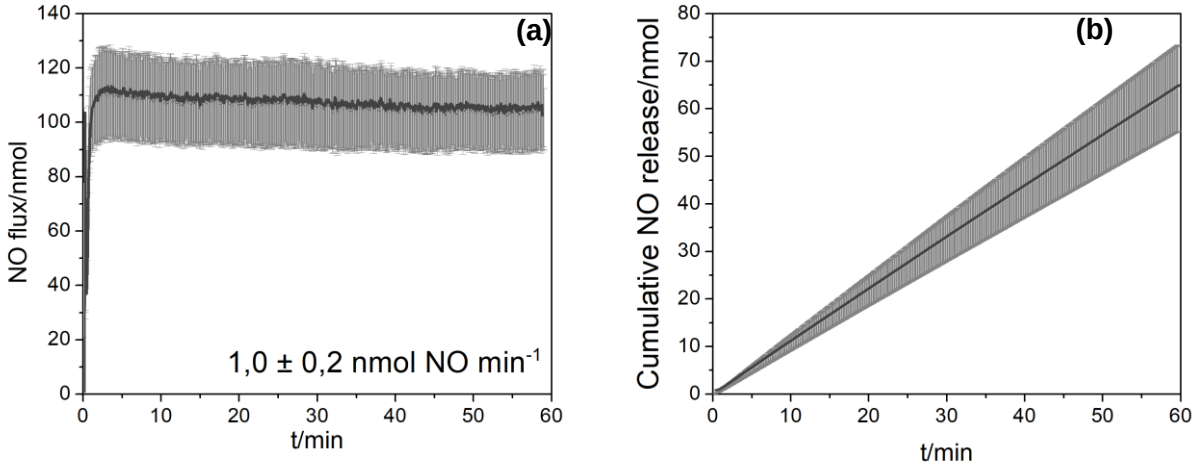

Fig. 29(a) Real time NO release from aqueous SNAP and **(b)** cumulative NO release, obtained from the integration of the curve in (a). The curves were obtained after the injection of 333 µL of SNAP 9 mM in 10 mL PBS containing 100 µM of EDTA at 37 ºC, protected from light. The shaded area corresponds to the SD of triplicates.

Fig.30 shows the real time NO release profiles of PLLA-SNAP 10, PLLA-SNAP 20, PLLA-SNAP/PLLA-SNAP 10, and PLLA/PEO-SNAP 10 samples. The monitoring was carried out during 1h. The initial rates of NO release (I_r) were calculated from the slopes of the curves after 5 min of measurement, during which a short burst release is observed in all cases. This short burst release can be assigned to the elution of the fraction of SNAP molecules which are more exposed a loosely bound on the surface. The I_r of PLLA-SNAP 10 and PLLA-SNAP 20 monolayers were 11 ± 1 pmol cm^{-2} min^{-1} and 23 ± 3 pmol cm^{-2} min^{-1}, respectively. This difference is considered to be statistically significant (Fig.30a and b). Therefore, doubling the SNAP concentration led to a 2-fold higher I_r as well as a 2-fold higher cumulative NO released after 1 h, suggesting that the distribution of SNAP in the PLLA matrix is homogeneous and the amount of SNAP exposed at the surface (which elutes in the 1 h period) is directly proportional to the SNAP concentration.

The real time NO release profile of the PLLA-SNAP/PLLA-SNAP 10 is shown in Fig.30c. The I_r obtained was 11 ± 2 pmol cm^{-2} min^{-1} which is statistically

equal to the I_r monolayer (11 ± 1 pmol cm^{-2} min^{-1}). Therefore, a second layer did not increase the I_r indicating that NO release occurs only at the outermost surface of the coating. This result supports the proposal of using PLLA-SNAP coatings for sustained NO release.

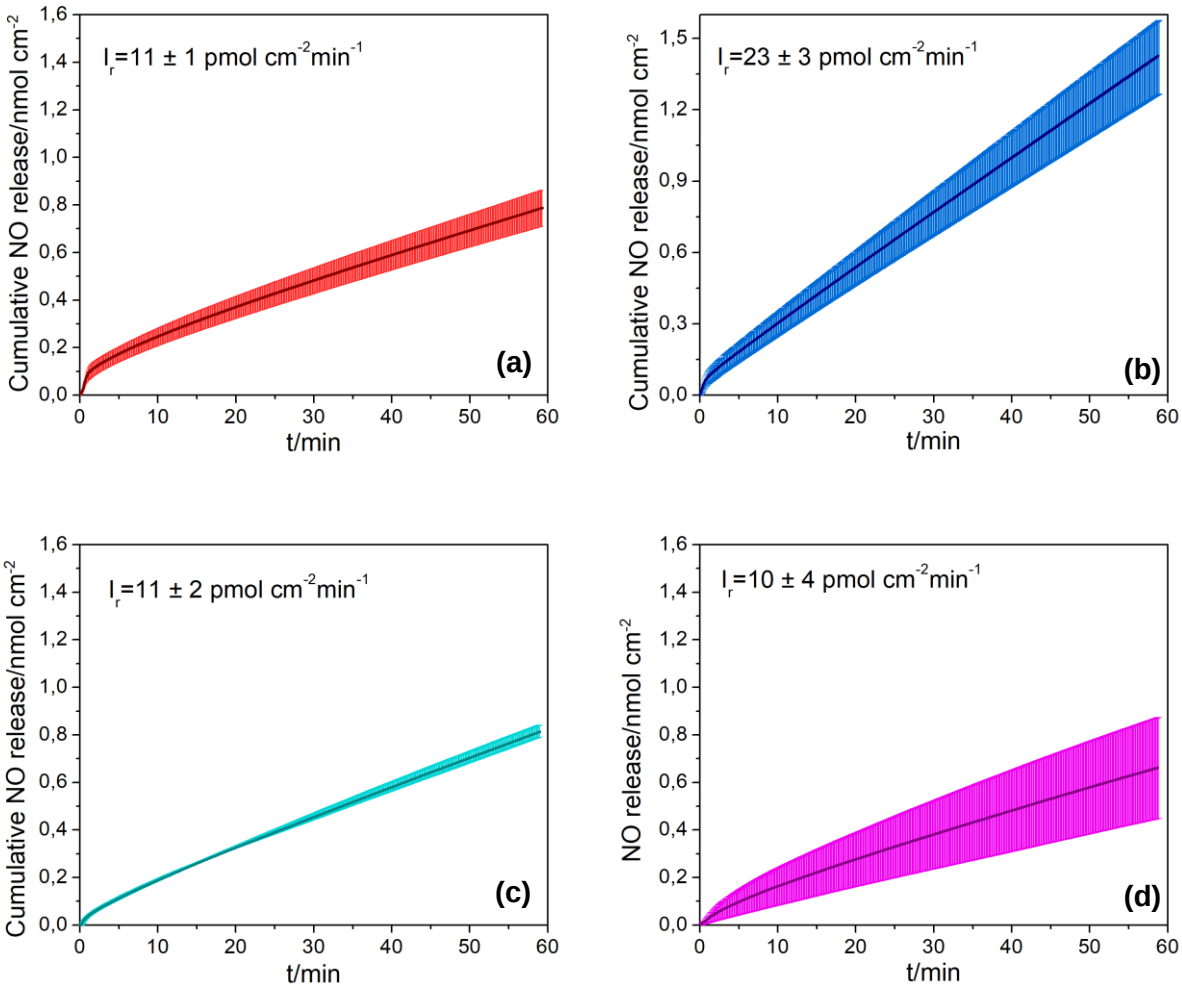

Fig. 30. Real time NO release profiles of **(a)** PLLA-SNAP 10, **(b)**, PLLA-SNAP 20, **(c)** PLLA-SNAP/PLLA-SNAP 10 and **(d)** PLLA/PEO-SNAP 10. NO release measurements were carried out in PBS at 37 ºC protected from light. The shaded area corresponds to the SD of triplicates.

In the case PLLA/PLLA-SNAP (second monolayer of PLLA), the real time NO release did not show significant release during 1 h, since the NO release was below the detection limit of the method (data not shown). This result indicates that a PLLA topcoat acts as a protective coating and is capable of blocking NO release from the underneath PLLA-SNAP coating during a short term exposition to the aqueous medium. Finally, Fig.30d shows the real time NO release profile of the PLLA/PEO-

SNAP 10. The I_r obtained was 10 ± 4 pmol cm^{-2} min^{-1} which is statistically equal to the I_r obtained for the PLLA-SNAP 10. Therefore, the presence of PEO does not change the kinetics of NO release suggesting that SNAP is exclusively dissolved in the PLLA matrix.

The rate of real time NO release obtained for aqueous SNAP solution and for SNAP incorporated in the PLLA and PLLA/PEO matrices are shown in Fig.31 and table 6, in comparison with the rates of endogenous NO production by the surface of endothelial cells lining blood vessels, as well as the rates of NO release necessary for inhibiting platelet adhesion and thrombus formation and bacterial adhesion.[36,68,77] It can be seen that the rates of NO release of 6 - 20 pmol cm^{-2} min^{-1}obtained are lower than the rate displayed by healthy endothelial cells from the inner walls of the blood stream.[68,77] On the other hand, they are higher than the required flux to inhibit the bacterial adhesion and to prevent thrombus formation;[36] These values suggest that SNAP-doped polymeric coatings have potential to be employed as contacting blood biomaterial and blood–contacting biomaterials. In comparison with NO fluxes reported for SNAP-doped CarboSil® based coatings, 50 – 550 nmol cm^{-2} min^{-1},[59,68,77] the values obtained in the present study are lower showing that PLLA degradation can be used as tool to modulate the rate of NO release from SNAP.

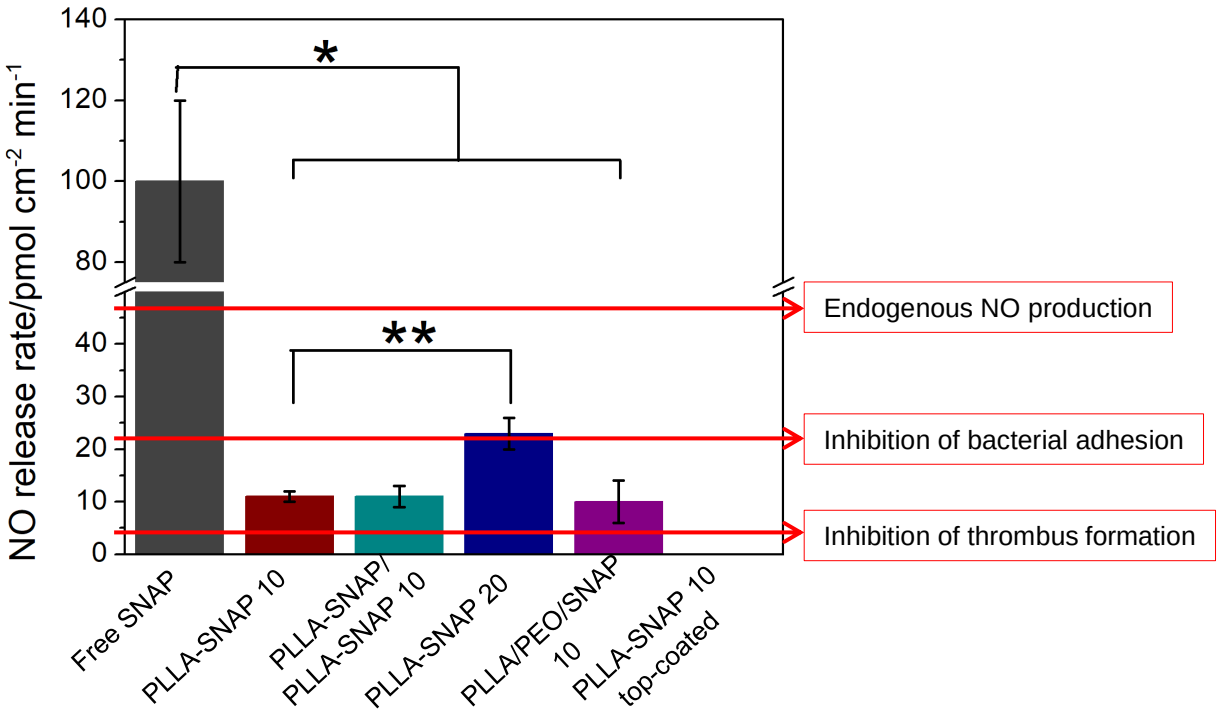

Fig. 31. Comparison of the NO release rates from different coatings obtained from the NO release profiles during 1h in PBS at 37 ºC protected from light with the endogenous NO release rates provided by the surface of endothelial cells and the NO release rates necessary for inhibiting thrombus formation and bacterial adhesion.[36,68,77] PLLA/PLLA-SNAP 10sample did not show significant NO release. (*) $p < 0.001$. (**) $p < 0.02$.

Table 6. t-test for statistical significance evaluation (p values) for of NO release rates.

Coating	Initial rate ± SD /pmol cm^{-2} min^{-1}	Free SNAP	PLLA-SNAP 10
Free SNAP	1.0 ± 0,2[a]	-	-
PLLA-SNAP 10	11 ± 1	0.0010	-
PLLA-SNAP/PLLA-SNAP 10	11 ± 2	0.0010	1
PLLA-SNAP 20	23 ± 3	0.0011	0.0028
PLLA/PEO-SNAP 10	10 ± 4	0.0010	0.6960

[a] Units for NO release rate of SNAP in PBS are nmol min^{-1}.

Fig.32 shows the schematic illustration of the NO release mechanism proposed for SNAP-doped coatings base on the NO release mechanism described by Yaqi Wo., *et al.*

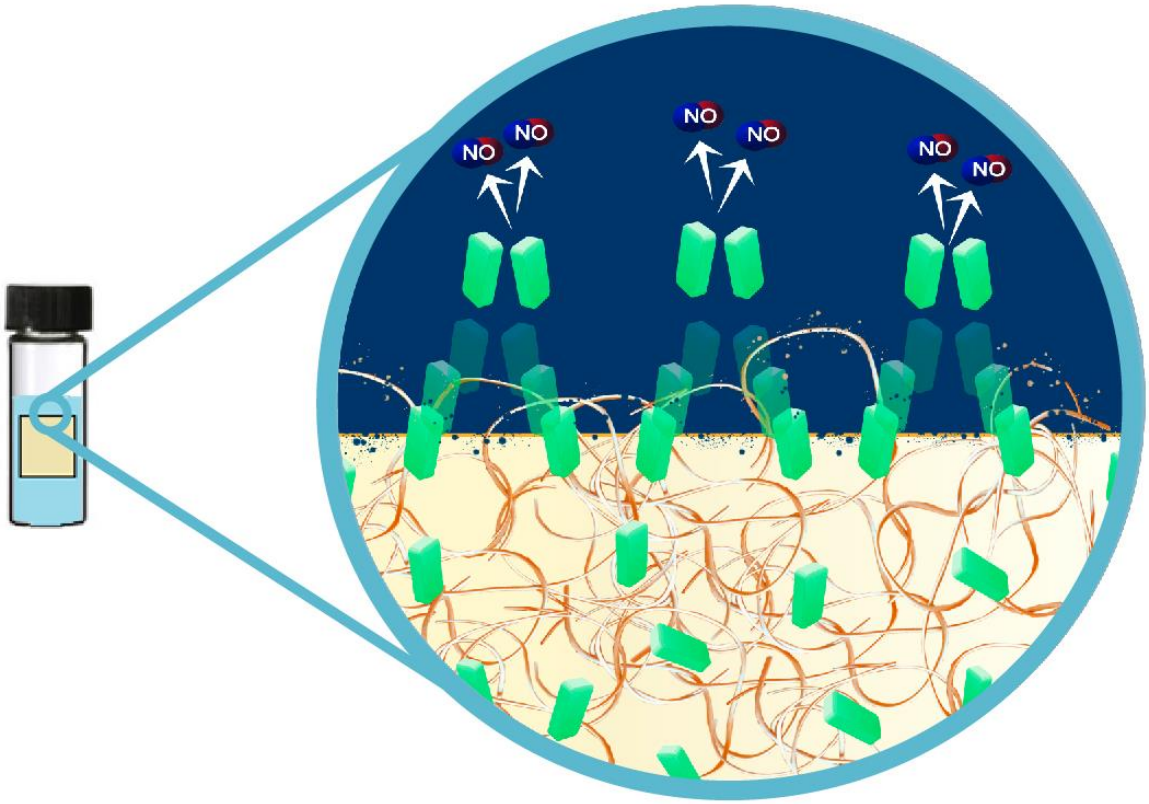

Fig 32. Schematic illustration of the NO release from the PLLA-SNAP coatings after their immersion in water or physiological medium (PBS at 37 ºC). Green parallelepipeds represent SNAP molecules, which are released from the polymeric matrix as the PLLA degradation takes place. Two NO molecules are released when the disulphide dimer is formed.

The SNAP molecules most exposed to the aqueous solution at physiological conditions dissolve and diffuse in the aqueous medium at the solid/liquid interface. Once in solution, collisions between two SNAP molecules or between pre-formed thiyl radical and an intact SNAP molecule leads to free NO release according to Eqs.17 and 19. After this phase the slow degradation of PLLA at physiological conditions is expected to control the dissolution and decomposition of SNAP molecules which are beneath the surface, leading to slow NO release phase, controlled by the rate of PLLA hydrolysis.

4.4. Quantification of short-term NO release

The reaction of a RSNO with a nucleophile such as ascorbic acid is another decomposition pathway, in which NO acts as a leaving group due to the strongly polarized S–N bond. This reaction depends on both ascorbate concentration and solution pH. Under certain pH, the acid may be in the protonated or deprotonated form.[158] Under the accelerated conditions used herein, ascorbate di-anion stoichiometrically reacts with SNAP releasing NO, and can be used to calculate the SNAP dose.

The initial SNAP doses in the coatings measured by the ascorbate method were proportional, to the SNAP charges used in the PLLA matrix, and raged from 14 ± 1 nmol cm^{-2} to 31 ± 7 nmol cm^{-2}. It must be noted however that these doses correspond to the amount of SNAP close to the surface which was accessed by the reducing ascorbate anion, and do not represent the total SNAP content of the samples. These values reflect the NO release from the superficial SNAP, which the fraction of SNAP molecules most exposed a loosely bound on the surface.

4.5. Long-term NO release from PLLA-SNAP and blended PLLA/PEO coatings

Long-term monitoring of the NO release process from the coatings immerged in PBS at 37 ºC as carried out by quantifying the total NO released and accumulated over time in a vial containing the samples. In this case, the NO release could depended on the hydrolytic degradation of PLLA, which takes place by chain scission, leading to decreased polymer M_w.[760] This chemical reaction depends on pH, temperature and the length of the chains.[160] The mechanism proposed comprehends the polymer degradation followed by SNAP leaching to the aqueous media and, ultimately NO release. NO is expected to be easily oxidized to nitrite and nitrate by dissolved oxygen in the PBS medium as shown in Eq.4.[19] The cumulative value, was measured using the VCl_3 reduction method which reduces nitrite and nitrate back to

free NO (Eq.14). This implies that the released NO does not exceed PBS solubility limit and therefore does not evolve from the aqueous medium.

Fig.33 depicts the kinetic curves of NO release assembling data from different samples under different conditions. The long-term NO releasing assays comprehend three stages beginning with the physiological condition (PBS at 37 ºC), followed by the raise of temperature and finishing with the raise of pH.

Considering the real time NO release rate (I_r obtained before), of 11 pmol cm^{-2} min^{-1} after 7 h of incubation in PBS at 37 ºC, the PLLA-SNAP 10 monolayer and bilayer samples are expected values of cumulative NO dose of 5 nmol cm^{-2} for both since the I_r are the same, while in Fig.33a, the initial NO release values after 7h were about the same order of magnitude 20 nmol cm^{-2}. The same trend can be observed in the Fig.33b for the PLLA-SNAP 20 monolayer and bilayer. Considering the real time NO release rate of 23 pmol cm^{-2} min^{-1} (I_r obtained before), the expected dose of NO released after 7 h is 10 nmol cm^{-2} for both samples, while in Fig.33b the initial NO release values after 7 h were around 60 nmol cm^{-2}.

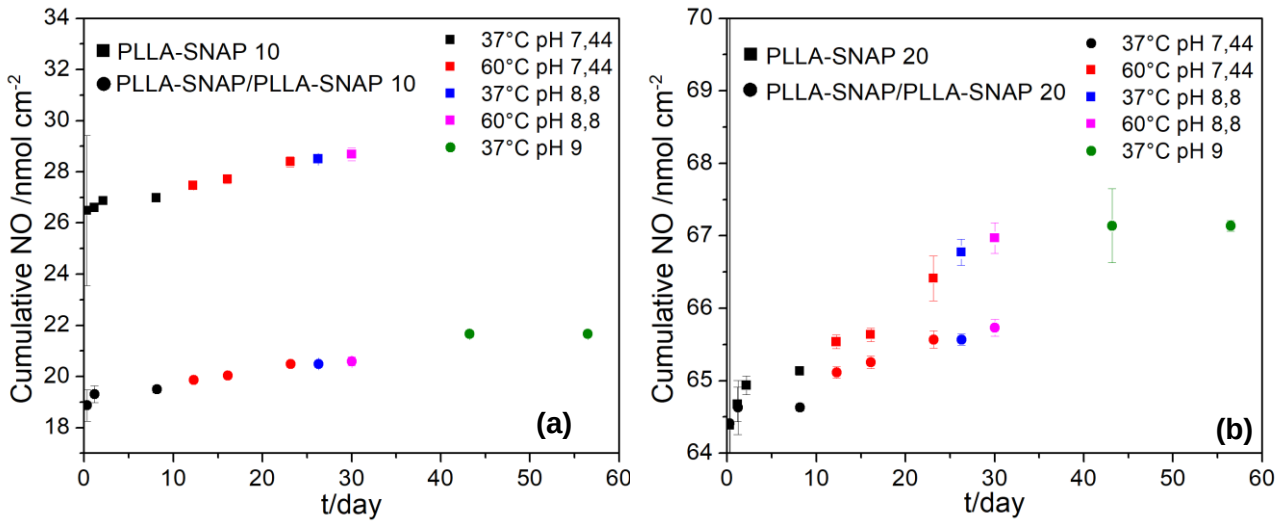

Fig. 33. Cumulative NO release under physiological (black squares and circles) and accelerated conditions (colored squares and circles) from **(a)** PLLA-SNAP 10 monolayer (square) and bilayer (circle) and **(b)** PLLA-SNAP 20 monolayer (square) and bilayer (circle). Data mean ± SD (n = 3).

Since after 8 days at 37 °C the cumulative NO released reached a plateau (Fig.33a and b), further measurements were taken under accelerated hydrolysis conditions at pH 8.8.[67] The total NO release from monolayer samples of SNAP 10 wt%

and 20 wt% were 28.7 ± 0.2 nmol cm^{-2} and 67.0 ± 0.2 nmol cm^{-2}, reaching complete NO release after 30 days.

Using bilayer coatings, NO release was prolonged for 13 days under accelerated conditions, 37 °C and pH = 9, reaching a total NO release of 21.7 ± 0.1 nmol cm^{-2} and 67.3 ± 0.5 nmol cm^{-2}, respectively, in both cases, the monolayer cumulative NO profiles were slightly higher than the bilayer cumulative NO profiles (Fig.33a and b) due probably to the fluctuation in the experimental data inherent to this protocol.

A comparison between the expected values of cumulative NO release of 5 and 10 nmol cm^{-2} (before 7 h, for both SNAP concentration) and values of SNAP quantification of 14 and 31 nmol cm^{-2} (short-term measurements, for both concentration), are values lower than the initial cumulative obtained, which were 20 and 60 nmol cm^{-2}. These differences allow us to conclude that the initial NO release is governed by the superficial SNAP and as this superficial SNAP is released, the NO release is now governed by the PLLA degradation (more than 7 h), which exposes the SNAP to the surface and the SNAP decomposition happens (Fig.32). The other conclusion is that under prolonged hydrolytic conditions PLLA hydrolysis lead to higher amounts of NO release.

Samples with the second coating of neat PLLA showed the same trend (Fig.34). Initial values of the NO release from PLLA/PLLA-SNAP 10 and PLLA/PLLA-SNAP 20 samples were in the same order of magnitude of 0.7 ± 0.2 nmol cm^{-2} and 1 ± 0.4 nmol cm^{-2}, after 8 hours, respectively. The total NO released were 2.54 ± 0.04 nmol cm^{-2} and 3.2 ± 0.2 nmol cm^{-2}, respectively. NO release was verified up to 40 days in both cases under accelerated conditions (increasing temperature and pH). Therefore, a PLLA topcoat decreases substantially the NO release in comparison with other coatings, due to PLLA topcoat protecting effect.

Additionally, the long-term NO release from the immersion of PLLA/PEO-SNAP 10 took 32 days in PBS at 37 ºC (Fig.35). The initial NO release value was 75 ± 3 nmol cm^{-2} after 6 h; PLLA/PEO-SNAP 10 led to a 3-fold increase in the initial NO release relative to PLLA-SNAP 10. After 32 days the total NO released was 95.8 ± 0.6 nmol cm^{-2}. This result indicates that by blending PLLA with PEO, the NO release can be modulated leading to a significant increase in the total NO release.

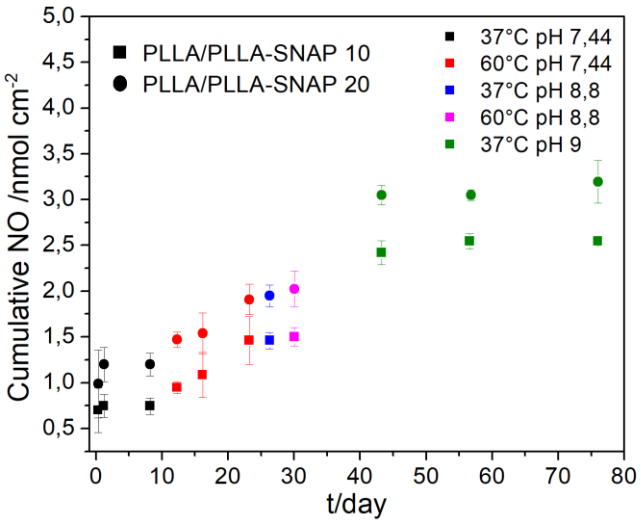

Fig. 34. Cumulative NO release under physiological and accelerated conditions of PLLA/PLLA-SNAP 10(squarer) and PLLA/PLLA-SNAP 20(circle). Data mean ± SD (n = 3).

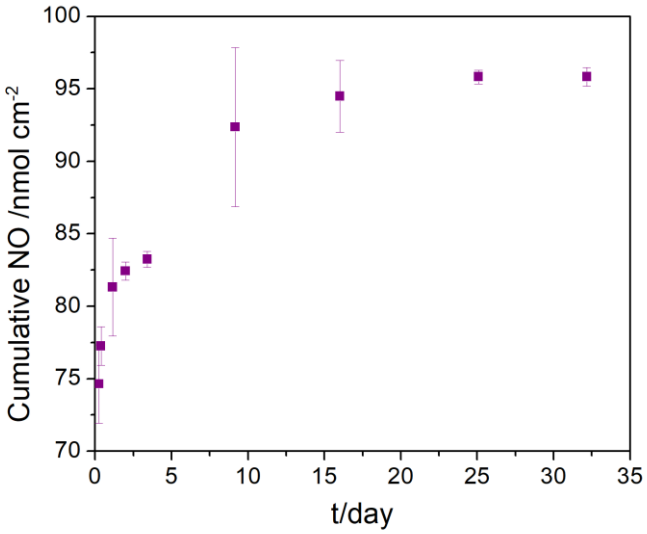

Fig. 35. Cumulative NO release under physiological of PLLA/PEO-SNAP 10. Data mean ± SD (n = 3).

It is interesting to notice that the presence of PEO in the coating, PLLA/PEO samples, increased the hydrophilicity if the material compared with PLLA only ($p < 0.003$), as shown by the contact angle measurements (Fig.36). This higher wettability may contribute to a faster hydrolytic degradation process, corroborating the higher cumulative NO release observed for the PLLA/PEO-SNAP samples. On the other hand, the hydrophilicity was not affected by the presence of SNAP.

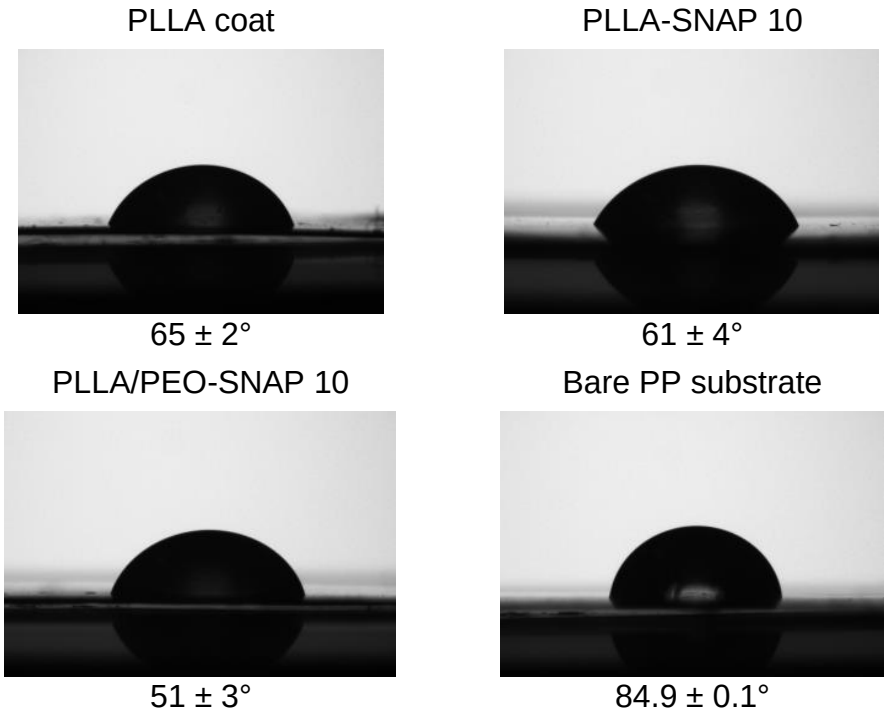

Fig. 36. Contact angle measurements on PLLA coat, PLLA-SNAP 10, PLLA/PEO-SNAP 10 coatings onto PP substrate and bare PP substrate samples.

Fig.37 shows the sulfur element mapping of the PLLA-SNAP 10 sample, which allows inferring the SNAP distribution within the coating is homogeneous. Fig.38 shows the EDS spectra obtained during the hydrolysis assay. It can be seen that the peak assigned to sulfur disappears after hydrolyzes, suggesting that the SNAP located in the surface was leached out.

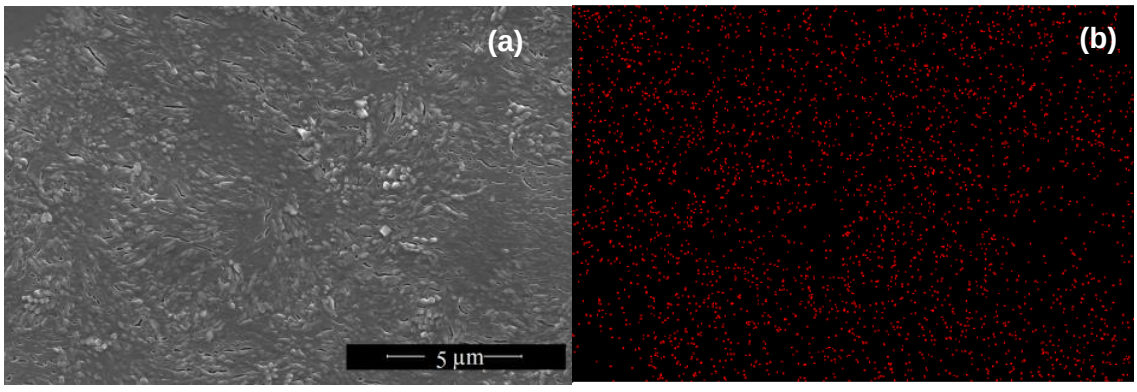

Fig. 37 Sulfur element mapping of PLLA-SNAP 10 before hydrolysis in PBS at 37 ºC.

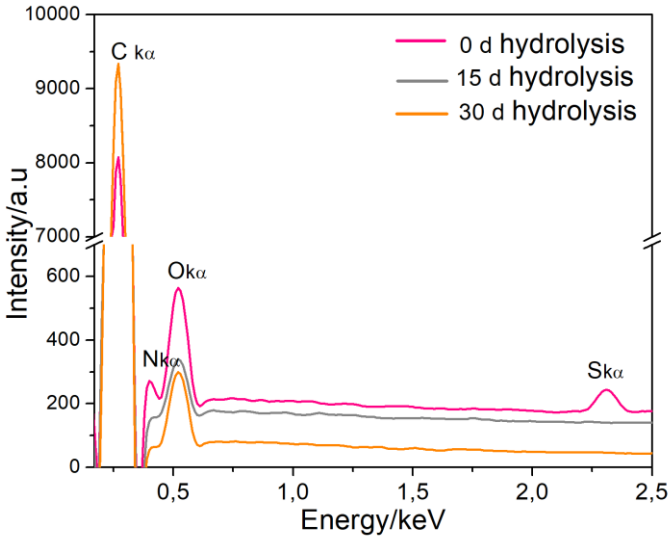

Fig. 38 Smoothed spectrum of long-term hydrolysis of PLLA-SNAP 10 before immersion (0 d), after 15 d and 30 d after immersion in PBS at 37 ºC.

The morphological changes due to the hydrolysis in PBS at 37 ºC are shown in Fig. 39. The micrographs of hydrolyzed PLLA-SNAP monolayer displayed an erosion process of the polymeric coating, resulting in the formation of fissures that grew as the hydrolysis proceeded (Fig.39a). For bilayer coatings (Fig.39b and c), the polymeric erosion is more evident; since the cracks and fissures in the region between pores grew.

In the case of PLLA-SNAP/PLLA-SNAP 10, it is possible to distinguish that the topcoat suffered degradation, resulting in pore formation after 15 days. After 30 days the inner region of the pores presented no changes. In contrast, in PLLA/PLLA-SNAP 10the inner coating is visible and the topcoat is hydrolyzed; the size of the initial cavities increased and fissures appeared. The morphology of the inner coating resembles the morphology of a monolayer coating. After 30 days the inner and topcoat cannot be distinguished, suggesting that the inner coating began to hydrolyze as well. For blended coating (Fig.39d), the decreasing of number of pores and the increasing of pore size generated by the degradation process from 15 days until 30 days might be observed. The inner region of the pores in both coatings seems to hydrolyze as well, these regions appear deeper. Additionally, micrographs of hydrolysis blended coatings indicate no phase segregation of the polymer constituents of the blend.

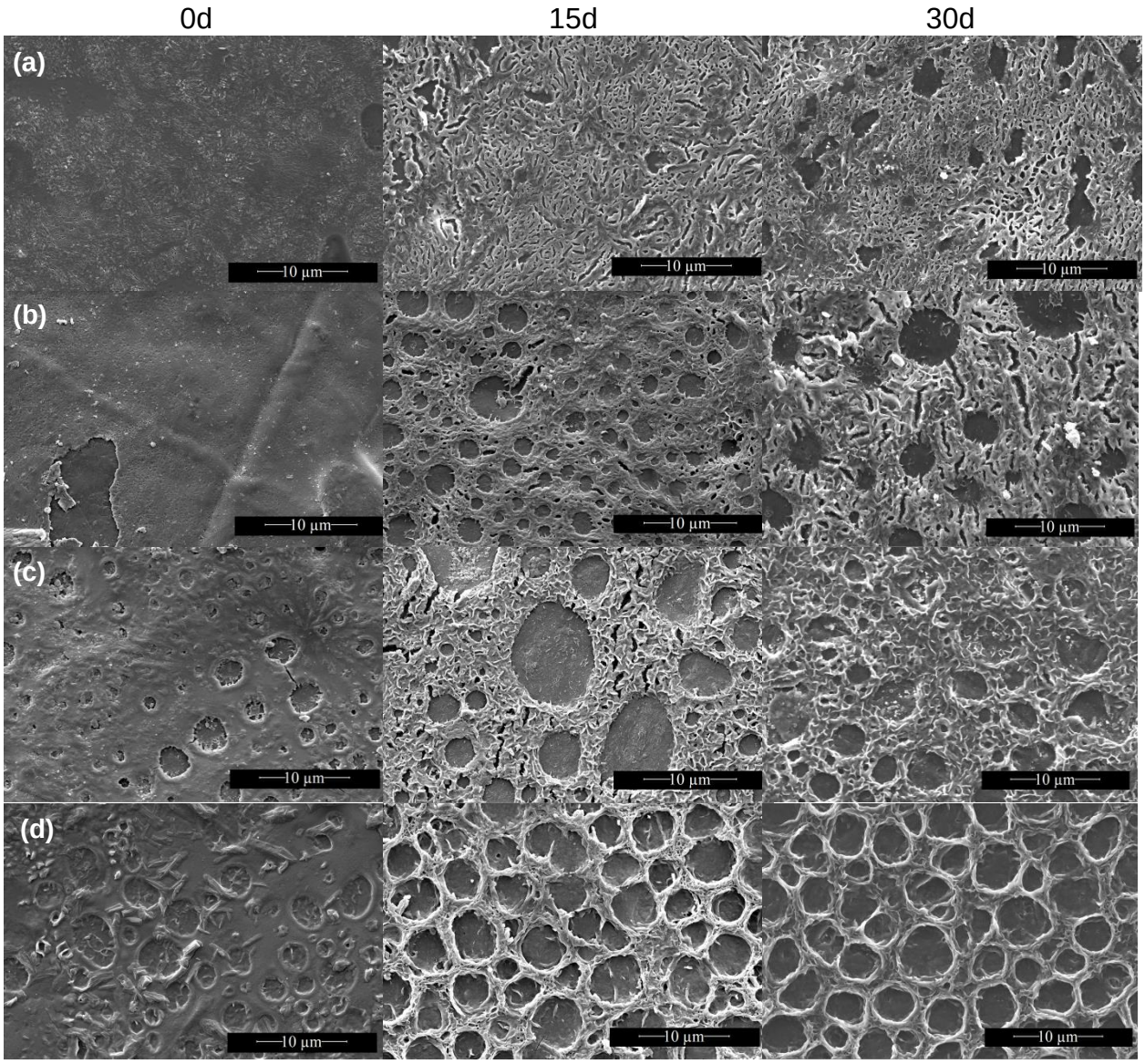

Fig. 39. SEM micrographs of *in vitro* hydrolysis for before immersion (left), after 15 days (middle) and 30 days (right) of immersion in PBS at 37 ºC of **(a)** PLLA-SNAP 10, **(b)** PLLA-SNAP/PLLA-SNAP 10, **(c)** PLLA/PLLA-SNAP 10 and **(d)** PLLA/PEO-SNAP 10.

5. CONCLUSIONS AND PERSPECTIVES

Homogeneous and PLLA-SNAP coatings can be obtained on the surface of polypropylene by the spin coating.

PLLA-SNAP coatings are able to modulate the rate and dose of NO release to aqueous environments.

PLLA-SNAP coatings are able to release NO during prolonged times in a process governed by the slow hydrolysis of the PLLA matrix.

The rates of NO release from PLA/SNAP coatings can be adjusted to levels with potential to inhibit bacterial adhesion and thrombus formation in blood contacting medical devices.

PLLA/PEO-SNAP coatings showed faster hydrolytic degradation process obtaining higher cumulative NO release values.

As futures perspectives, firstly, NO release profiles could be obtained for longer times and for the different PLLA/PEO compositions. The store stability of the PLLA-SNAP and PLLA/PEO-SNAP coatings could be evaluated. Secondly, NO release profiles for some medical devices coated with PLLA-SNAP by dip coating could be evaluated. Finally, biological assays could be performed in order to evaluate the potential biological activity of the PLLA-SNAP coatings in inhibiting platelet, bacterial adhesion and tissue regeneration as well as evaluate the cytotoxicity of the coatings.

6. REFERENCES

[1] Vila-Petroff, M. G., Lakatta, E. G., and Sollott, S. J. (1998). Nitric oxide: a multifaceted modulator of cardiac contractility. *The Asia Pacific Heart Journal*, *7*(1), 38-42.

[2] Dierks, E. A., *et al*. (1996).Nitric oxide (NO•), the only nitrogen monoxide redox form capable of activating soluble guanylyl cyclase. *Biochemical pharmacology*,*51*(12),1593-1600.

[3] Cals-Grierson, M. M., and Ormerod, A. D. (2004). Nitric oxide function in the skin. *Nitric oxide*, *10*(4), 179-193.

[4] Weidensteiner, C., *et al*. (2013). Effects of the nitric oxide donor JS-K on the blood-tumor barrier and on orthotopic U87 rat gliomas assessed by MRI. *Nitric Oxide*, *30*, 17-25.

[5] Pitsikas, N. (2015). The role of nitric oxide donors in schizophrenia: Basic studies and clinical applications. *European journal of pharmacology*, *766*, 106-113.

[6] Raghavan, S. A. and Dikshit, M. (2004). Vascular regulation by the L-arginine metabolites, nitric oxide and agmatine. *Pharmacological research*, *49*(5), 397-414.

[7] McCarthy, H. O. and Coulter, J. A. (Eds.). (2011). Nitric Oxide: Methods and Protocols. Humana Press. DOI: 10.1007/978-1-61737-964-2.

[8] Ignarro, L.J., and Freeman, B. (Eds). (2010). Nitric oxide biology and pathobiology. (2Ed). Academia Press. ISBN: 978-0-12-373866-0.

[9] Hughes, M. N. (2008). Chemistry of nitric oxide and related species. In Methods in enzymology (Vol. 436, pp. 3-19). Academic Press.

[10] Shaw, A. W., and Vosper, A. J. (1977). Solubility of nitric oxide in aqueous and nonaqueous solvents. *Journal of the Chemical Society, Faraday Transactions 1: Physical Chemistry in Condensed Phases*, *73*, 1239-1244.

[11] Culotta, E., and Koshland Jr, D. E. (1992). NO news is good news. *Science*, 258(5090), 1862-1866.

[12] Bailar, H.J., *et al*. (Eds). (1973). Comprehensive Inorganic Chemistry. Chapter 19 NITROGEN. Pergamon. ISBN 9781483283135.

[13] Butler, A. R., and Nicholson, R. (2003). *Life, death and nitric oxide*(Vol. 33). Royal Society of Chemistry.

[14] McCleverty, J. A. (2004). Chemistry of nitric oxide relevant to biology. *Chemical reviews*, 104(2), 403-418.

[15] Siegel, M. W., *et al*. (1972). Molecular Photodetachment Spectrometry. I. The Electron Affinity of Nitric Oxide and the Molecular Constants of NO^-. *Physical Review A*, 6(2), 607.

[16] Chalasinski, G., and Kukawska-Tarnawska, B. (1990). Ab initio studies of the structure and energies of the nitric oxide-helium and nitric oxide-argon complexes. *Journal of Physical Chemistry*, 94(9), 3450-3454.

[17] Teillet-Billy, D., and Fiquet-Fayard, F. (1977). The NO^{-3} Σ^- and $^1\Delta$ resonances: theoretical analysis of electron scattering data. *Journal of Physics B: Atomic and Molecular Physics*, 10(4), L111.

[18] Anthony, A. R., and Rhodes, P. (1997). Chemistry, Analysis, and Biological Roles of S-Nitrosothiols. *Analytical biochemistry*, 249(1), 1-9.

[19] Ignarro, L. J., *et al*. (1993). Oxidation of nitric oxide in aqueous solution to nitrite but not nitrate: comparison with enzymatically formed nitric oxide from L-arginine. *Proceedings of the National Academy of Sciences*, 90(17), 8103-8107.

[20] Ford, P. C., Wink, D. A., and Stanbury, D. M. (1993). Autoxidation kinetics of aqueous nitric oxide. *Febs Letters*, 326(1-3), 1-3.

[21] Liu, X., *et al*. (1998). Accelerated reaction of nitric oxide with O_2 within the hydrophobic interior of biological membranes. *Proceedings of the National Academy of Sciences*, 95(5), 2175-2179.

[22] Alderton, W. K., Cooper, C. E., and Knowles, R. G. (2001). Nitric oxide synthases: structure, function and inhibition. *Biochemical journal*, 357(3), 593-615.

[23] Wang, P. G., Cai, T. B., and Taniguchi, N. (Eds.). (2005). Nitric oxide donors: for pharmaceutical and biological applications. John Wiley and Sons. ISBN-13 978-3-527-31015-9.

[24] Major, T.C.,*et al*. (2010).The attenuation of platelet and monocyte activation in a rabbit model of extracorporeal circulation by a nitric oxide releasing polymer. *Biomaterials*, *31*(10), 2736-2745.

[25] Zhu, H., Ka, B., and Murad, F. (2007). Nitric oxide accelerates the recovery from burn wounds. *World journal of surgery*, *31*(4), 624-631.

[26] Hetrick, E. M., & Schoenfisch, M. H. (2007). Antibacterial nitric oxide-releasing xerogels: Cell viability and parallel plate flow cell adhesion studies. *Biomaterials*, *28*(11), 1948-1956.

[27] Amadeu, T. P., *et al*. (2008). Nitric oxide donor improves healing if applied on inflammatory and proliferative phase. *Journal of Surgical Research*, *149*(1), 84-93.

[28] Traish, A. M., Botchevar, E., and Kim, N. N. (2010). Biochemical factors modulating female genital sexual arousal physiology. *The journal of sexual medicine*, *7*(9), 2925-2946.

[29] Griffith, T. M., *et al.* (1984). The nature of endothelium-derived vascular relaxant factor. *Nature*, 308(5960), 645.

[30] Martin, W., *et al.* (1986). Depression of contractile responses in rat aorta by spontaneously released endothelium-derived relaxing factor. *Journal of Pharmacology and Experimental Therapeutics*, 237(2), 529-538.

[31] Koprowski, H., and Maeda, H. (Eds.). (2012). The role of nitric oxide in physiology and pathophysiology (Vol. 196). Springer Science and Business Media. DOI: 10.1007/978-3-642-79130-7.

[32] Busse, R., Hecker, M., and Fleming, I. (1994). Control of nitric oxide and prostacyclin synthesis in endothelial cells. *Arzneimittel-Forschung*, 44(3A), 392-396.

[33] Marsden, P. A., *et al*. (1992). Molecular cloning and characterization of human endothelial nitric oxide synthase. *FEBS letters*, 307(3), 287-293.

[34] Binder, C., Schulz, M., Hiddemann, W., and Oellerich, M. (1999). Induction of inducible nitric oxide synthase is an essential part of tumor necrosis factor-alpha-induced apoptosis in MCF-7 and other epithelial tumor cells. *Laboratory investigation; a journal of technical methods and pathology*, 79(12), 1703-1712.

[35] Farias-Eisner, R., *el al*. (1994). Nitric oxide is an important mediator for tumoricidal activity in vivo. *Proceedings of the National Academy of Sciences*, 91(20), 9407-9411.

[36] Kim, J., *et al*. (2014). A platform for nitric oxide delivery. *Journal of Materials Chemistry B*, *2*(4), 341-356.

[37] Jen, M. C.,*et al*. (2012). Polymer-based nitric oxide therapies: Recent insights for biomedical applications. *Advanced functional materials*, *22*(2), 239-260.

[38] Hogg, N. (2002). The biochemistry and physiology of S-nitrosothiols. *Annual review of pharmacology and toxicology*, 42(1), 585-600.

[39] Wang, P. G.,*et al*. (2002). Nitric oxide donors: chemical activities and biological applications. *Chemical reviews*, *102*(4), 1091-1134.

[40] Napoli, C., and Ignarro, L. J. (2003). Nitric oxide–releasing drugs. *Annual review of pharmacology and toxicology*, 43(1), 97-123.

[41] Field, L., *et al*. (1978). An unusually stable thionitrite from N-acetyl-D, L-penicillamine; X-ray crystal and molecular structure of 2-(acetylamino)-2-carboxy-1, 1-dimethylethyl thionitrite. *Journal of the Chemical Society, Chemical Communications*, (6), 249-250.

[42] Oae, S., and Shinhama, K. (1983). Organic thionitrites and related substances. A review. *Organic Preparations and Procedures International*, 15(3), 165-198.

[43] Seabra, A. B., *et al*. (2004). Topically applied S-nitrosothiol-containing hydrogels as experimental and pharmacological nitric oxide donors in human skin. *British Journal of Dermatology*, 151(5), 977-983.

[44] Dicks, A., and áHerves Beloso, P. (1997). Decomposition of S-nitrosothiols: the effects of added thiols. *Journal of the Chemical Society, Perkin Transactions 2*, (8), 1429-1434.

[45] Byler, D. M., Gosser, D. K., and Susi, H. (1983). Spectroscopic estimation of the extent of S-nitrosothiol formation by nitrite action on sulfhydryl groups. *Journal of Agricultural and Food Chemistry*, 31(3), 523-527.

[46] Oae, S., Kim, Y. H., Fukushima, D., and Shinhama, K. (1978). New syntheses of thionitrites and their chemical reactivites. *Journal of the Chemical Society, Perkin Transactions* 1, (9), 913-917.

[47] Bonnett, R., Holleyhead, R., Johnson, B. L., and Randall, E. W. (1975). Reaction of acidified nitrite solutions with peptide derivatives: Evidence for nitrosamine and thionitrite formation from ^{15}N NMR studies. *Journal of the Chemical Society, Perkin Transactions 1*, (22), 2261-2264.

[48] Vaughn, M. W., Kuo, L., and Liao, J. C. (1998). Estimation of nitric oxide production and reaction rates in tissue by use of a mathematical model. *American Journal of Physiology-Heart and Circulatory Physiology*, 274(6), H2163-H2176.

[49] Starrett, M. A., *et al*. (2012). Wireless platform for controlled nitric oxide releasing optical fibers for mediating biological response to implanted devices. Nitric Oxide, 27(4), 228-234.

[50] Frost, M. C., *et al*. (2002). In vivo biocompatibility and analytical performance of intravascular amperometric oxygen sensors prepared with improved nitric oxide-releasing silicone rubber coating. *Analytical chemistry*, 74(23), 5942-5947.

[51] Fung, H. L., *et al*. (1988). Mechanisms for the pharmacologic interaction of organic nitrates with thiols. Existence of an extracellular pathway for the reversal of nitrate vascular tolerance by N-acetylcysteine. *Journal of Pharmacology and Experimental Therapeutics*, 245(2), 524-530.

[52] Gaston, B., *et al*. (1993). Endogenous nitrogen oxides and bronchodilator S-nitrosothiols in human airways. *Proceedings of the National Academy of Sciences*, 90(23), 10957-10961.

[53] Morris, S. L., Walsh, R. C., and Hansen, J. N. (1984). Identification and characterization of some bacterial membrane sulfhydryl groups which are targets of bacteriostatic and antibiotic action. *Journal of Biological Chemistry*, 259(21), 13590-13594.

[54] Morris, S. L., & Hansen, J. N. (1981). Inhibition of Bacillus cereus spore outgrowth by covalent modification of a sulfhydryl group by nitrosothiol and iodoacetate. *Journal of bacteriology*, 148(2), 465-471.

[55] Fang, F. C. (1997). Perspectives series: host/pathogen interactions. Mechanisms of nitric oxide-related antimicrobial activity. *The Journal of clinical investigation*, *99*(12), 2818-2825.

[56] Marcinkiewicz, J. (1997). Nitric oxide and antimicrobial activity of reactive oxygen intermediates. *Immunopharmacology*, *37*(1), 35-41.

[57] Lautner, G., Meyerhoff, M. E., and Schwendeman, S. P. (2016). Biodegradable poly (lactic-co-glycolic acid) microspheres loaded with S-nitroso-N-acetyl-D-penicillamine for controlled nitric oxide delivery. *Journal of Controlled Release*, *225*, 133-139.

[58] McCarthy, C. W., *et al*. (2016). Transition-metal-mediated release of nitric oxide (NO) from S-nitroso-N-acetyl-d-penicillamine (SNAP): potential applications for endogenous release of NO at the surface of stents via corrosion products. *ACS applied materials & interfaces*, 8(16), 10128-10135.

[59] Brisbois, E. J., *et al*. (2013). Long-term nitric oxide release and elevated temperature stability with S-nitroso-N-acetylpenicillamine (SNAP)-doped Elast-eon E2As polymer. *Biomaterials*, 34(28), 6957-6966.

[60] Frost, M. C., and Meyerhoff, M. E. (2004). Controlled photoinitiated release of nitric oxide from polymer films containing S-nitroso-N-acetyl-DL-penicillamine derivatized fumed silica filler. *Journal of the American Chemical Society*, 126(5), 1348-1349.

[61] Kark, R. P., *et al*. (1971). Mercury poisoning and its treatment with N-acetyl-D, L-penicillamine. *New England Journal of Medicine*, 285(1), 10-16.

[62] Pagnotto, L. D., Brugsch, H. G., and Elkins, H. B. (1960). Treatment of chronic mercurialism with N-acetyl-penicillamine. *American Industrial Hygiene Association Journal*, 21(5), 419-422.

[63] Walshe, J. M. (1956). Penicillamine, a new oral therapy for Wilson's disease. *The American journal of medicine*, 21(4), 487-495.

[64] Yadav, A., and Flora, S. J. S. (2016). Nano drug delivery systems: a new paradigm for treating metal toxicity. *Expert opinion on drug delivery*, 13(6), 831-841.

[65] Dias, A.B. (2018). Blenda degradável de Poli(ácido L- láctico)/poli(acetato de vinila) para liberação localizada de óxido nítrico. (Master Thesis) Universidade Estadual de Campinas. Campinas, São Paulo.

[66] Aaseth, J., *et al*. (2018). Chelator combination as therapeutic strategy in mercury and lead poisonings. Coordination Chemistry Reviews, 358, 1-12.

[67] Wo, Y., *et al*. (2017). Study of crystal formation and nitric oxide (NO) release mechanism from S-nitroso-N-acetylpenicillamine (SNAP)-doped CarboSil polymer composites for potential antimicrobial applications. *Composites Part B: Engineering*, *121*, 23-33.

[68] Wo, Y., *et al*. (2015). Origin of long-term storage stability and nitric oxide release behavior of CarboSil polymer doped with S-nitroso-N-acetyl-D-penicillamine. *ACS applied materials & interfaces*, *7*(41), 22218-22227.

[69] Maharana, T., Mohanty, B., and Negi, Y. S. (2009). Melt–solid polycondensation of lactic acid and its biodegradability*. Progress in polymer science*, 34(1), 99-124.

[70] Willians D.F. (1999).The Williams dictionary of biomaterials. Liverpool University Press. ISBN: 0-85323-921-5.

[71] Nair, L. S., and Laurencin, C. T. (2007). Biodegradable polymers as biomaterials. *Progress in polymer science*, 32(8-9), 762-798.

[72] Jo, Y. S., *et al*. (2009). Micelles for delivery of nitric oxide. Journal of the American Chemical Society, 131(41), 14413-14418.

[73] Johnson, T. A., *et al*. (2010). Reduced ischemia/reperfusion injury via glutathione-initiated nitric oxide-releasing dendrimers. Nitric Oxide, 22(1), 30-36.

[74] Storm, W. L., *et al*. (2014). Superhydrophobic nitric oxide-releasing xerogels. *Acta biomaterialia*, 10(8), 3442-3448.

[75] Kim, J., *et al*. (2011). NONOates–polyethylenimine hydrogel for controlled nitric oxide release and cell proliferation modulation. *Bioconjugate chemistry*, 22(6), 1031-1038.

[76] Kakisawa, H., *et al.* (2010). Room temperature fabrication of SiO_2/polyacrylic ester multilayer composites by spin-coating. *Materials Science and Engineering*: *B*, 173(1), 94-98.

[77] Xu, L. C., *et al*. (2017). Inhibition of bacterial adhesion and biofilm formation by dual functional textured and nitric oxide releasing surfaces. *Acta biomaterialia*, *51*, 53-65.

[78] Xu, L. C., Meyerhoff, M. E., and Siedlecki, C. A. (2019). Blood coagulation response and bacterial adhesion to biomimetic polyurethane biomaterials prepared with surface texturing and nitric oxide release. *Acta biomaterialia*, *84*, 77-87.

[79] Major, T. C., *et al*. (2011). The hemocompatibility of a nitric oxide generating polymer that catalyzes S-nitrosothiol decomposition in an extracorporeal circulation model. *Biomaterials*, *32*(26), 5957-5969.

[80] Pant, J., *et al*. (2017). Tunable nitric oxide release from S-nitroso-N-acetylpenicillamine via catalytic copper nanoparticles for biomedical applications. *ACS applied materials & interfaces*, *9*(18), 15254-15264

[81] Riccio, D. A., *et al*. (2012). Photoinitiated nitric oxide-releasing tertiary S-nitrosothiol-modified xerogels. *ACS applied materials & interfaces*, *4*(2), 796-804

[82] Frost, M. C., and Meyerhoff, M. E. (2005). Synthesis, characterization, and controlled nitric oxide release from S‐nitrosothiol‐derivatized fumed silica polymer filler particles. Journal of Biomedical Materials Research Part A: An Official Journal of The Society for Biomaterials, The Japanese Society for Biomaterials, and The

Australian Society for Biomaterials and the Korean Society for Biomaterials, 72(4), 419-419.

[83] Mowery, K. A., *et al*. (2000). Preparation and characterization of hydrophobic polymeric films that are thromboresistant via nitric oxide release. *Biomaterials*, *21*(1), 9-21.

[84] Lin, C. E.,*et al*. (2004). Combination of paclitaxel and nitric oxide as a novel treatment for the reduction of restenosis. *Journal of medicinal chemistry*, *47*(9), 2276-2282.

[85] Wu, B.,*et al*. (2007). Polymeric coatings that mimic the endothelium: combining NO release with surface-bound active thrombomodulin and heparin. *Biomaterials*, *28*(28), 4147-4155.

[86] Reynolds, M. M., Frost, M. C., and Meyerhoff, M. E. (2004). Nitric oxide-releasing hydrophobic polymers: preparation, characterization, and potential biomedical applications. *Free Radical Biology and Medicine*, 37(7), 926-936.

[87] Nair, L. S., and Laurencin, C. T. (2007). Biodegradable polymers as biomaterials. *Progress in polymer science*, 32(8-9), 762-798.

[88] Moon, S. I., *et al*. (2000). Melt polycondensation of L-lactic acid with Sn (II) catalysts activated by various proton acids: A direct manufacturing route to high molecular weight Poly (L-lactic acid). *Journal of Polymer Science Part A: Polymer Chemistry*, *38*(9), 1673-1679.

[89] Ajioka, M., *et al*. (1995). Basic properties of polylactic acid produced by the direct condensation polymerization of lactic acid. *Bulletin of the Chemical Society of Japan*, 68(8), 2125-2131.

[90] Kowalski, A., Duda, A., and Penczek, S. (2000). Kinetics and mechanism of cyclic esters polymerization initiated with tin (II) octoate. 3. Polymerization of L, L-dilactide. *Macromolecules*, 33(20), 7359-7370.

[91] Xu, H., *et al*. (2006). The Effect of Crystallization on the Solid State Polycondensation of Poly (L‐lactic Acid). *Journal of Macromolecular Science, Part B*, 45(4), 681-687.

[92] Middleton, J. C., and Tipton, A. J. (2000). Synthetic biodegradable polymers as orthopedic devices. *Biomaterials*, 21(23), 2335-2346.

[93] Righetti, M. C., *et al*. (2015). Enthalpy of melting of α`-and α-crystals of poly (l-lactic acid). *European Polymer Journal*, 70, 215-220.

[94] Pyda, M., Bopp, R. C., and Wunderlich, B. (2004). Heat capacity of poly (lactic acid). *The Journal of Chemical Thermodynamics*, 36(9), 731-742.

[95] Magoń, A., and Pyda, M. (2009). Study of crystalline and amorphous phases of biodegradable poly (lactic acid) by advanced thermal analysis. *Polymer*, 50(16), 3967-3973.

[96] Fukushima, K., and Kimura, Y. (2006). Stereocomplexed polylactides (Neo‐PLA) as high‐performance bio‐based polymers: their formation, properties, and application. *Polymer International*, 55(6), 626-642.

[97] Wunderlich, B. (2005). Thermal analysis of polymeric materials. Springer Science and Business Media. ISBN 3-541-23629-5

[98] Wunderlich, B. (2003). Reversible crystallization and the rigid–amorphous phase in semicrystalline macromolecules. *Progress in Polymer Science*, 28(3), 383-450.

[99] Wasanasuk, K., *et al*. (2011). Crystal structure analysis of poly (l-lactic acid) α form on the basis of the 2-dimensional wide-angle synchrotron X-ray and neutron diffraction measurements. *Macromolecules*, 44(16), 6441-6452.

[100] Pan, P., *et al*. (2008). Polymorphic transition in disordered poly (L-lactide) crystals induced by annealing at elevated temperatures. *Macromolecules*, 41(12), 4296-4304.

[101] Cartier, L., *et al*. (2000). Epitaxial crystallization and crystalline polymorphism of polylactides. *Polymer*, 41(25), 8909-8919.

[102] Zhang, J., *et al*. (2006). Confirmation of Disorder α Form of Poly (L-lactic acid) by the X-ray Fiber Pattern and Polarized IR/Raman Spectra Measured for Uniaxially-Oriented Samples. *Macromolecular symposia*. Vol. 242, No. 1, pp. 274-278.

[103] Cho, T. Y., and Strobl, G. (2006). Temperature dependent variations in the lamellar structure of poly (L-lactide). Polymer, 47(4), 1036-1043.

[104] Eling, B., Gogolewski, S., and Pennings, A. J. (1982). Biodegradable materials of poly (l-lactic acid): 1. Melt-spun and solution-spun fibres. *Polymer*, *23*(11), 1587-1593.

[105] Jiménez, A., Peltzer, M., and Ruseckaite, R. (Eds.). (2014). Poly (lactic acid) science and technology: processing, properties, additives and applications. Royal Society of Chemistry. ISBN: 978-1-78262-480-6

[106] Maurus, P. B., and Kaeding, C. C. (2004). Bioabsorbable implant material review. *Operative Techniques in Sports Medicine*, 12(3), 158-160.

[107] Piemonte, V., and Gironi, F. (2013). Lactic acid production by hydrolysis of poly (lactic acid) in aqueous solutions: an experimental and kinetic study. *Journal of Polymers and the Environment*, 21(1), 275-279.

[108] Day, J. N. E., and Ingold, C. K. (1941). Mechanism and kinetics of carboxylic ester hydrolysis and carboxyl esterification. *Transactions of the Faraday Society*, 37, 686-705.

[109] McMurry, J. E. (2008). Organic Chemistry. Cengage Learning. ISBN: 0-495-11258-5.

[110] Schliecker, G., *et al*. (2003). Characterization of a homologous series of D, L-lactic acid oligomers; a mechanistic study on the degradation kinetics in vitro. *Biomaterials*, 24(21), 3835-3844

[111] De Jong, S. J., *et al*. (2001). New insights into the hydrolytic degradation of poly (lactic acid): participation of the alcohol terminus. *Polymer*, 42(7), 2795-2802.

[112] Saha, S. K., and Tsuji, H. (2006). Effects of molecular weight and small amounts of d-lactide units on hydrolytic degradation of poly (l-lactic acid)s. *Polymer Degradation and Stability*, 91(8), 1665-1673.

[113] Tsuji, H. (2010) Hydrolytic degradation. In: Auras, R., *et al.* (eds) Poly (lactic acid): synthesis, structures, properties, processing, and applications. Wiley, Hoboken.. DOI:10.1002/9780470649848.

[114] Rasal, R. M., Janorkar, A. V., and Hirt, D. E. (2010). Poly (lactic acid) modifications. *Progress in polymer science*, 35(3), 338-356.

[115] Younes, H. and Cohn, D. (1988). Phase separation in poly (ethylene glycol)/poly (lactic acid) blends. *European polymer journal*, *24*(8), 765-773.

[116] Nijenhuis, A. J.,*et al*. (1996). High molecular weight poly (L-lactide) and poly (ethylene oxide) blends: thermal characterization and physical properties. *Polymer*, *37*(26), 5849-5857.

[117] Jiang, W., and Schwendeman, S. P. (2001). Stabilization and controlled release of bovine serum albumin encapsulated in poly (D, L-lactide) and poly (ethylene glycol) microsphere blends. *Pharmaceutical research*, *18*(6), 878-885.

[118] Höglund, A., *et al*. (2009). Surface modification changes the degradation process and degradation product pattern of polylactide. *Langmuir*, 26(1), 378-383.

[119] Källrot, M., Edlund, U., and Albertsson, A. C. (2007). Covalent grafting of poly (L-lactide) to tune the in vitro degradation rate. *Biomacromolecules*, 8(8), 2492-2496.

[120] Odelius, K., *et al*. (2011). Porosity and pore size regulate the degradation product profile of polylactide. *Biomacromolecules*, 12(4), 1250-1258.

[121] Wypych, G. (2016). Handbook of polymers. Elsevier.

[122] Bailey, F. E. and Koleske, J. Y., (1976). Poly(ethylene oxide), Academic Press. ISBN 978-0-12-073250-0.

[123] Lee, J. H., Lee, H. B., and Andrade, J. D. (1995). Blood compatibility of polyethylene oxide surfaces. *Progress in polymer science*, *20*(6), 1043-1079.

[124] do Carmo Rufino, T., and Felisberti, M. I. (2016). Confined PEO crystallisation in immiscible PEO/PLLA blends. *RSC Advances*, 6(37), 30937-30950.

[125] Lourenco, A. M. (1859). *Éther intermédiaire du glycol*. 49, 619 (1859).

[126] Wurtz, A. C. (1859). Synthèse du glycol avec l'oxyde d'éthylène et l'eau. *CR Acad. Sci*, *49*, 813-815.

[127] Hill, F. N., Bailey, F. E., and Fitzpatrick, J. T. (1958). High molecular weight polymers of ethylene oxide polymerization with alkaline earth carbonate catalysts. *Industrial & Engineering Chemistry*, *50*(1), 5-7.

[128] Kjellander, R. (1981). R. Kjellander and E. Florin, J. Chem. Soc. Faraday Trans. 1 77, 2053 (1981). J. Chem. Soc. Faraday Trans. 1, 77, 2053.

[129] Desai, N. P., and Hubbell, J. A. (1991). Solution technique to incorporate polyethylene oxide and other water-soluble polymers into surfaces of polymeric biomaterials. Biomaterials, 12(2), 144-153.

[130] Arrighi, V., Cowie, J. M., Fuhrmann, S., & Youssef, A. (2010). Miscibility criterion in polymer blends and its determination. *Encyclopedia of polymer blends*, 153-198.

[131] Nofar, M., *et al.*(2018). Poly (lactic acid) blends: Processing, properties and applications. *International journal of biological macromolecules*.

[132] Younes, H., and Cohn, D. (1988). Phase separation in poly (ethylene glycol)/poly (lactic acid) blends. *European polymer journal*, *24*(8), 765-773.

[133] Nijenhuis, A. *et al.* (1996). High molecular weight poly (L-lactide) and poly (ethylene oxide) blends: thermal characterization and physical properties. *Polymer*, *37*(26), 5849-5857.

[134] Nakane, K., *et al.* (2004). Porous poly (l-lactic acid)/poly (ethylene glycol) blend films. *Journal of applied polymer science*, *94*(3), 965-970.

[135] Sungsanit, K., Kao, N., and Bhattacharya, S. N. (2012). Properties of linear poly (lactic acid)/polyethylene glycol blends. *Polymer engineering & science*, *52*(1), 108-116.

[136] Hu, Y., *et al.* (2003). Aging of poly (lactide)/poly (ethylene glycol) blends. Part 1. Poly (lactide) with low stereoregularity. *Polymer*, *44*(19), 5701-5710.

[137] Hu, Y., *et al.* (2003). Aging of poly (lactide)/poly (ethylene glycol) blends. Part 2. Poly (lactide) with high stereoregularity. *Polymer*, *44*(19), 5711-5720.

[138] Riley, T., *et al.* (2003). Core− shell structure of PLA− PEG nanoparticles used for drug delivery. *Langmuir*, *19*(20), 8428-8435.

[139] Seck, T. M., *et al.* (2010). Designed biodegradable hydrogel structures prepared by stereolithography using poly (ethylene glycol)/poly (D, L-lactide)-based resins. *Journal of Controlled Release*, *148*(1), 34-41.

[140] Oliveira, J. E., *et al.* (2013). Properties of poly (lactic acid) and poly (ethylene oxide) solvent polymer mixtures and nanofibers made by solution blow spinning. *Journal of Applied Polymer Science*, *129*(6), 3672-3681.

[141] Serra, T., *et al.* (2014). Relevance of PEG in PLA-based blends for tissue engineering 3D-printed scaffolds. *Materials Science and Engineering: C*, *38*, 55-62.

[142] Prudente, A., *et al.* (2013). Impregnation of implantable polypropylene mesh with S-nitrosoglutathione-loaded poly (vinyl alcohol). *Colloids and Surfaces B: Biointerfaces*, 108, 178-184.

[143] de Souza, G. F. P., and de Oliveira, M. G. (2016). Intratablet S-nitrosation: A New Approach for the Oral Administration of S-nitrosothiols as Nitric Oxide Donors. *Journal of pharmaceutical sciences*, *105*(1), 359-361.

[144] Fox Jr, T. G., *et al*. (1950). Second-order transition temperatures and related properties of polystyrene. I. Influence of molecular weight. *Journal of Applied Physics*, *21*(6), 581-591.

[145] Turnbull, D., and Cohen, M. H. (1961). Free-volume model of the amorphous phase: glass transition. *The Journal of chemical physics*, *34*(1), 120-125.

[146] Jamshidi, K., Hyon, S. H., and Ikada, Y. (1988). Thermal characterization of polylactides. *Polymer*, *29*(12), 2229-2234.

[147] Zhang, J., *et al.* (2005). Crystal modifications and thermal behavior of poly (L-lactic acid) revealed by infrared spectroscopy. *Macromolecules*, *38*(19), 8012-8021.

[148] Delpouve, N., Saiter, A., and Dargent, E. (2011). Cooperativity length evolution during crystallization of poly (lactic acid). *European Polymer Journal*, *47*(12), 2414-2423.

[149] McCarthy, C. W., Goldman, J., and Frost, M. C. (2016). Synthesis and Characterization of the Novel Nitric Oxide (NO) Donating Compound, S-nitroso-N-acetyl-D-penicillamine Derivatized Cyclam (SNAP-Cyclam). *ACS applied materials & interfaces*, *8*(9), 5898-5905.

[150] Li, C. Q., *et al*. (2017). Mechanical and dielectric properties of graphene incorporated polypropylene nanocomposites using polypropylene-graft-maleic anhydride as a compatibilizer. *Composites Science and Technology*, *153*, 111-118.

[151] Garlotta, D. (2001). A literature review of poly (lactic acid). *Journal of Polymers and the Environment*, *9*(2), 63-84.

[152] Fernandes, J. S., Reis, R. L., and Pires, R. A. (2017). Wetspun poly-L-(lactic acid)-borosilicate bioactive glass scaffolds for guided bone regeneration. *Materials Science and Engineering: C*, *71*, 252-259.

[153] Weng, Y. X., *et al*. (2013). Biodegradation behavior of poly (butylene adipate-co-terephthalate)(PBAT), poly (lactic acid)(PLA), and their blend under soil conditions. Polymer Testing, 32(5), 918-926.

[154] Neumann, I. A.,*et al*. (2017). Biodegradable poly (l-lactic acid)(PLLA) and PLLA-3-arm blend membranes: The use of PLLA-3-arm as a plasticizer*. Polymer Testing*, 60, 84-93.

[155] Lai, W. C., *et al*. (2004). The effect of end groups of PEG on the crystallization behaviors of binary crystalline polymer blends PEG/PLLA. *Polymer*, *45*(9), 3073-3080.

[156] Sundararajan, S., Samui, A. B., and Kulkarni, P. S. (2017). Synthesis and characterization of poly (ethylene glycol)(PEG) based hyperbranched polyurethanes as thermal energy storage materials. *Thermochimica Acta*, *650*, 114-122.

[157] Abdelrazek, E. M., *et al*. (2017). Structural, optical, morphological and thermal properties of PEO/PVP blend containing different concentrations of biosynthesized Au nanoparticles. *Journal of Materials Research and Technology*.

[158] Stamler, J. S., and Toone, E. J. (2002). The decomposition of thionitrites. *Current opinion in chemical biology*, *6*(6), 779-785.

[159] Haitham, A. S. D., and Ferro, A. (2000). S-Nitrosothiols: a class of nitric oxide-donor drugs. *Clinical science*, *98*(5), 507-520.

[160] Conn, D., and Younes, H. (1989). Compositional and structural analysis of PELA biodegradable block copolymers degrading under in vitro conditions. *Biomaterials,*10(7),466-474.

SUPPLEMENTARY MATERIAL

Calibration curve for nitrite determination

The NO is detected by the NOA equipment as mV units. Using a calibration curve the mV signal is converted to NO flux as mol min^{-1} units. The calibration curve is obtained adding known aliquots of $NaNO_2$ 20 µM in triplicate. According to Eq.S-1, the nitrite ion is quantitatively reduced to NO by the iodide ion, which is in excess in the 0.1 M acetic acid solution (NaI 0.1 M)

$$2I^- + 4H^+ + 2NO_2^- \rightarrow 2NO + I_2 + 2H_2O \qquad \text{S-1}$$

The calibration curve is performed at 37 °C, the sample vessel contains 10 mL of reducing agent in acid solution. Aliquots of 20, 40, 60, 80 and 100 µL of $NaNO_2$ 20 µM are added in sequence and a figure is obtained in function of time (Fig.S-1a). The NO amount added in each aliquot is proportional to the area (mV min) of the peak, which is known by the integration of the respective peak. Afterwards, the area values are plotted against the known NO nmol as Fig.S-1b shows. Finally, a linear fit is realized in order to obtain the equation that defines the line.

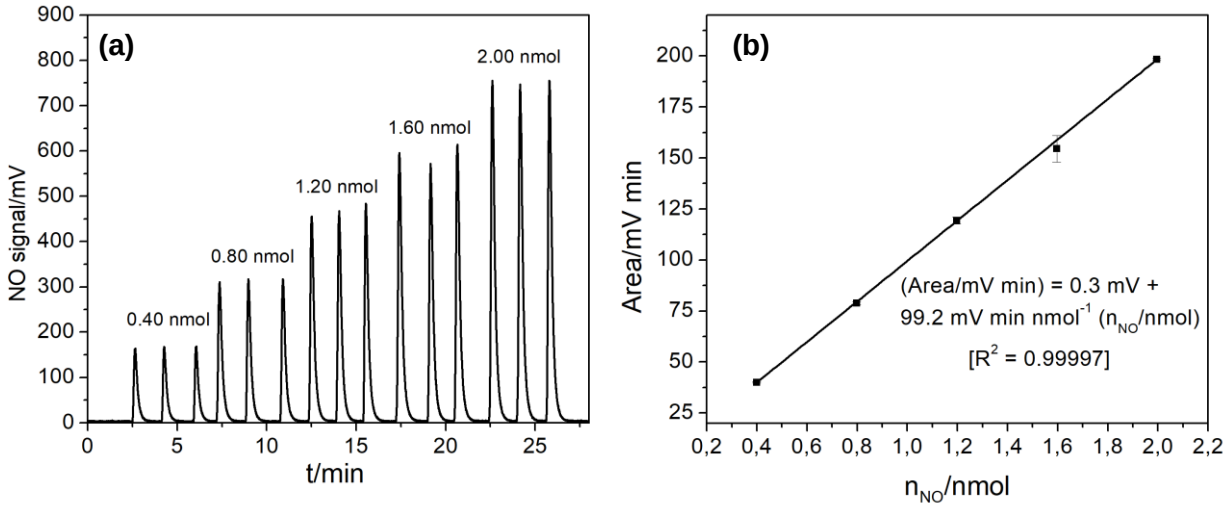

Fig. S-1(a). Representative graphic obtained by the aliquots addition in triplicate (20, 40, 60, 80 and 100 µL of $NaNO_2$), the added NO nmol are indicated above each set of peaks. **(b)** Calibration curve is by the peak integration of (a) and its equation is obtained by the linear regression of the mean ± SD.

Calibration curve for nitrate determination (vanadium (III) chloride method)

In this method the NO is detected by the NOA equipment as mV units as the current measurements. According to Eq.B-1,VCl_3 in hydrochloric acid (saturated solution) reduces nitrite species to nitric oxide. Using a calibration curve the mV signal is converted to NO flux as mol min^{-1} units. The calibration curve is obtained adding known aliquots of $NaNO_3$ 20 µM in triplicate.

$$3V^{+3} + 2NO_3^- + H_2O \rightarrow 2NO + 3VO_2^+ + 4H^+ \qquad \text{B-1}$$

The calibration curve is performed at 85 °C, the sample vessel contains 10 mL of reducing agent in acid solution. Aliquots of 20, 40, 60, 80 and 100 µL of $NaNO_3$ 20 µM are added in sequence and a figure is obtained in function of time (Fig.S-2a). The NO amount added in each aliquot is proportional to the area (mV min) of the peak, which is known by the integration of the respective peak. Afterwards, the area values are plotted against the known NO nmol as Fig.S-2b shows. Finally, a linear fit is realized in order to obtain the equation that defines the line.

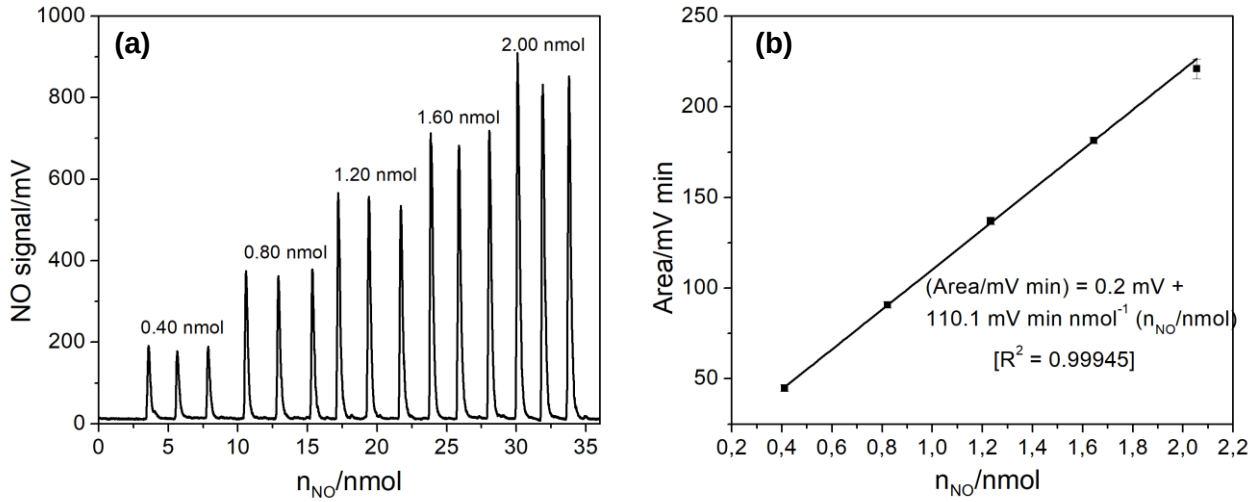

Fig. S-2(a). Representative graphic obtained by the aliquots addition in triplicate (20, 40, 60, 80 and 100 µL of $NaNO_2$), the added NO nmol are indicated above each set of peaks. **(b)** Calibration curve is by the peak integration of (a) and its equation is obtained by the linear regression of the mean ± SD.

Thermal history of PLLA

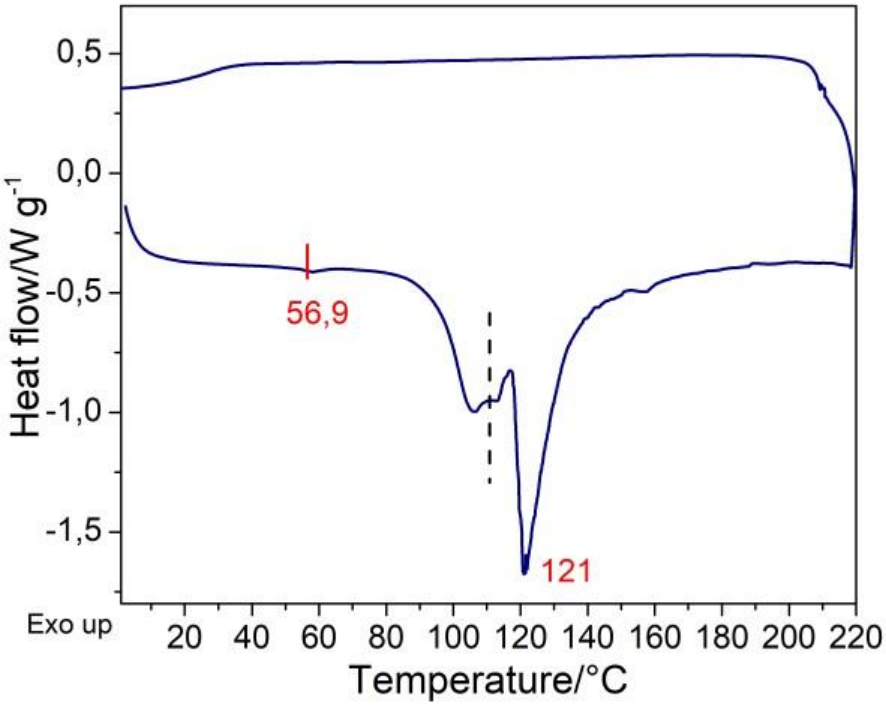

Fig. S-3. Thermogram of PLLA by DSC showing the thermal history (first heating and cooling cycle, with 10 °C min^{-1}) displaying the temperatures related to the thermal events, the glass transition temperature at 56,9 °C and the melting temperature at 121 °C. The dashed line indicates the absence of the first melting temperature, instead of there is undefined peak in the multiple melting peaks depicted as a result of the PLLA polymorphism, whereas during cooling no crystallization peaks are obtained since the crystallization kinetics from the melt is slow and cannot be perceptible.

SEM micrograph of polypropylene substrate

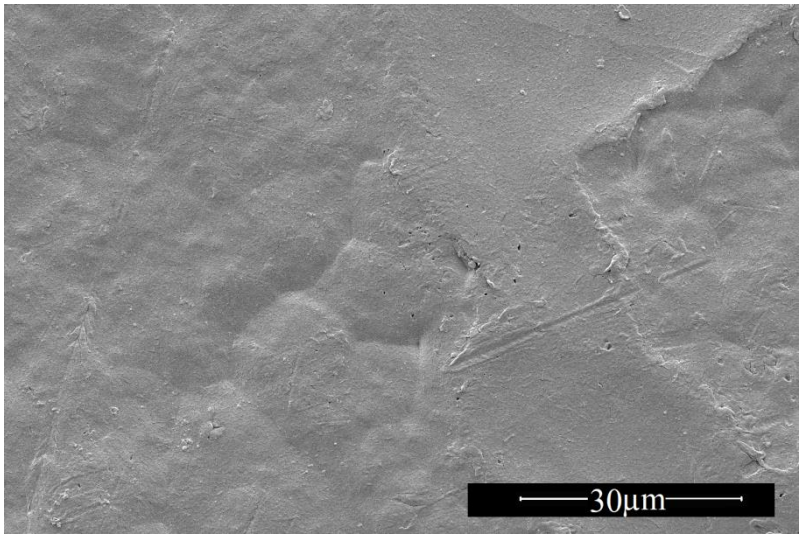

Fig. S-4. SEM micrograph of bare PP substrate allowed evaluating the surface morphology. The PP surface display crystalline sites along the PP sheet supporting the diffraction pattern of the PP which suggested a crystalline structure. In comparison with PP coated, the coatings showed different morphologies with or without cavities observed along the surface.

Thermal history of PEO

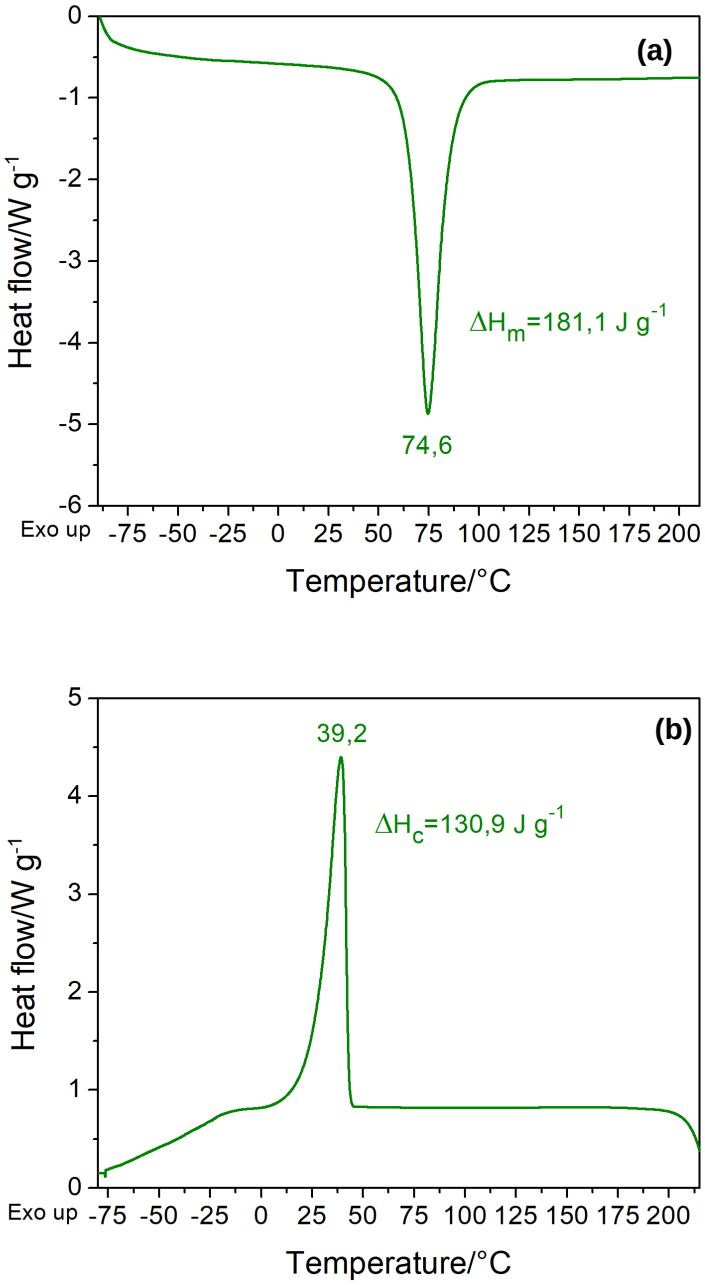

Fig. S-5. Thermogram of PEO by DSC showing the thermal history **(a)** first heating cycle the T_g could not be observed; Possibly, the amorphous phase volumetric fraction decreasing as a result of the high crystallinity degree. Additionally, a large sharp endothermic peak is observed at 74.6 °C related to T_m. **(b)** In the cooling cycle the crystallization is depicted at 39 °by intense exothermic peak. The enthalpy values are shown in each figures and the glass transition temperature, the melting temperature and the crystallization temperature are summarized in Table.5.

Thermal history of PLLA/PEO 70:30

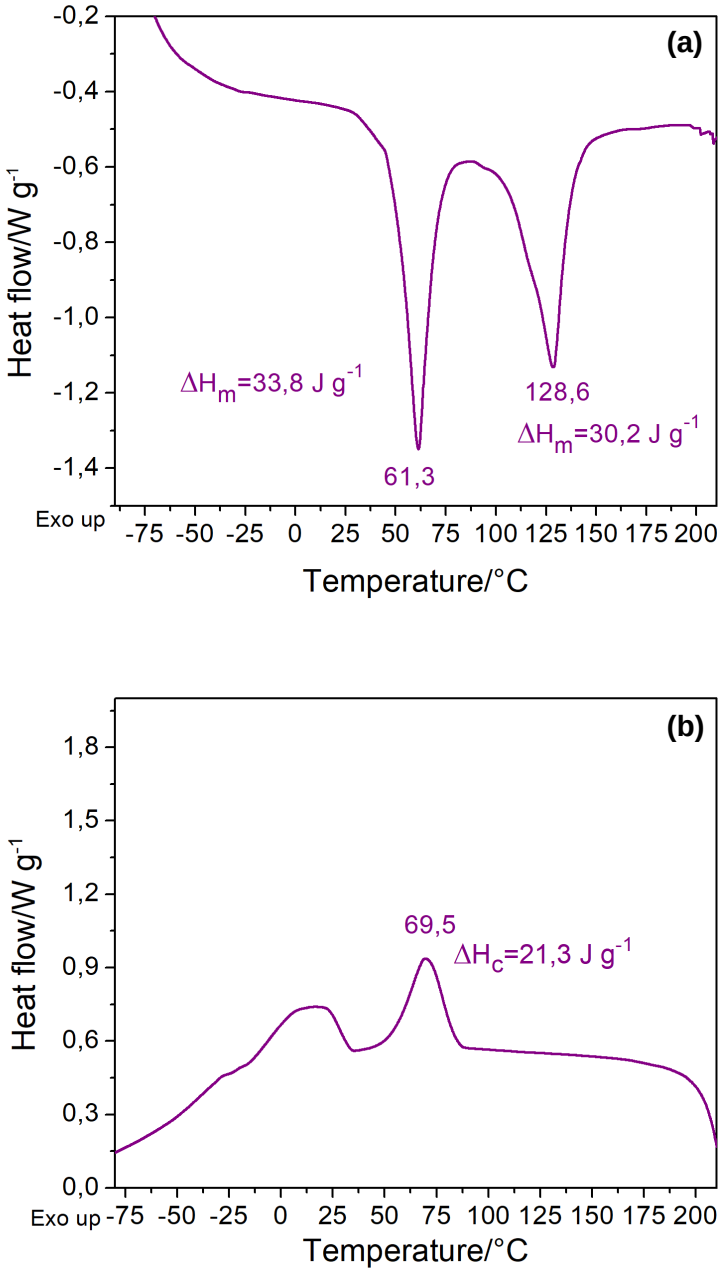

Fig. S-6. Thermogram of PLLA/PEO 70:30 by DSC showing the thermal history **(a)** first heating cycle the T_g could not be observed due to its overlap with PEO melting peak as well as the PLLA T_g. Additionally, both T_m suffered a reduction of intensity and a shift, as well as significant reduction on both PLLA and PEO melting enthalpies. **(b)** In the cooling cycle the crystallization is depicted at 69.5 °C by weak exothermic peak, suffered a reduction of intensity and a shift. The irregular peak about 0 to 25 °C could indicate presence of water in the blend. These thermal events values might indicate blend miscibility as aforementioned and are summarized in Table.5.

APPENDIX. A – License to reproduce Figure 3

ELSERVIER LICENSE
TERMS AND CONDITIONS

Jan 08, 2019

This Agreement between University of Campinas -- Yuliana Pérez Sánchez ("You") and Elsevier ("Elsevier") consists of your license details and the terms and conditions provided by Elsevier and Copyright Clearance Center.

License Number	4504180715716
License date	Jan 08, 2019
Licensed Content Publisher	Elsevier
Licensed Content Publication	Elsevier Books
Licensed Content Title	Nitric Oxide
Licensed Content Author	Christopher G. Kevil,David J. Lefer
Licensed Content Date	Jan 1, 2010
Licensed Content Pages	17
Start Page	587
End Page	603
Type of Use	reuse in a thesis/dissertation
Intended publisher of new work	other
Portion	figures/tables/illustrations
Number of figures/tables/illustrations	1
Format	electronic
Are you the author of this Elsevier chapter?	No
Will you be translating?	No
Original figure numbers	Figure.1
Title of your thesis/dissertation	Nitric Oxide-releasing polyester coatings to improve the biocompatibility of implantable medical devises
Expected completion date	Jan 2019
Estimated size (number of pages)	90
Requestor Location	University of Campinas Rua Carlos Gomes, 241 Cidade Universitária CEP: 13083970, Campinas, São Paulo 6145Brazil Attn: University of Campinas
Publisher Tax ID	GB 494 6272 12
Total	0.00 USD

APPENDIX. B – License to reproduce Figure 5

STANDARD ACS AUTHORCHOICE/EDITORS´S
CHOICE AGREEMENTS

Dec 31, 2018

This ACS article is provided to You under the terms of this Standard ACS AuthorChoice/Editors' Choice usage agreement between You and the American Chemical Society ("ACS"), a federally-chartered nonprofit located at 1155 16th Street NW, Washington DC 20036. Your access and use of this ACS article means that you have accepted and agreed to the Terms and Conditions of this Agreement. ACS and You are collectively referred to in this Agreement as "the Parties").

Link: https://pubs.acs.org/page/policy/authorchoice_termsofuse.html

Posted: 03/06/2014

APPENDIX. C – License to reproduce Figure 6

JOHN WILEY AND SONS LICENSE
TERMS AND CONDITIONS

Dec 31, 2018

This Agreement between University of Campinas -- Yuliana Pérez Sánchez ("You") and John Wiley and Sons ("John Wiley and Sons") consists of your license details and the terms and conditions provided by John Wiley and Sons and Copyright Clearance Center.

License Number	4499440725749
License date	Dec 31, 2018
Licensed Content Publisher	John Wiley and Sons
Licensed Content Publication	Advanced Functional Materials
Licensed Content Title	Polymer-Based Nitric Oxide Therapies: Recent Insights for Biomedical Applications
Licensed Content Author	Michele C. Jen, María C. Serrano, Robert van Lith, et al
Licensed Content Date	Nov 17, 2011
Licensed Content Volume	22
Licensed Content Issue	2
Licensed Content Pages	22
Type of use	Dissertation/Thesis
Requestor type	Author of this Wiley article
Format	Electronic
Portion	Figure/table
Number of figures/tables	1
Original Wiley figure/table number(s)	Scheme 1
Will you be translating?	No
Title of your thesis / dissertation	Nitric Oxide-releasing polyester coatings to improve the biocompatibility of implantable medical devises
Expected completion date	Jan 2019
Expected size (number of pages)	90
Requestor Location	University of Campinas Rua Carlos Gomes, 241 Cidade Universitária CEP: 13083970, Campinas, São Paulo 6145 Brazil Attn: University of Campinas
Publisher Tax ID	EU826007151
Total	0.00 USD

APPENDIX. D – License to reproduce Figure 6

ELSEVIER LICENSE
TERMS AND CONDITIONS

Dec 31, 2018

This Agreement between University of Campinas -- Yuliana Pérez Sánchez ("You") and Elsevier ("Elsevier") consists of your license details and the terms and conditions provided by Elsevier and Copyright Clearance Center.

License Number	4499450617527
License date	Dec 31, 2018
Licensed Content Publisher	Elsevier
Licensed Content Publication	Nitric Oxide
Licensed Content Title	Reduced ischemia/reperfusion injury via glutathione-initiated nitric oxide-releasing dendrimers
Licensed Content Author	Timothy A. Johnson,Nathan A. Stasko,Jessica L. Matthews,Wayne E. Cascio,Ekhson L. Holmuhamedov,C. Bryce Johnson,Mark H. Schoenfisch
Licensed Content Date	Jan 1, 2010
Licensed Content Volume	22
Licensed Content Issue	1
Licensed Content Pages	7
Start Page	30
End Page	36
Type of Use	reuse in a thesis/dissertation
Intended publisher of new work	other
Portion	figures/tables/illustrations
Number of figures/tables/illustrations	1
Format	print
Are you the author of this Elsevier article?	No
Will you be translating?	No
Original figure numbers	Figure 2
Title of your thesis/dissertation	Nitric Oxide-releasing polyester coatings to improve the biocompatibility of implantable medical devises
Expected completion date	Jan 2019
Estimated size (number of pages)	90
Requestor Location	University of Campinas,Rua Carlos Gomes, 241. Cidade Universitária,CEP: 13083970, Campinas, São Paulo 6145,Brazil Attn: University of Campinas
Publisher Tax ID	GB 494 6272 12

APPENDIX. E – License to reproduce Figure 6

Copyright Clearance Center

Dec 31, 2018

Title:	Micelles for Delivery of Nitric Oxide
Author:	Yun Suk Jo, André J. van der Vlies, Jay Gantz, et al
Publication:	Journal of the American Chemical Society
Publisher:	American Chemical Society
Date:	Oct 1, 2009

PERMISSION/LICENSE IS GRANTED FOR YOUR ORDER AT NO CHARGE

This type of permission/license, instead of the standard Terms & Conditions, is sent to you because no fee is being charged for your order. Please note the following:

- Permission is granted for your request in both print and electronic formats, and translations.
- If figures and/or tables were requested, they may be adapted or used in part.
- Please print this page for your records and send a copy of it to your publisher/graduate school.
- Appropriate credit for the requested material should be given as follows: "Reprinted (adapted) with permission from (COMPLETE REFERENCE CITATION). Copyright (YEAR) American Chemical Society." Insert appropriate information in place of the capitalized words.
- One-time permission is granted only for the use specified in your request. No additional uses are granted (such as derivative works or other editions). For any other uses, please submit a new request.

If credit is given to another source for the material you requested, permission must be obtained from that source.

APPENDIX. F – License to reproduce Figure 8

JOHN WILEY AND SONS LICENSE
TERMS AND CONDITIONS

Dec 31, 2018

This Agreement between University of Campinas -- Yuliana Pérez Sánchez ("You") and John Wiley and Sons ("John Wiley and Sons") consists of your license details and the terms and conditions provided by John Wiley and Sons and Copyright Clearance Center.

License Number	4499490581850
License date	Dec 31, 2018
Licensed Content Publisher	John Wiley and Sons
Licensed Content Publication	Polymer International
Licensed Content Title	Stereocomplexed polylactides (Neo-PLA) as high-performance bio-based polymers: their formation, properties, and application
Licensed Content Author	Kazuki Fukushima, Yoshiharu Kimura
Licensed Content Date	Apr 6, 2006
Licensed Content Volume	55
Licensed Content Issue	6
Licensed Content Pages	17
Type of use	Dissertation/Thesis
Requestor type	University/Academic
Format	Electronic
Portion	Figure/table
Number of figures/tables	1
Original Wiley figure/table number(s)	Figure 1
Will you be translating?	No
Title of your thesis / dissertation	Nitric Oxide-releasing polyester coatings to improve the biocompatibility of implantable medical devises
Expected completion date	Jan 2019
Expected size (number of pages)	90
Requestor Location	University of Campinas Rua Carlos Gomes, 241 Cidade Universitária CEP: 13083970 Campinas, São Paulo 6145 Brazil Attn: University of Campinas
Publisher Tax ID	EU826007151
Total	0.00 USD